Meteorological Modeling for the August 2000 Houston-Galveston Ozone Episode: PBL Characteristics, Nudging Procedure, and Performance Evaluation

John W. Nielsen-Gammon
Department of Atmospheric Sciences
Texas A&M University

a report to the Technical Analysis Division,
Texas Natural Resource Conservation Commission
February 28, 2002

Contact Information:
John W. Nielsen-Gammon
Department of Atmospheric Sciences
3150 TAMU
College Station, TX 77843-3150
Phone: 979-862-2248 Fax: 979-862-4466

This report is the third in a series describing meteorological modeling efforts for the August 2000 ozone episode. Previous reports are available from the author and from the Texas Natural Resource Conservation Commission.
Report 1: Initial Modeling of the August 2000 Houston-Galveston Ozone Episode (Dec. 19, 2001)
Report 2: Evaluation and Comparison of Preliminary Meteorological Modeling for the August 2000 Houston-Galveston Ozone Episode (Feb. 5, 2002)

Summary

This report describes evaluations of the performance of various configurations of the MM5 modeling system, as compared to planetary boundary layer (PBL) structure and profiler winds. Soundings from the three sounding sites are grouped by time of day and by regime. Systematic differences between the different model runs are found; the differences between the models and observations vary from site to site. Higher vertical resolution did not produce improved boundary layer structure. The MCNC runs had well-mixed PBL's, even at night, but were too shallow during the day. Most of the runs with the MRF PBL were similar and performed fairly well. One area of possible concern is the systematic underestimate of the strength of the sea breeze inversion, an error which may lead to too much diffusion of constituents into and out of the advancing marine air. The Gayno-Seaman PBL scheme appeared to be more realistic, but its sea breeze inversion was too strong.

Wind errors were computed at a variety of heights, grouped by weather regime, and with 24-hour running means and departures from running means. Most of the model error was associated with the departures from the running means. The MRF PBL schemes tended to perform best overall. All model runs except MCNC developed large biases at heights above 1 km. The MCNC run was worst during Regime 1 but was best during Regime 2 when other model runs produced only a small fraction of the observed low-level jet speeds.

Based on these and previously-reported evaluations of various model configurations, a particular configuration was chosen. This configuration uses the MRF PBL with 43 vertical levels and one-way nesting. The soil moisture availability is specified to decrease during the model integration, to simulate evaporation of rain that fell just prior to the ozone episode. A new subroutine was added to the MM5 to permit model restarts with updated soil moisture.

The nudging strategy is then outlined. The approach followed here uses a large time window for nudging so as to effectively average out possibly erroneous hour-to-hour variations in low-level winds that were introduced during the quality assurance process. The default value for nudging strength is used. No nudging is performed prior to August 25 because the convection on the previous days are not resolved by the profiler network and any attempt at nudging would cause aliasing in the model fields.

The final model run, called the "driver" run, also utilizes lower-tropospheric nudging of water vapor on the 12 km grid. This nudging is designed to suppress a robust outflow boundary which sweeps through Houston on August 31 in the model forecasts but not in the observations. The nudging successfully prevents convection from developing on the 4 km grid and reinforcing the outflow, but a weak wind surge does reach Houston during the evening.

The thermodynamic performance of the driver run is very similar to its predecessor runs, since no nudging is applied to the temperature field. The wind field is dramatically improved, at least by comparison to the profiler data. Since this data set was used to nudge the model in the first place, further objective verification of the improvement due to nudging is necessary.

The wind and temperature fields during the high ozone days of the episode are examined in detail. On two of the days, August 30 and 31, the model wind and

temperature fields have realistic large-scale and small scale features and further improvement is unlikely. Three other days, August 26, August 29, and September 1, are generally accurate but have wind errors which are likely to lead to position errors in the simulation of ozone by a photochemical model. The remaining day, August 25, had erroneous or too-light surface winds. On this day, high values of ozone are likely to be simulated by a photochemical model, but it is possible that the mixture of ozone precursors that leads to the high ozone will be fundamentally different due to the transport errors.

In summary, the driver model run produces generally accurate daytime lower-tropospheric temperatures and winds. On most days of the episode, the meteorological fields appear to be adequate for driving the particular combination of mixing and chemical processes that lead to high ozone on each of those days.

Table of Contents

List of Figures

(figures appear consecutively in the back of this report)

Figure 6b: Model sounding from dec30grid4 model run, Houston Southeast/Lamarque, 2300 UTC Aug. 30 2000.

Figure 6c: Model sounding from dec16grid4 model run, Houston Southeast/Lamarque, 2300 UTC Aug. 30 2000.

Figure 6d: Model sounding from feb9grid4 model run, Houston Southeast/Lamarque, 2300 UTC Aug. 30 2000.

Figure 6e: Model sounding from feb16grid4 model run, Houston Southeast/Lamarque, 2300 UTC Aug. 30 2000.

Figure 7: Daytime PBL depths, Houston Downtown site. First set is from Airsonde observations; other sets are from model runs.

Figure 8: Mean PBL potential temperatures, Houston Downtown Airsonde site. First set is observations, remaining sets are model runs.

Figure 9a: Observed sounding, 1400 UTC Aug. 30, 2000, Houston Downtown Airsonde site.

Figure 9b: Model sounding from dec30grid4 model run, Houston Downtown, 1400 UTC Aug. 30 2000.

Figure 9c: Model sounding from MCNC model run, Houston Downtown, 1400 UTC Aug. 30 2000.

Figure 10a: Observed sounding, 2316 UTC Aug. 31, 2000, Houston Downtown Airsonde site.

Figure 10b: Model sounding from dec30grid4 model run, Houston Downtown, 2300 UTC Aug. 31 2000.

Figure 10c: Model sounding from dec16grid4 model run, Houston Downtown, 2300 UTC Aug. 31 2000.

Figure 10d: Model sounding from MCNC model run, Houston Downtown, 2300 UTC Aug. 31 2000.

Figure 11a: Observed sounding, 0804 UTC Aug. 31, 2000, Houston Downtown Airsonde site.

Figure 11b: Model sounding from dec16grid4 model run, Houston Downtown, 0800 UTC Aug. 31 2000.

Figure 11c: Model sounding from dec30grid4 model run, Houston Downtown, 0800 UTC Aug. 31 2000.

Figure 11d: Model sounding from feb9grid4 model run, Houston Downtown, 0800 UTC Aug. 31 2000.

Figure 12: Daytime PBL depths, Wharton Power Plant site. First set is from GPS rawinsonde observations; other sets are from model runs.

Figure 13: Mean PBL potential temperatures, Wharton Power Plant GPS rawinsonde site. First set is observations, remaining sets are model runs.

Figure 14a: RMS Errors between model runs and profiler data, vertical level nearest to 200 m. (u,v): total wind components. (urm,vrm) 24-hour running mean wind components. (udp,vdp) departures from 24-hour running mean. Profiler data set has been passed through ETL quality control.

Figure 14b: RMS Errors between model runs and profiler data, vertical level nearest to 400 m.

Figure 14c: RMS Errors between model runs and profiler data, vertical level nearest to 700 m.

Figure 14d: RMS Errors between model runs and profiler data, vertical level nearest to 1000 m.

Figure 15: Biases of modeled wind components at indicated levels (m), measured against ETL quality-controlled profiler data.

Figure 16: Comparison of model RMS error using ETL quality-controlled profiler data (ww) and AL quality-controlled profiler data (con).

Figure 17a: RMS error of the departures from the 24-hour running mean of each wind component during Regime 1, measured against ETL quality-controlled profiler data.

Figure 17b: RMS error of the departures from the 24-hour running mean of each wind component during Regime 2, measured against ETL quality-controlled profiler data.

Figure 18: RMS error of the departure from 24-hour running means for Regime 1 and Regime 2, measured against ETL quality-controlled profiler data. RMS errors are computed at the 200m, 400m, 700m, and 1000m levels and averaged.

Figure 19: RMS error of the departure from 24-hour running means for entire ozone episode, measured against ETL quality-controlled profiler data. RMS errors are computed at the 200m, 400m, 700m, and 1000m levels and averaged.

Figure 20: Time series of wind speed (top, m/s) and direction (bottom, degrees) at the 400 m level at the Houston Southwest profiler site. Solid black: AL profiler data; Dashed black: ETL profiler data; Blue: dec6grid4; Green: dec30grid4; Red: MCNC; Purple: Obs nudging with default soil moisture; Brown: Driver run (with obs nudging)

Figure 21: Time series of wind speed (top, m/s) and direction (bottom, degrees) at the 400 m level at the Liberty profiler site. Colors as in Fig. 20.

Figure 22: Time series of u (east-west) component of wind (top, m/s) and v (north-south component of wind (bottom, m/s) at the 250 m level at the Lamarque profiler site. Colors as in Fig. 20.

Figure 23: Time series of u (east-west) component of wind (top, m/s) and v (north-south component of wind (bottom, m/s) at the 250 m level at the Liberty profiler site. Colors as in Fig. 20.

Figure 24: Time series of u (east-west) component of wind (top, m/s) and v (north-south component of wind (bottom, m/s) at the 250 m level at the Wharton Power Plant profiler site. Colors as in Fig. 20.

Figure 25: Time series of u (east-west) component of wind (top, m/s) and v (north-south component of wind (bottom, m/s) at the 1000 m level at the Lamarque profiler site. Colors as in Fig. 20.

Figure 26: Time series of u (east-west) component of wind (top, m/s) and v (north-south component of wind (bottom, m/s) at the 1500 m level at the Wharton Power Plant profiler site. Colors as in Fig. 20.

Figure 27: Total RMS error, RMS error of the 24-hour running mean, and RMS error of the departure from the 24-hour running mean, by wind component and height above ground, driver model run. Compare with Fig. 14.

Figure 28: Bias as a function of wind component and height, driver model run. Compare with Fig. 15.

Figure 29: Driver model run RMS error of the departure from 24-hour running mean by regime, as a function of wind component and height. Compare with Fig. 18.

Figure 30a: Surface observations (black) and driver model run simulated winds (red) and temperatures (purple, C), 16 UTC August 25 2000.The observed wind speed in the lower right corner is 3.2 m/s; this scale is retained in the figures that follow. The model data is 2 m temperature and 10 m wind, output from the MRF PBL scheme.

Figure 30b: Observations and driver model simulation, 18 UTC August 25.

Figure 30c: Observations and driver model simulation, 20 UTC August 25.

Figure 30d: Observations and driver model simulation, 22 UTC August 25.

Figure 31a: Observations and driver model simulation, 16 UTC August 26.

Figure 31b: Observations and driver model simulation, 18 UTC August 26.

Figure 31c: Observations and driver model simulation, 20 UTC August 26.

Figure 31d: Observations and driver model simulation, 22 UTC August 26.

Figure 32a: Observations and driver model simulation, 16 UTC August 29.

Figure 32b: Observations and driver model simulation, 18 UTC August 29.

Figure 32c: Observations and driver model simulation, 2000 UTC August 29.

Figure 32d: Observations and driver model simulation, 22 UTC August 29.

Figure 33a: Observations and driver model simulation, 18 UTC August 30.

Figure 33b: Observations and driver model simulation, 20 UTC August 30.

Figure 33c: Observations and driver model simulation, 22 UTC August 30.

Figure 34a: Observations and driver model simulation, 18 UTC August 31.

Figure 34b: Observations and driver model simulation, 20 UTC August 31.

Figure 34c: Observations and driver model simulation, 22 UTC August 31.

Figure 35a: Observations and driver model simulation , 16 UTC September 1.

Figure 35b: Observations and driver model simulation, 18 UTC September 1.

Figure 35c: Observations and driver model simulation, 20 UTC September 1.

Figure 35d: Observations and driver model simulations, 22 UTC September 1.

List of Tables

Introduction

Texas A&M University (TAMU) has been contracted by the Texas Natural Resource Conservation Commission (TNRCC) to develop a high-quality meteorological simulation of the August 25-September 1, 2000 Houston-Galveston ozone episode. According to their timetable, TNRCC shall begin photochemical modeling of the episode on March 1, 2002, and therefore the best possible meteorological model output must be available on or before February 28, 2002.

During the fall and winter of 2001-2002, this meteorological modeling work has followed a procedure designed to take full advantage of both the raw meteorological data and the knowledge gained from the Texas 2000 Air Quality Study (TexAQS-2000), which included the ozone episode of interest. The modeling philosophy and initial modeling results are described in the report dated December 19, 2001, and titled "Initial Modeling of the August 2000 Houston-Galveston Ozone Episode", available from TNRCC and at http://www.met.tamu.edu/results. This report will henceforth be referred to as Report 1. Further modeling work, including an evaluation of cloud cover, precipitation, temperatures, and winds, is described in the report dated February 5, 2002, and titled "Evaluation and Comparison of Preliminary Meteorological Modeling for the August 2000 Houston-Galveston Ozone Episode", also available from TNRCC and at http://www.met.tamu.edu/results.

The purpose of the present report is to document the model run recommended for input to a photochemical model by TNRCC, to describe the procedures used to assimilate TexAQS-2000 observations into this and other model runs, and to evaluate the performance of the model with respect to planetary boundary layer (PBL) structure, low-level winds, and other characteristics important for photochemical modeling. Since no model is perfect, it is critical to understand the performance limitations of the meteorological model so that the subsequent performance of the photochemical model may be placed in the proper context. The performance of preliminary modeling by the Microcomputer Center of North Carolina (MCNC), which has been used as part of a separate photochemical modeling effort, is similarly evaluated. The characteristics of several other model runs are compared here in order to provide a basis for possible future meteorological modeling work on this episode. Finally, recommendations are made for additional investigations which may be expected to lead to improved understanding and model simulations of meteorological conditions that are associated with high levels of ozone in the Houston-Galveston area.

2. Comparison of Planetary Boundary Layer Characteristics

Previous reports have compared model simulations of maximum and minimum temperatures and have summarized the daytime planetary boundary layer (PBL) performance at the Wharton Power Plant (WPP) sounding site. In this section, the non-nudged MM5 simulations are compared to soundings from all three radiosonde launch sites by day and by time of day.

Particular emphasis is placed on the development of nighttime inversions and daytime well-mixed layers and the vertical structure of winds and temperatures associated with sea breezes. Inversion depths and well-mixed PBL depths are estimated subjectively. Where the PBL is not capped by a clear layer of high stability, the PBL top was estimated based on an increase of potential temperature (generally, at least 1 C from its PBL minimum) and a decrease of mixing ratio with height. A few soundings are neglected when the PBL height is ambiguous.

2a) Description of model runs

Eight model runs are compared. Five of the runs have been documented in previous reports. They are:
dec6grid4: 43 levels, MRF PBL, dry soil moisture
dec30grid4: Same as dec6grid4, but with very dry soil moisture
dec16grid4: Same as dec30grid4, but with Gayno-Seaman PBL
oct25grid4: Same as dec6grid4, but with the lowest two levels combined
mcnc: Forecast mode, 31 levels, Blackadar PBL, normal soil moisture, other differences

Three model runs are new to this report. The **feb9grid4** model run is identical to the dec30grid4 run, except that it uses the original Hong and Pan PBL scheme on which the current implementation of the MRF PBL is based. The original scheme has much smaller vertical diffusion in the free atmosphere. Based on analysis of the evolution of the nighttime low-level jet during Regime 2, it was hypothesized that the erroneously low wind speeds in the model were a consequence of excessive vertical mixing of momentum, and the feb9grid4 model run was designed to test this hypothesis.

The **feb16grid4** model run is identical to the feb9grid4 model run, except that an additional eleven layers were added to the lower part of the model domain, effectively doubling the resolution at the bottom of the PBL. This test was conducted to see if nocturnal surface-based inversions would be simulated more realistically, in turn leading to improvements in the simulation of the decoupling of winds aloft from the nighttime PBL and development of the low-level jet.

Finally, the **feb18grid4** model run is identical to the feb6grid4 run, except that no nudging is used on the 12 km grid and two-way nesting is used on the 12-4 km grid interface. This run was designed to test the hypothesis that the one-way heavily nudged lateral boundary conditions were inhibiting a large-scale inertial adjustment on the 4 km grid associated with the nighttime low-level jet.

It is virtually certain that some other untested combination of settings would provide at least a slightly better simulation than any of the ones that we have tried. Therefore, the fact that a model run with setting A performed better than a model run with setting B does not mean that setting A is better than setting B with other model

configurations. This is particularly true of the mcnc run, which did not have the advantage of model adjustments designed for the Houston meteorological environment.

2b) Subjective vs. Objective Estimate of PBL Heights

The subjective assessment of PBL heights for daytime soundings at the Houston Southeast (HSE) site is compared to the MRF PBL scheme's computed PBL height in Fig. 1. The subjective assessments were made by viewing plotted soundings, and PBL heights are recorded in millibars. During this period, one millibar equals approximately 9 meters, so MRF PBL's are consistently higher than subjective PBL's by about 30 %. The only outlier occurred during a sea breeze episode, where the subjectively-estimated height was 30 mb and the model-reported height was 1660 m. This was actually a close call, since the model-reported height at the next upstream grid point was a much more consistent 340 m.

The subjective assessments appear to more accurately reflect the PBL structure. For example, Fig. 2a shows the HSE sounding for 1952 UTC (1352 LST) Aug. 30, 2000. In a perfectly well-mixed boundary layer, the temperature (right-hand) graph would be exactly parallel to the red background lines (constant potential temperature) and the dewpoint (left-hand) graph would be exactly parallel to the blue background lines (constant water vapor mixing ratio). This sounding is nearly perfectly well-mixed from the lowest data point (about 20 mb above the ground) to a pressure of 870 mb. Above that point, the potential temperature increases and the dew point decreases and becomes more erratic. The top of this boundary layer is unambiguous.

Figure 2b shows the corresponding dec6grid4 model sounding. As in the observed sounding, the air a short distance above the ground has constant potential temperature and mixing ratio. Right next to the ground, a superadiabatic layer (in which potential temperature decreases with height) is simulated. This is a sign of heating of the atmosphere by the ground, and is commonly found in simulated and observed soundings. Over the same shallow layer, the mixing ratio decreases slightly, a sign of the evaporation from the ground which is expected during daytime.

There is no sharp upper boundary to the layer of uniform potential temperature and mixing ratio. Between 875 mb and 835 mb, the potential temperature increases slightly and the mixing ratio decreases slightly. Over the next model layer, between 835 mb and 810 mb, potential temperature and mixing ratio change significantly, in a manner which is very similar to the observed changes between 870 mb and 840 mb. The top of the model PBL is therefore determined to be 835 mb, for a total PBL depth of 160 mb.

The simulated height of the 835 mb level is 1725 m. The PBL height at this point according to the MRF PBL scheme, by contrast, is 2010 m, or 810 mb, which is at the top of the capping inversion at this location. The MRF PBL height at adjacent grid points ranges from 1800 m to 2285 m, corresponding to pressures between 825 mb and 780 mb. None of these heights or pressures correspond with the simulated base of the inversion at the top of the PBL. It therefore appears that the MRF PBL height is systematically above the top of the well-mixed layer in the simulations. Care must be taken when determining vertical mixing characteristics for photochemical modeling so that strong vertical mixing is not assumed to take place near the top of the reported daytime MRF PBL.

2c) Houston Southeast Composites

The Houston Southeast (HSE) sounding site was used for Airsonde launches (pressure, temperature, and humidity) and was colocated with the Lamarque (LAM) wind profiler. The HSE site is about 13 km northwest of West Bay, which separates Galveston Island from the mainland and is wider than Galveston Island itself. This close proximity to the coastline makes the temperature and PBL structure spatially nonuniform under onshore flow conditions. Model PBL errors may be caused by errors in the onshore wind speed and errors in the resolution of the coastline and Galveston Island, in addition to standard sources of model error. Therefore, while the site is valuable for recording the thermodynamic structure of the atmosphere behind the sea breeze front, this site is not particularly useful for assessing PBL changes during Regime 1 (August 25-29), when winds were predominantly onshore. During Regime 2 (August 30-September 1), winds were offshore during most of the day, and the observed PBL structure can be assumed to be representative of fairly homogeneous overland conditions.

Average PBL heights from the observations and from eight model runs are shown in Fig. 3 for five classes of soundings. The first class, 17 UTC during Regime 1, consists of soundings during the time that the PBL was growing and winds were light. All model runs overestimate the depth of the late morning PBL here, some by a factor of two or more. This set actually consists of only two soundings, from Aug. 25 and Aug. 29. Model performance on Aug. 29 was actually fairly good. The observed PBL depth was 110 mb, while the simulated PBL depths ranged from 110 mb to 160 mb. The errors occurred with the Aug. 25 sounding. On that day, the 17 UTC observed PBL depth was only 50 mb, and the mean PBL potential temperature was 27 C. The model simulations, however, typically had a deeper and warmer PBL on Aug. 25 than on Aug. 29. This error is likely to be due to an underestimate of evaporation from the ground on Aug. 25. Rainfall occurred in the area during the previous two days, and the wet conditions appear to have contributed to a reduced surface heating rate. The other two Regime 1 groupings include three soundings apiece and so are not as influenced by Aug. 25. Furthermore, as the day progresses, the relative amount of evaporation should decrease as water is lost to the atmosphere.

The 20 UTC Regime 1 observed soundings show little change from the 17 UTC soundings. This is an indication that marine air is suppressing the growth of the boundary layer, so that the total boundary layer depth depends not just on local thermodynamics but also on the advection of air from the coastline. The only model run that has correctly simulated this aspect of the PBL is dec16grid4, which is within 20 mb of the observed PBL depth on all three days.

At 2300 UTC, HSE/LAM is under the strong influence of the Gulf breeze. The sounding from Aug. 26 (Fig. 4a) is typical. The well-mixed, humid layer of air in the lowest 70 mb is the Gulf breeze, overlaid with a weak inversion and drier, more stable air above. Winds from the Lamarque profiler show onshore winds throughout the lowest half of the sounding, with the strongest onshore winds (the sea breeze) beneath the inversion.

The dec6grid4 model sounding features a somewhat higher inversion, near 900 mb. This inversion is not the top of the sea breeze. In this and other model soundings using the MRF PBL, both the sea breeze and the return flow are within a weakly stratified

layer. In this instance, there is no true return flow, but the onshore flow is weakest just beneath the capping inversion. Below the inversion, the weakly stratified layer is not quite well mixed: the stability gradually increases up to the capping inversion and the mixing ratio decreases with height at all levels. This seems unrealistic: high-resolution observations of sea breezes in other environments typically show a weak to moderate inversion overlaying the strongest onshore flow, with the return flow strongest above the inversion.

The dec16grid4 run (Fig. 4c), with the Gayno-Seaman PBL scheme, produces a much more realistic sea breeze structure, with strong onshore flow in the well-mixed layer beneath the inversion and weak offshore or onshore flow above the inversion. The height of the inversion and depth of the sea breeze are in agreement with observations. However, the inversion is too strong in the dec16grid4 run, about twice as strong as in the observations, suggesting that the sea breeze circulation may be too vigorous.

The MCNC run (Fig. 4d) is similar to the dec6grid4 run, in that both have most of the sea breeze and return flow confined to a deep layer without a strong inversion. The MCNC run is even less realistic than dec6grid4, though: the marine air is thoroughly well-mixed, with not even weak stratification present below the inversion. As will be seen, the MCNC model tends to produce well-mixed PBLs in too many situations.

Summarizing the performance on this and other strong sea breeze days during Regime 1, the observations lie somewhere between the simulations with the MRF PBL and the Gayno-Seaman PBL, with Gayno-Seaman producing too strong a sea breeze inversion and the MRF PBL producing no inversion at all at the top of the sea breeze, just weak stratification which increases with height. The MRF PBL depth is also too large within the sea breeze. On balance, the Gayno-Seaman PBL simulations most closely resemble the observations within a strong sea breeze flow.

During Regime 2, daytime offshore flow sharpened the sea breeze but prevented its advance until late in the day. The Lamarque soundings imply that the sea breeze was later arriving on Aug. 31 than on Aug. 30; no 23 UTC sounding is available for Sept. 1. So as to avoid model timing errors being muddled with systematic PBL errors, we shall present soundings from 20 UTC Aug. 31 and 23 UTC Aug. 30.

At 20 UTC (Fig. 5a), the observed sounding includes a shallow, strong superadiabatic layer which may partly be due to inadequate ventilation of the sonde prior to launch. Above this, the atmosphere is well mixed in mixing ratio and slightly stable in potential temperature up to about 870 mb. There is no inversion overlaying the PBL; the air above the PBL is likely to have originated as PBL air farther inland where temperatures were warmer.

Most model runs had PBL's which were too warm and deep. One of the worst offenders was dec30grid4 (Fig. 5b). It was too warm by about 2 C, and the PBL was about 1 km too deep. Mixing ratios were reasonably correct, though. The only run with the proper PBL depth was the MCNC run (Fig. 5c), although the temperatures were slightly too cold (producing a stronger than observed inversion at the top of the PBL) and mixing ratios were slightly too moist.

The sea breeze at Houston Southeast during Regime 2 was shallower than during Regime 1 and the potential temperature difference between the sea breeze air and the air above the sea breeze was larger. Both of these differences are to be expected from the

more offshore larger-scale wind component during Regime 2. In Fig. 6a, the sea breeze is seen to be only about 30 mb (250 m) deep, with a deeper stable layer above it.

Model behavior is similar to the deeper sea breeze day (Fig. 4) in most model runs, although none of the models are able to simulate sufficiently cool air within the sea breeze. The dec30grid4 model run (Fig. 6b) shows that the MRF PBL scheme's sea breeze is similar to that in Regime 1 (Fig. 4b), with smooth stable layer rather than an inversion overlying the marine air. The scheme at least is able to capture the variation in the depth of the PBL between Regime 1 and Regime 2. The dec16grid4 run (Fig. 6c) has the proper height but too abrupt an inversion. Although this run comes close, it and the other runs modify (heat) the marine air too rapidly as it comes onshore.

The Hong-Pan PBL scheme does not fare well with this shallow sea breeze. The feb9grid4 run, otherwise identical to the dec30grid4 run, has a well-mixed layer through the first 90 mb (Fig. 6d), with apparently too much onshore mass flux due to the deeper onshore layer. An increase of vertical resolution might have been expected to better resolve any stable layer atop the marine air; instead, the feb16grid4 run (Fig. 6e) cannot simulate a stable layer at all and is well mixed through the sea breeze and the return current. It appears that the daytime MRF PBL mixing (identical in the Hong-Pan and MRF implementations) is more robust when the low-level resolution is increased. In agreement with this characteristic, the oct25grid4 simulation (not shown) tends to have slightly shallower daytime PBL's, with its coarser vertical spacing at the ground.

At night, surface-based inversions would form regularly. During Regime 1, the five nighttime soundings indicated an average inversion strength of 4 C over a depth of about 20 mb. Three of the model runs, dec16grid4 (Gayno-Seaman), MCNC (Blackadar), and oct25grid4 (low vertical resolution), did not generate a surface-based inversion at most or all of the sounding times. The other five runs produced inversions that averaged between 0.4 C and 1.2 C. The strongest inversions were in the feb16grid4 run, which had the highest vertical resolution.

During Regime 2, analysis of the nighttime inversion is complicated by a sometimes separate inversion near the base of the low-level jet. But all model runs produces surface inversions that averaged too shallow and too weak.

2d) Houston Downtown Composites

The Houston Downtown sounding site was about a mile north of the center of downtown Houston. While it is within an area whose land use is classified as urban, it lies between a core urban area dominated by skyscrapers and mixed use commercial-residential neighborhoods.

During Regime 1, all models underestimated the PBL depth (Fig. 7) and PBL potential temperature (Fig. 8) at 14 UTC, while by 23 UTC all models were overestimating PBL depth and potential temperature. The cause of the time lag between the modeled and actual PBL diurnal cycle is unknown. Contributing to the problem is a 30-minute radiation time step that was used for all but the MCNC runs. However, this coarse time step would be expected to only cause a 15-minute delay in PBL evolution, and even the MCNC run shares the biases of the other models.

Besides the timing error, there is a general tendency for the model forecasts to be too warm (and consequently too deep) with their PBL during Regime 1. This warm bias

changes from day to day, with the largest warm bias occurring on Aug. 25 and most models having no bias on Aug. 29. As at Houston Southeast, this is likely to be due to the precipitation and subsequent evaporation near the beginning of the ozone episode. Moisture profiles from the Houston Downtown site were erratic, so this hypothesis lacks direct observational support

The second half of the episode saw much greater variability among the models. Most model PBL's are too shallow at 14 UTC, due to an erroneous nighttime inversion structure. In the observations, a shallow well-mixed layer develops soon after sunrise (Fig. 9a). A typical model sounding (Fig. 9b), from dec30grid4, has the PBL too shallow and PBL temperatures too warm. This combination can be attributed to the overlying inversion being too low, so that the surface air warms up quickly. This error may be dynamically related to the tendency, discussed in Report 2, for the model to produce a nighttime low-level jet which is too close to the ground. The only model that tended to have a PBL of the proper depth at 14 UTC was the MCNC run (Fig. 9c). The structure of the model sounding is very good, but the PBL itself is several degrees too warm.

By late afternoon, the PBL would be very deep, as shown, for example, in Fig. 10a. A shallow stable layer is present at the very bottom of the sounding, indicating that the daytime PBL has begun to decouple from the ground as the sun descends toward the horizon. Also note that the residual PBL is not quite neutrally stratified. These subtleties are missed by the model, which has difficulty getting the depth of the PBL correct.

Most model runs come reasonably close. For example, dec30grid4 (Fig. 10b) has a PBL that is slightly too warm and too deep, but both temperatures and moisture are similar to observations. The dec16grid4 run (Fig. 10c), on the other hand, has difficulty producing sufficient mixing; neutrally stratified conditions are only found below 840 mb. The MCNC run (Fig. 10d) is similar. Both are also too moist, although the dec16grid4 run used the same soil moisture as dec30grid4.

At night during Regime 1, surface-based inversions were much less strong at Houston Downtown than at Houston Southeast. This may be due to the greater terrain slope at Houston Downtown and the dense forest surrounding Houston Southeast. Most model runs typically produced inversions of the proper depth and magnitude. The MCNC run did not produce a nighttime inversion at the Downtown site, as it failed to do at Houston Southeast also. The oct25grid4 run only produced an inversion or stable layer at three of the five sounding times.

During regime 2, the temperature structure was strongly affected by the nighttime low-level jet. In a typical observed sounding (Fig. 11a), a very shallow surface inversion was capped by a 20 mb thick well-mixed layer, the mixing presumably due to mechanical mixing caused by the strong wind shear beneath the jet. Above this neutral layer was a strong inversion, a deeper stable layer, and above 920 mb, very weak stratification.

Models failed to duplicate this structure, especially the neutral layer near the ground. The dec16grid4 run, which was most effective at producing a deep low-level jet, lacked both the surface inversion and the neutral layer above it (Fig. 11b). The dec30grid4 run shows a similar problem, but also exhibits poorer jet structure. Based on doppler lidar data at the nearby LaPorte site, the maximum wind speeds should be near 975 mb. Not only is the dec30grid4 run too shallow, but there is an apparent discontinuity in the winds between levels 3 and 4 above the ground. While this

discontinuity marks the transition from the stable PBL regime to the free atmosphere regime in the MRF PBL, the exact cause of the discontinuity is not known.

The feb9grid4 run was designed to improve the simulation of the low-level jet. Unfortunately, while the jet speed increased over dec30grid4, other aspects of the simulation became less realistic. The corresponding feb9grid4 sounding (Fig. 11d) has westerly winds over a deeper layer, but there still exists a wind discontinuity at the top of the low-level inversion. Above this inversion is a well-mixed layer where winds are constant. This layer coincides with the levels in the observed sounding which are most stably stratified. So while the low-level jet is deeper, its structure remains unrealistic.

2e) Wharton Power Plant Composites

Many of the model simulations discussed here were compared to soundings from the Wharton Power Plant (WPP) site (near Beltway 8 northwest of Houston) in Report 2. Here we present more complete summary statistics. Unfortunately, most of the nighttime soundings failed to capture data in the lowest part of the atmosphere, so the nighttime surface-based inversion remained largely unobserved, except for the day discussed in Report 2.

The daytime PBL observations and model performance are shown in Figs. 12 and 13. Since WPP is far from the coastline, its daytime PBL was not directly affected by the sea breeze during either Regime 1 or Regime 2, so all days are composited together. There was, as at other sites, a tendency for model simulations to have too deep a PBL during the early part of the episode and too shallow a PBL during the latter part of the episode.

Overall, PBL performance is best for the dec30grid4 and dec6grid4 model runs, with dec6grid4 being better during the earlier part of the episode and dec30grid4 being better during the latter half of the episode. The Gayno-Seaman run, dec16grid4, exhibited similar difficulties in simulating a deep PBL as at Houston Downtown during Regime 2. The Hong-Pan runs, feb9grid4 and feb16grid4, deepened the PBL too quickly, and the feb16grid4 run failed to deepen it further. The feb18grid4 run, here as elsewhere, is too warm, probably because of the very dry soil moisture that was used on the 12 km grid in order to couple two-way to the very dry 4 km grid. The oct25grid4 is similar to the dec6grid4 run but the PBL is not sufficiently deep. Finally, the PBL in the MCNC model run is much too shallow during the afternoon.

Temperature errors tend to track PBL depth errors. Most model runs are not warm enough; dec30grid4 and feb18grid4 are the exceptions. The MCNC model run averages as much as 3 C too cool compared to the observations and most of the other models.

2f) Summary of PBL Comparisons

The comparison of simulated and observed PBL's focused on four phenomena: the nighttime inversion, the daytime PBL, the sea breeze, and the nighttime low-level jet. For the nighttime inversion and the daytime PBL, differences between the models tended to be similar from station to station, while the most accurate simulation varied. The MM5 does not have a uniform land surface; several categories, including urban, agricultural, forest, and marsh are represented here. Apparently the variations in land use

that the MM5 is missing are the cause of a significant fraction of the model error. This implies that the "best" model configuration cannot be determined from a comparison with observed PBL's at only three stations, particularly when one was close to the coastline. A better approach would be examination of maximum and minimum surface temperatures, for which more observing sites are available. This test was carried out in Report 2, and it was found that the dec6grid4 was more accurate (with respect to maximum temperatures) during the early part of the episode, and dec30grid4 was more accurate during the later part of the episode. The additional model runs conducted since Report 2 are inferior according to the above PBL analysis, so no maximum/minimum temperature statistics are computed.

The sea breeze and low-level jet are dynamic features of the atmospheric circulation and depend in a complex way on the PBL parameterization as well as other factors. Observations from the two airsonde sites showed a similar structure to the sea breeze, with day-to-day variations larger than spatial variations. Each model run also predicted similar structures at Houston Downtown and Houston Southeast, implying that the two stations are sufficient for a comparative assessment of the models. The best model run appeared to be dec16grid4, followed by dec6grid4 and dec30grid4. Interestingly, the model runs bracket the observations, with dec16grid4 having a sea breeze stable layer that is too strong and the MRF PBL runs having a sea breeze stable layer that is too weak. The MCNC run fails to produce a stable layer at all.

The low-level jet is not well handled by any of the models. The best of the set seems to be the MCNC model run, with the dec16grid4 run second best.

3. Comparison of Wind Performance

In Report 2, the model runs to date were evaluated through examination of surface wind fields and time-height cross sections at profiler locations. Here, we present summary statistics of wind performance for the eight model runs discussed in this report. A detailed wind evaluation of the non-nudged model runs conducted during February is not provided here because our analysis indicates these model runs are not the best candidates for use in photochemical models. Figures analogous to those presented in Report 2 may be accessed from http://www.met.tamu.edu/results.

As was also discussed in Report 2, there is some ambiguity regarding the profiler data set. The most recent quality control, by the Environmental Technology Laboratory (ETL), seems to have introduced spurious velocities during the daytime PBL to a degree that varies from profiler to profiler. On the other hand, the ETL quality control has clearly improved the profiler winds, particularly at higher altitudes.

We hypothesize that the automated component of the ETL profiler data processing algorithm, called Weber-Wuertz, emphasizes strong, coherent velocity signals during light wind periods, and that these velocity signals are caused by profiler sampling of boundary-layer rolls and other small-scale turbulence. If this is the case, any errors introduced by the ETL processing should be largely bias-free, except to the extent that average wind speeds may be slightly overestimated. Since raw profiler data is known to have a low bias at low wind speeds due to ground clutter, the two errors may compensate for each other. Here we shall use the ETL-processed data for performance assessment, recognizing that actual model performance is better than this data set would indicate.

Figures 14a-d show the RMS error of the various model runs at 200 m, 400 m, 700 m, and 1000 m, respectively. The plots include overall RMS errors as well as RMS errors in the 24-hour running mean and RMS errors of the departures from the running mean. All three types of RMS errors tend to be largest at 400 m, where the sea breeze and low-level jet are both strong. The MCNC run is the exception; its winds are least accurate at 200 m, suggesting that a performance analysis using surface data would underestimate MCNC model accuracy.

Considering the overall RMS errors, the errors in the u component of the wind are almost always larger than the errors in the v component. This is at first surprising, considering that during Regime 1 there is more variability in the v component of the wind. But the v component is directly forced by the land-sea contrast, while the u component appears to be an inertial response to the v (primarily onshore) component. Apparently, the nighttime simulation of u, involving inertial oscillations and complex temperature structures, is most difficult for the models.

The 24-hour running mean RMS errors are only about half as large as the overall RMS errors. Errors are largest for the u component, except for the mcnc run. The RMS errors of the departure from a running mean account for most of the overall RMS error at all levels, indicating that the winds are dominated by phenomena with periods of 24 hours or less. The systematic and unsystematic model errors did not show a clear signal.

Comparing model runs, the December runs have the lowest RMS error at 200 mb and 400 m. At 700 m and 1000 m, most model runs show similar behavior, except that dec16grid4 and feb18grid4 are noticeably worse.

The model biases (Fig. 15) are rather different for the MCNC run and the other runs. The MCNC run has a nearly steady bias of −1m/s in the u component; the v component bias shifts from negative to positive with height. The other runs are fairly similar, and show an increasing bias in the u component with height. According to thermal wind laws, this model bias may be associated with erroneously cool temperatures in the models between 1000 m and 3000 m. These biases should largely vanish with observation nudging to the profiler data.

The daytime winds are of particular interest, since most ozone in Houston appears to be produced on the same day that its precursors are emitted. In Fig. 16, the model winds are compared to two sets of profiler data: the ETL (ww) data and the Aeronomy Laboratory (AL) (Con) data. At this level (400 m), the AL profiler data is smoother than the ETL data. Whether that smoothness more closely reflects the real atmosphere is not known for certain; what is certain is that the noisiness in the ETL data is not predictable, and therefore the RMS errors for the ETL data are higher than the RMS errors for the AL data. During the day, the best models, essentially indistinguishable from each other in this statistic, are the oct25grid4, dec6grid4, dec30grid4, and feb9grid4 runs.

Some differences are found in the model scores between Regime 1 and Regime 2. During Regime 1 (Fig. 17a), the u component of the diurnal wind becomes progressively worse with height in all but the MCNC runs. Apparently the model is not properly simulating the vertical propagation of the inertia-gravity waves associated with the diurnal wind cycle. The v component does not exhibit a systematic variation with height. Overall, a few model runs stand out as being worse than the others: dec16grid4, feb18grid4, and MCNC.

During Regime 2 (Fig. 17b), the largest errors are typically found at 400 m, the approximate level of the low-level jet. The MCNC model, which was the worst performer during Regime 1, is the best performer during Regime 2. The feb9grid4 run, which was intended to minimize the errors at 400 m and 700 m during Regime 2, did just that, but errors at other levels tend to be slightly larger compared to dec30grid4. The feb18grid4 and dec16grid4 runs have the highest RMS errors.

Finally, Fig. 18 summarizes the performance of the models in simulating the diurnal wind cycle (departure from the 24-hour running mean) during Regimes 1 and 2. The feb18grid4 run stands out as a poor performer; dec16grid4 is not so bad but is clearly worse than the remaining model runs. Again, MCNC is worst during Regime 1 and best during Regime 2.

4. Selection of Optimal Model Configuration

The performance evaluations in this report and previous reports have failed to produce a clear top performer with respect to meteorological conditions. Some of the model runs can be easily dismissed as inferior, however, at least in the exact configuration evaluated here. The oct25grid4 run is not a candidate for photochemical modeling because its vertical resolution is too coarse near the ground; its statistics have been included here to show the impact of the removal of a single level. The feb18grid4 run produced a worse thermodynamic simulation than most other runs as well as worse wind fields. The feb16grid4 run failed to improve in most areas on the feb9grid4 run.

The dec16grid4 run produced attractive simulations of the sea breeze front, performed well with regard to maximum temperatures, and may be useful in combination with one of the other runs in bracketing the range of possible sea breeze behavior. But the daytime PBL structure was too shallow at the inland sites and the wind fields (see Report 1) begin to simulate boundary layer eddies. There are undoubtedly eddies present in the atmospheric PBL, but they are unlikely to have the same shape, scale, and structure as the ones that the dec16grid4 simulation produces. Furthermore, the effect of these eddies is already being parameterized by the PBL scheme. In a photochemical model, the result would be erratic horizontal advection of constituents. The problem is exacerbated when, according to TNRCC protocol, the meteorological model output is sampled at a time frequency (1 hour) much larger than the time scale of the PBL eddies. Finally, since data assimilation increments are computed at the observation locations, a simulated eddy passing over a station location would affect the nudging increment over a broad area, degrading the data assimilation. Many of these problems may be solvable, through a combination of higher resolution and sophisticated nudging techniques, but with current technology the dec16grid4 run is not a viable option.

The MCNC run performs better than the other runs in some ways, significantly worse in others. On balance, the temperature performance is poor, and the wind performance is poor during Regime 1 and superior during Regime 2. The MCNC run also appeared to have the worst structure for the sea breeze itself. The MCNC should perform well in many circumstances, particularly ahead of the sea breeze front during Regime 2, but some of the other model runs seem to be better performers overall.

The dec30grid4 and feb9grid4 runs are statistically indistinguishable. Similarly, one would expect that a Hong-Pan run with dec6grid4 soil moisture would be indistinguishable from the dec6grid4 run. For present purposes, the dec30grid4 run is preferred over the feb9grid4 run for the following reasons: (1) the MRF implementation of Hong and Pan is more widely used than the original Hong and Pan; (2) the original Hong and Pan PBL scheme produces unrealistic wind discontinuities at the top of the nighttime PBL under many circumstances; and (3) given essentially equivalently performing schemes, the standard version of the scheme is preferable.

The final two model runs under consideration are dec6grid4 and dec30grid4. Following a recommendation in Report 2, we essentially adopt both of them. Specifically, we propose to run the innermost grid with successive land use files whose soil moisture decreases during the period of the episode. The maximum temperatures of dec30grid4 began outperforming the maximum temperatures of dec6grid4 on Aug. 28, so the switch should occur at the beginning of Aug. 28. Meanwhile, both runs were too

warm and had boundary layers that were too deep on August 25. Given the considerable evidence for moist conditions on that day, and likely moist conditions on previous days while rainfall was occurring, we propose to use the standard soil moisture during the first four days of the model run (Aug. 22-25), and switch to the dec6grid4 soil moisture on Aug. 26.

Examination of the dec6grid4 wind fields in Report 2 suggested that the daytime heat island was too strong. In the dec30grid4 land use file, the urban soil moisture was set to be 0.1 larger than the surrounding agricultural areas, while in dec6grid4 the urban soil moisture was 0.1 smaller than the surroundings. We propose to cure the daytime heat island by adjusting the urban soil moisture upward from its original dec6grid4 values. Finally, for consistency, we shall increase the urban soil moisture in the normal configuration during the first four days of grid 4.

The drought was confined to Texas, Oklahoma, and parts of the Southeast, so reduced soil moisture should not necessarily be widespread on the outermost grids. We propose to use the default soil moisture on grids 1 and 2, and dry soil moisture (consistent with dec6grid4) on grid 3.

The following table shows the recommended soil moisture characteristics for the best model run of the August 2000 ozone episode.

Table 1: Soil moisture changes for August 2000 ozone episode modeling

Name	Category	108 km and 36 km grids	12 km grid	4 km, 00 UTC Aug. 22 to 00 UTC Aug. 26	4 km, 00 UTC Aug. 26 to 00 UTC Aug. 28	4 km, 00 UTC Aug. 28 to 12 UTC Sept. 2
Urban and built-up land	1	.10	.10	.30	.20	.20
Dryland cropland and pasture	2	.30	.20	.30	.20	.10
Cropland/grassland mosaic	5	.25	.15	.25	.15	.10
Grassland	7	.15	.10	.15	.10	.10
Deciduous broadleaf forest	11	.30	.30	.30	.25	.15
Evergreen needleleaf forest	14	.30	.20	.30	.20	.10

Because different grids have different soil moisture, the nesting between the 36 km and 12 km grids and between the 12 km and 4 km grids will be one-way. Version 3.4 of MM5 is also unable to easily handle changes in soil moisture; it discards the updated information. To fix this problem, a new subroutine has been written (domain/initial/initld.F) to reinitialize the land surface characteristics on restart.

Another change made to the previously documented (Regime 1) configuration of MM5 is to reduce the radiation time step to 5 minutes from 30 minutes. Finally, the model run is started at 0000 UTC August 22, three days before the ozone episode itself, by the request of TNRCC.

5. Selection of Data Assimilation Configuration

Based on previously-reported tests, the 108 km, 36 km, and 12 km grids are being nudged to Eta Data Assimilation System (EDAS) analyses. This type of data assimilation is called analysis nudging. This section discusses the use of observations from TexAQS-2000 to directly alter the simulation on the 4 km grid. This type of data assimilation is called observation nudging.

5a) Nudging to Observations

Observation nudging proceeds as follows. At each model time step, or at a slower frequency specified by the user, observations taken close to the model time are located. At each observation site, the difference between the observation and the current model value (call it an increment) is computed. In a second loop through all grid points, for each nearby observation, a weight is computed that is largest for those observations closest in space and time. The weights are squared, multiplied by the increment, summed, and divided by the sum of the weights. The result is multiplied by a final factor that controls how rapidly the model should come into agreement with the observations. The final product is added to the modeled fields at each time step, so that gradually the model-simulated fields get closer and closer to the observed fields.

In an ideal world, there will be enough observations to resolve all significant features in space and time. In practice, there are typically far fewer observations than necessary.

Surface observations are particularly difficult to assimilate, for there is no good way for the model to determine the vertical extent of the portion of the atmosphere that wind represents. For example, a southeast wind might imply southeasterlies throughout the lowest 2 km of the atmosphere, or it might imply a sea breeze circulation with northwesterlies at a height of 1-2 km.

The profiler network in place during TexAQS-2000 is an excellent resource for data assimilation, unprecedented in the history of Texas. Five profilers were fully operational during the August ozone episode. (A doppler lidar was also operating, but as of this writing, the lidar data is not yet reliable enough to be used for modeling.) These profilers are too widely spaced to resolve the primary local-scale circulation: the Galveston Bay breeze.

As explained in Report 1, our approach for utilizing the profiler data is to improve the model by comparison to available data so as to allow the model to generate sea breezes and diurnal wind cycles that are so realistic that the observation nudging would have little effect on the sea breeze. The dec6grid4 and dec30grid4 model runs do fairly well with the onset of the sea breeze, but the performance statistics go down when the alongshore component becomes significant later in the night. Particularly during Regime 2, the low-level nighttime winds are unrealistic. This error impacts nighttime transport as well as daytime transport the following morning as those winds mix down to the surface. Thus, the nudging will have to correct for the larger-scale biases as well as systematic errors in the diurnal wind cycle.

Four parameters control the observational nudging characteristics in the MM5. These are the time interval, the vertical radius of influence, the horizontal radius of influence, and the nudging strength.

The spatial separation of the profilers (about 30-50 km) imposes an effective time scale on features the profiler network can resolve. The sea breeze front, for example, would be difficult to resolve with the network because its location and orientation cannot be specified with only five stations. Because the MM5 has shown itself to be able to simulate Gulf and Bay breezes, we need not nudge toward something with such a small spatial scale. The diurnal wind cycle, on the other hand, is a very large-scale dynamical response that is seen in all five profilers. This wind, which to a large extent controls the buildup and transport of ozone, must be simulated well.

The nudging time interval is the period of time in which a given observation is used in full force in nudging. The nudging for each observation ramps up and down, so the total period of influence is twice the nudging time interval. Since the most rapidly varying feature of interest progresses through one complete cycle in 24 hours, the nudging time window must be less than 12 hours or so or else the diurnal cycle would be smoothed almost out of existence by the nudging. On the other hand, we do not want to nudge large areas of the model domain to local, small-scale, transient features, so either the data must be temporally smoothed or the nudging time scale must be large enough to effectively accomplish that smoothing itself. We adopt a nudging time interval of 240 minutes, which is about as large as it can be without causing significant degradation of the signal.

The profiler data is available between about 150 m and 2000-3500 m. The vertical resolution is sufficient that there is an observation for every model level within the vertical interval in which data exist. The vertical radius of influence can be used to force the impact of the nudging to extend above and below the span of the profiler data. One disadvantage of doing this is that there is no data to support the nudging directly, and any significant vertical radius of influence would smooth any realistic vertical structure in the observations. Since the Regime 2 low-level jet has considerable vertical structure, we adopt the default vertical radius of influence of 0.001.

The horizontal radius of influence controls the distance from the observation over which the model simulation is nudged. Within uniform networks, an appropriate length scale would be about twice the station spacing. For the particular application to the Aug. 2000 ozone episode, the profiler network is not uniform. We must therefore ask a different question: over what length scale do we expect model errors to be correlated? The phenomena we wish to correct through nudging include the large-scale winds as well as the diurnal wind cycle, which theoretically has a fairly large scale of its own. We therefore adopt a radius of influence of 150 km, so that the profiler data can influence the model solution over most of the coastal plain.

Finally, the nudging factor controls how tightly the model is forced to agree with the observations. Too large a value, and the model dynamics become unrealistic. Too small, and the agreement between models and observations is not as good. We have performed two tests, one with the nudging coefficient equal to .0001 and one with the nudging coefficient equal to .0004. The latter is the default value, but if a weaker coefficient works, the better the dynamics of the simulation. Unfortunately, a test with

.0001 failed to produce satisfactory winds during the early stages of the simulation. The results reported here therefore use a nudging factor of 0.0004.

In order for the MM5 to ingest the nudging data, it must be reformatted. We have written a program to do this, and have tested the program by nudging the MM5 with very small radii of influence to confirm that the model has the data in the right place.

We do not nudge the entire run to observations, but instead begin at 2330 UTC August 24, 2000. We wait until the convection of the previous two days is largely gone, because thunderstorms unresolved by the profiler network would produce unrepresentative nudging increments.

5b) Nudging to Bogus Observations

A bogus observation is an observation that does not exist but that is presented to the model as an observation so that its assimilation will produce a phenomenon known to be present or to be occurring. Bogus soundings have been commonly used to initialize numerical forecasts of hurricanes, since the structure of hurricanes is well-known but any individual hurricane is poorly resolved by observations.

In almost all model runs, including a control run with nudging (Fig. 20), convection develops during Aug. 31 in the northeast part of the domain. Analysis of this convection shows that it originates with air moving upward from the PBL, but that the triggering mechanism was a couple of convective cells which enter the 4 km domain from the 12 km domain. The convection develops strong downdrafts and organizes gust fronts which sweep through Houston early on the evening of Aug. 31, presumably clearing out any remaining pollution. Since such a gust front did not pass through Houston on Aug. 31, the convection must be suppressed somehow.

Possible techniques for suppressing the convection would be to suppress it on the 12 km domain so that (hopefully) it isn't triggered on the 4 km domain, or suppressing it on the 4 km domain so that the triggering doesn't actually trigger anything. Suppression can occur through warming of air aloft or cooling and drying of air near the surface. The least intrusive technique would be to dry the air near the ground, since that would have minimal impact on the pressure gradients or wind fields. This nudging would have to take place at night when the PBL is shallow, because the MM5 does not allow nudging of temperature or moisture within the boundary layer.

To determine the proper domain to nudge onto, the wind fields were examined to see if the convecting air originated within the 4 km grid or whether it was advected onto the 4 km grid from the 12 km grid. Winds were predominantly into the domain, so the first convective cell, which developed near 18 UTC, consisted of air that had mostly been outside the 4 km domain six hours earlier. Nudging must therefore take place at least on the 12 km grid. Vertical profiles of mixing ratio showed that fairly high mixing ratios (in the neighborhood of 10 g/kg) extended at least to the 700 mb level in the area where the northeastern boundary of the 4 km grid was located.

Bogus mixing ratio "observations" of 3 g/kg were created along a strip within the 12 km grid that contains the northeastern boundary of the 4 km grid. The fortran code that generated the bogus observations is as follows:

```
open(unit=1,name='mixr3.nudg',form='unformatted')
```

```
do ih=2,16,2
  day=24400.+float(ih)

  do in=50,85,5
    x=float(in)
    do jn=60,70,5
      y=float(jn)
      do kn=24,43
        z=float(kn)
        write(1) day,y,x,z,99999.,99999.,99999.,.003,99999.
      end do
    end do
  end do

  do in=70,85,5
    x=float(in)
    do jn=50,55,5
      y=float(jn)
      do kn=24,43
        z=float(kn)
        write(1) day,y,x,z,99999.,99999.,99999.,.003,99999.
      end do
    end do
  end do

end do

close(1)
end
```

The bogus observations span the time period from 02 UTC Aug. 31 to 16 UTC Aug. 31, at two-hour intervals. A nudging half-window of two hours ensures continuous nudging toward dry mixing ratio values. Beyond 16 UTC, additional nudging on the 12 km grid would have little impact because the observations would be within the boundary layer and the air that is to participate in the undesirable convection is well within the 4 km grid by that time.

6. Overall Wind Performance

Because of the newness of the model runs discussed here, an exhaustive performance evaluation has not yet been done. Below, the simulated winds are compared to profiler data. This comparison will overestimate the degree of improvement caused by nudging, since no profilers were withheld from the nudging. However, since the horizontal radius of influence for nudging was so large, the modeled winds at each profiler site include nudging increments from all the other profilers as well as the coincident one, so perfect agreement would not be expected even if the nudging coefficients were excessively large.

6a) Time Series

Time series comparisons of modeled and observed winds can be plotted either as wind speed and direction or u and v wind components. Wind speed and direction are more familiar, but wind component plots are more straightforward to interpret and translate directly into spatial translation errors in the east-west and north-south directions. Here we show a couple of examples of wind speed and direction plots before focusing on the wind components.

The wind speed and direction from the 400 m level at Houston Southwest (HOU) is shown in Fig. 20. Two lines are provided for the observed winds, corresponding to the ETL and AL quality controlled profiler data sets. Five model runs are also plotted: dec6grid4, dec30grid4, MCNC, and two model runs with observation nudging. The first uses standard soil moisture (nudgwet) and the second uses the recommended model configuration, including decreasing the soil moisture as described in section 4 (driver).

Most of the curves lie on top of each other, meaning that most of the model simulations are consistent with the observations. The MCNC run wind speed deviates considerably from observed speeds at night. The wind speed from the driver run, in brown, closely tracks the observed wind speed during the first part of the episode (Regime 1). In Regime 2, starting on Aug. 30, low-level jets form whose strength is underestimated by all the model simulations. The driver run is closer than the other runs to the observed wind speeds, but it still falls short by about 3 m/s.

The wind direction plot graphically illustrates the flow reversals that occurred during the first and last few days of the ozone episode. The MCNC and driver runs are the only two runs that simulated a full flow reversal on Aug. 25. The MCNC flow reversal was several hours too early, and the driver flow reversal was a couple of hours too late. Through most of the rest of the period, the MCNC run shows frequent wind direction errors, while the other models track well. On Aug. 31, large wind direction errors are found in dec6grid4 and dec30grid4 at a time when wind speeds are also large, implying very large transport errors which observational nudging appears to cure.

During the latter half of the episode in particular, the winds at Houston Southwest should show the least improvement from observational nudging, since Houston Southwest is located upstream of most of the other profiler sites. As air passes through the Houston area, it experiences continual nudging so that by the time it exits the eastern edge of metropolitan Houston the winds should be in good agreement with observations. In Fig. 21, showing the winds at Liberty Municipal Airport, the behavior of the driver run

seems a bit better, but not remarkably so. The amplitude of the low-level jet is still underestimated, by about 2 m/s, but the timing of the strongest winds more closely follows the observed winds.

The separate wind components are shown at 250 m for Lamarque, Liberty, and Wharton in Figs. 22-24. At Lamarque, the dec6grid4, dec30grid4, and MCNC graphs frequently depart by two or more m/s from the observed wind components, while the nudged winds track the observations well. At the other two profiler sites, the dec6grid4 and dec30grid4 runs tend to have an excessively strong v component (onshore flow) during the evening, while the MCNC run is too weak with the onshore flow during the day. Again, the nudged model runs track the observations well. During Regime 2 at both inland sites, the agreement with the observations is less good, but the nudged simulations represent a clear improvement over the other simulations.

The 1000 m level at Lamarque (Fig. 25) is above the sea breeze front, and instead of a strong positive v component around 00 UTC the v component tends to be weak or negative. The nudged runs and the MCNC runs both track the diurnal variations at this level fairly well.

Farther up, the dec6grid4 and dec30grid4 runs exhibited a negative bias in the u component of wind. Fig. 26, from Wharton, shows that the observation nudging has almost completely eliminated the bias. Because of the noisiness of the observed winds it is difficult to assess the more rapid wind variations, but the agreement between the driver run and the v component in particular appears quite good.

6b) Statistical Measures

By standard statistical measures, the wind field above the ground at the profiler sites is tremendously improved. Figure 27 shows the RMS error for the two wind components at various heights, broken down into the total RMS error, the RMS error of the 24-hour running mean, and the RMS error of the departure from the running mean. The overall RMS errors are between 1.3 and 1.8 m/s and improve with height. By contrast, no non-nudged model runs had RMS errors below 2 m/s at any of the four levels. The improvement is largest in the running mean, where typical RMS errors have decreased by more than a factor of two.

Also tremendously improved are the model biases (Fig. 28). Most biases are less than 0.3 m/s below 2500 m. Even at 3000 m, where profiler data is more sparse, the biases are reduced by nearly a factor of two. Based on the improvement in the running mean RMS and overall bias, it appears that the observational nudging has accomplished its primary goal of correcting the large-scale, slowly-varying wind field.

In the diurnal component, or departures from the 24-hour running mean, the improvement is greatest during Regime 2. RMS errors in Regime 2 have decreased by a factor of two with the observational nudging. Regime 1 improvements are smaller, but the statistical model performance in Regime 1 still beats Regime 2.

7. Performance on High Ozone Days

7a) August 25, 2000

The surface meteorological observations from selected times during August 25 are overlaid on the driver model run for the same period. Recall from the previous section that the model winds evolved similarly to the profiler winds, but the evolution in the model lagged the observations by about two hours.

The surface winds tell a different story. At 16 UTC (Fig. 30a), observed winds are light but with a general northeasterly tendency. Model winds are also light, but tend to be from the southwest. This error was common to the unnudged simulations as well.

During the following few hours (Figs. 30b-c), observed winds strengthen from the east over land, and a sea breeze kicks in along the coast. The model fails to reproduce the strengthening easterlies over land; simulated winds are much too light. Finally, by late afternoon (Fig. 30d), the modeled winds begin to resemble the observed winds. Temperatures are well simulated throughout the day.

On this day, high ozone was first observed just southwest of the Houston Ship Channel, and the high ozone tracked westward and then northwestward during the afternoon. The model wind error should result in an ozone plume that is more concentrated and slower moving than was observed. The simulated plume should also track farther to the north than the observed plume. The wind speed error will be partly balanced by the too deep PBL over land (the increased soil moisture didn't cure the biases discussed in the non-nudged runs), which would tend to dilute ozone and its precursors. With the lighter wind speeds, the mix of pollutants in the core of the high ozone may be significantly different than was observed.

7b) August 26, 2000

On this day, an ozone exceedance was observed late in the day at Conroe, but aircraft observations detected high ozone north of Galveston Bay in the early afternoon in an area unobserved by surface monitors. The observations during the morning (Fig. 31a) show light easterly and northeasterly winds near the Ship Channel, which presumably allowed pollutants to build up and be transported eastward beyond the monitors. Modeled winds are also light and from the south, which is consistent with the general airflow but not the specific local winds near the Ship Channel. This deficiency in the modeled wind fields should keep the high ozone closer to the Ship Channel.

The bay and gulf breezes have intensified in both the model and observations by 18 UTC (Fig. 31b). Observed winds in the Ship Channel area are erratic and contradictory, so an assessment of the model performance is difficult there. The observed winds become consistent by 20 UTC (Fig. 31c), indicating the bay breeze has reached the Ship Channel. This feature is correctly forecasted by the model. The model also seems correct in its southeasterlies north of the Ship Channel, which would act to bring the ozone plume toward Conroe. West of Houston, the modeled southerlies are much weaker than the observations both at this time and two hours later (Fig. 31d), but the wind simulation elsewhere at the later time continues to be good.

From this simulation, one would expect the simulated plume to behave in a manner similar to the observed plume. The simulated plume should remain farther west, which may cause simulated ozone to be too high at stations near the Ship Channel.

7c) August 29, 2000

The observed ozone on August 29 behaved in a manner similar to August 26, except two sensors northeast of the Ship Channel, in addition to Conroe, experienced exceedances.

During the morning, the model simulation is excellent (Fig. 32a). The model correctly captures the southwest wind prevalent throughout the domain. Two hours later (Fig. 32b), the observations indicate that the winds become light and variable and the bay and gulf breezes begin in earnest. The model simulates the sea breezes well, and has nearly calm winds in place of light and variable ones.

At 20 UTC (Fig. 32c), observed winds over land are still a bit variable, but tend to be from the south. The model continues to produce very light winds over land. The error between the model and observations during this period is similar to the error on August 25, suggesting a systematic failure of the model or its configuration. Later in the day (Fig. 32d), winds continue to be too light well inland, but the sea breeze along the coastline is well simulated.

As with August 26, the model errors are such that the simulated ozone plume ought to be similar to the observed plume but move slower. The light winds over the city should cause ozone concentrations to increase too much there.

7d) August 30, 2000

This first day of Regime 2 saw high ozone south of the Ship Channel in stagnant winds late in the day, and even higher ozone behind the bay breeze that advanced into the stagnant air mass. To simulate the high ozone behind the bay breeze, the model must properly simulate the late morning and early afternoon advection pattern to carry pollutants over the bay.

Around midday (Fig. 33a), the model correctly simulates the light west-northwest flow over land. Over Galveston Bay, where observations are unavailable, the model has already initiated a weak bay breeze. Two hours later (Fig. 33b), the bay breeze is stronger and is starting to get picked up in the observations; the windflow over land looks good also, as do temperatures. By 22 UTC (Fig. 33c), winds have become light and variable over land and the bay breeze has penetrated farther inland. The model seems a bit slow with the bay breeze but otherwise looks good.

This appears to be a very successful simulation. Based on the available observations, the model correctly simulated the winds both ahead of and behind the bay breeze. Accuracy in simulated ozone will depend partly on how well the model produces the vertical structure of the bay breeze.

7e) August 31, 2000

This day was similar to the previous day, except the highest ozone was observed north of Galveston Bay rather than east of it. At 18 UTC (Fig. 34a), the model has the proper wind direction over Houston, but winds seem to be a bit light. By 20 UTC (Fig. 34b), the observations suggest that the northwest flow has broken down and winds have become light and variable. The model produces light winds over Houston rather than light and variable ones. AT 22 UTC (Fig. 34c), the bay breeze has kicked in along the northern shore, both in the observations and in the simulations. Indeed, the model correctly distinguishes between August 30, when the high ozone from Galveston Bay advected westward, and August 31, when the high ozone from Galveston Bay advected northward.

In Fig. 34c, the observed southwest winds north of the bay are not correctly represented in the model. Instead, the model shows a northeasterly wind surge. This wind surge is a consequence of convective activity in the third nest near the boundary of the 4 km nest. The outflow from the convection advances across the domain and has nearly reached Houston at this time. The bogus mixing ratio nudging has suppressed convective development within the 4 km domain, so this push of air is much weaker than in other simulations and does not appear to seriously degrade the nighttime simulation.

7f) September 1, 2000

This day was unlike any of the preceding days. Winds were directed from downtown Houston along the Ship Channel during the day, and a plume of high ozone was observed downwind as far as the Beaumont area.

Figure 35a shows that the model has the correct basic wind field, including the wind variations near Galveston Island, but has too weak a southerly component to the wind. A similar error persists two hours later (Fig. 35b), but the model seems to be doing a good job with the onset of the sea breeze. This behavior is similar at 20 UTC (Fig. 35c), but by 22 UTC (Fig. 35d), the model largely has the proper wind directions. The model has systematically underestimated the strength of the westerlies south of Houston and appears to have the sea breeze too far inland in this area. The anomalous observed easterly wind at Conroe, north of Houston, is the first indication of the outflow from a line of thunderstorms which advanced through the Houston area from the northeast during the following few hours. Figure 35d shows that the model has produced a convective outflow east of Houston, and the outflow sweeps through the city at about the same time as the observed outflow.

Based on model performance here, the simulated ozone should again be similar to the observed ozone, with a slight southward displacement in the position of the plume.

8. Suggestions for Future Work

The meteorological fields clearly have room for improvement. One fundamental problem that occurs on several days is the delayed onset of the large-scale southeasterlies over land ahead of the sea breeze front. This flaw seems to be the main deficiency in the simulations of August 25 and August 29; the impact of this flaw in the photochemical modeling remains to be seen but is likely to be significant. It is not known at this time whether this model shortcoming is a flaw in the model itself, the model configuration including the PBL scheme, or the nudging strategy. The observational nudging may contribute to this problem in at least two ways. First, the long time window for the nudging, while useful for damping out noise in the observations, also reduces the amplitude of the diurnal wind cycle. Alternate approaches, such as spectral filtering of the profiler data, may produce better performance. Second, wind profilers have a known negative speed bias at low wind speeds, so errors in the observations themselves may be causing the inland winds to be excessively damped. Tests of different nudging schemes should withhold individual profiler stations so as to allow objective evaluation of the performance of the nudging strategies.

Local-scale, probably shallow circulations appear to play an important role in the distribution of ozone, particularly on August 25 and 26. These local winds may be due to land use variations, or they may be caused by soil moisture inhomogeneities produced by variations in precipation on previous days. A scheme for assimilating precipitation or its remotely-sensed effects in the model may significantly improve the simulations on days such as August 26. To the extent that these land surface variations impact the PBL, they should be noticeable in aircraft or remotely-sensed temperature data.

A shortcoming of unknown significance in the observational nudging was the lack of data from the LaPorte doppler lidar due to an instrument calibration error. This data is being reprocessed by ETL. At a minimum the reprocessed data can become another observational nudging site equivalent to a profiler. Ideally, the low-level wind data from the doppler lidar can allow winds to be nudged all the way down to the ground and allow the model to correctly simulate the low-level wind structure near the Houston Ship Channel.

None of the PBL schemes tested so far produced the proper vertical structure of the sea breeze and its inversion. The MRF PBL scheme produced too weak an inversion, and depending on how vertical mixing is handled in the photochemical model, ozone and its precursors may be prone to diffuse too rapidly upward out of the advancing sea breeze air. Testing and possible modification of PBL schemes should continue if the vertical mixing proves to be a problem.

Time has not permitted much testing of different observational nudging configurations. It is extremely unlikely that the one selected here, while physically motivated and justifiable, is the optimal nudging configuration. In the short term, such tests can be conducted fairly quickly over a subset of the ozone episode. In the long term, other data assimilation techniques, such as ensemble Kalman filtering, have shown promise in other environments and should be tested for their ability to improve the assimilation of data along a coastline where forced circulations dominate.

A 1-km grid was run at an early stage of the model testing, and the output graphics from this simulation are available online. In view of the tendency of such high horizontal

resolution to produce explicit boundary-layer rolls and turbulence, observational data assimilation would be expected to perform less well on the 1 km grid than the 4 km grid. Since observational data assimilation was necessary to remove biases and other errors in the unnudged simulations, assimilation must be employed somehow when a 1 km grid is used. We propose that the 1 km grid be kept as small as possible so that the impact of assimilated data on the 4 km grid can be felt on the 1 km grid through the boundary conditions. The 1 km grid location should be chosen based on the output from the photochemical model so that it may be spatially confined to the important emitted plumes of the day, and should be free to vary from day to day within the episode. Alternatively, the 4 km output can be interpolated downscale to drive a higher-resolution photochemical model. From a meteorological standpoint, downscaling is preferable at scales such as this where additional wind patterns resolved at high resolution are likely to be inaccurate.

One area where a 1 km grid should produce a meteorological improvement is in the simulation of the sea breeze front. Previous model testing has shown that the front realistically collapses to a discontinuity when the horizontal grid spacing with the MRF PBL becomes less than about 3 km. Therefore, a 1 km meteorological grid may be appropriate for days such as August 30 and 31 when the interaction of the pollution with the sea breeze front and marine air appeared to be critical to the evolution of the high ozone event.

Due to the hurried nature of this model development, the final driver run has a few remaining loose ends. The 108 km and 36 km grids have been rerun with more appropriate (climatological) soil moisture and have been used to drive the 12 km grid. The 4 km grid should be rerun so as to be driven by the modified 12 km grid, although one would expect the differences on the 4 km grid to be imperceptible.

While model validation work has so far been extensive, a comprehensive statistical validation against surface meteorological data has not yet been performed. This will be done during the next few weeks so that the performance of the MM5 model can be objectively verified.

9. Conclusion

Despite a variety of tests, including direct modification of the MM5's vertical mixing scheme, the MM5 failed to reproduce some important aspects of the diurnal wind cycle, particularly during Regime 2 of the August ozone episode. Sounding data did not sample a wide enough range of conditions to fully validate the PBL structure of the model, but combined analysis of surface and sounding data suggests that a configuration with temporally-varying soil moisture is optimal and performs well. Nighttime temperature inversions were too weak, but this error is not critical to the driving of the land-sea breeze wind cycle.

Observational nudging succeeded in bringing the model into much closer agreement with the observations aloft, without disrupting the local scale sea breeze circulations. An analysis of the model simulations during high ozone days suggests that excellent performance can be expected on about half of the days. On one of the days (August 25), it seems likely that the simulated ozone may be qualitatively different from the actual ozone; on most of the other days, it seems that position errors are most likely.

Strategies for model improvements are far from having been exhausted, and there seem to be no fundamental reasons why acceptable meteorological simulations of the remaining days of the episode would not be within reach.

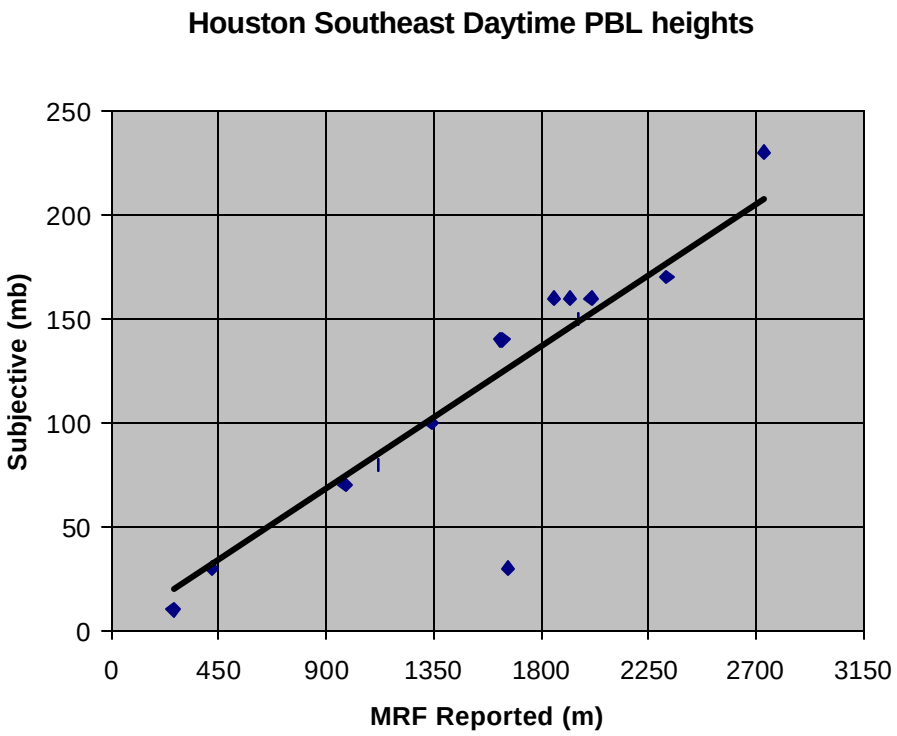

Figure 1: Comparison of estimates of daytime PBL heights simulated by the MM5, dec6grid4 model run. X axis: PBL height (m) computed and used by the MRF PBL parameterization. Y axis: PBL height (mb) estimated by inspection of MM5 model soundings. Approximate conversion from meters to mb is 1:9.

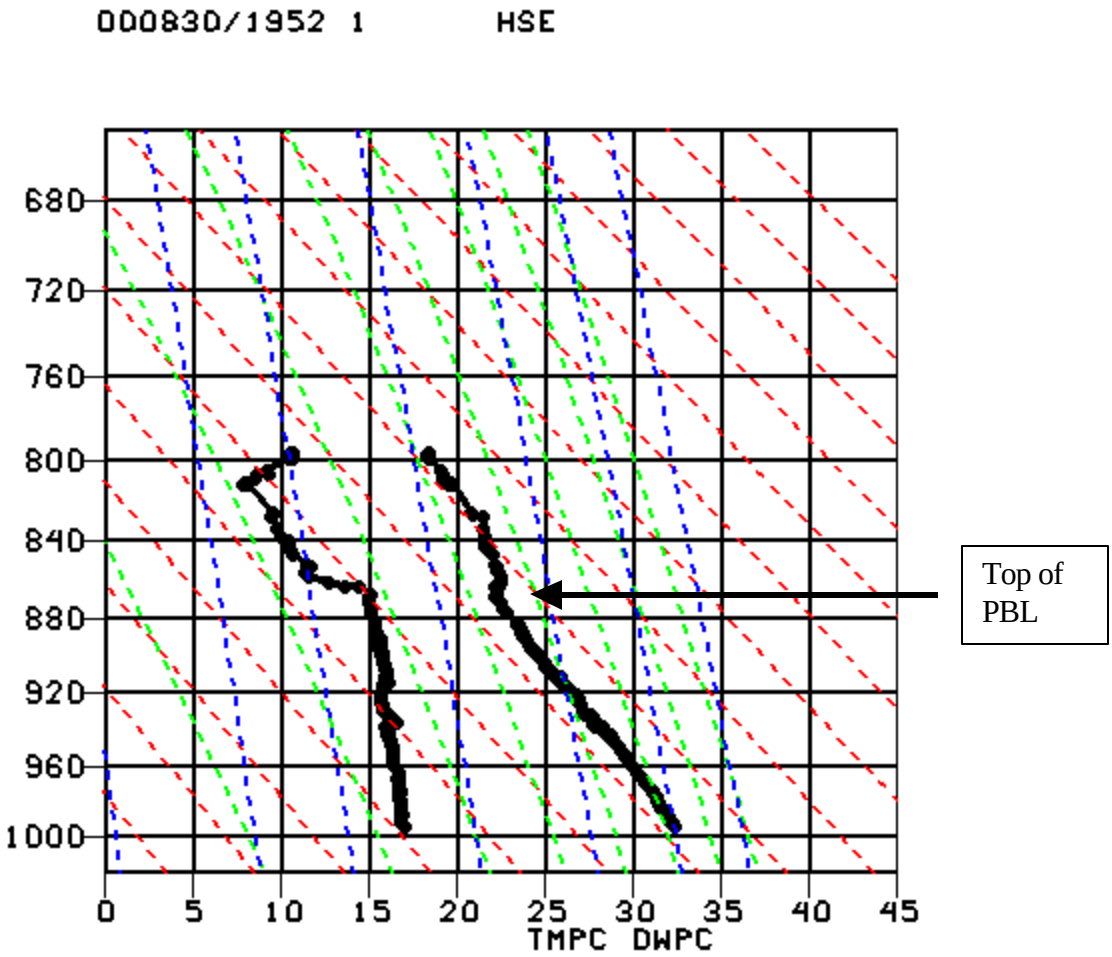

Fig. 2a: Observed sounding, Houston Southeast/Lamarque, 1952 UTC Aug. 30, 2000. Left graph is dewpoint, right graph is temperature. Temperature axis, along bottom, is in Celsius; vertical axis is pressure in mb. Red dashed background lines are dry adiabats, lines of constant potential temperature. Green dashed background lines are moist adiabats, lines of constant equivalent potential temperature. Blue background lines are lines of constant mixing ratio.

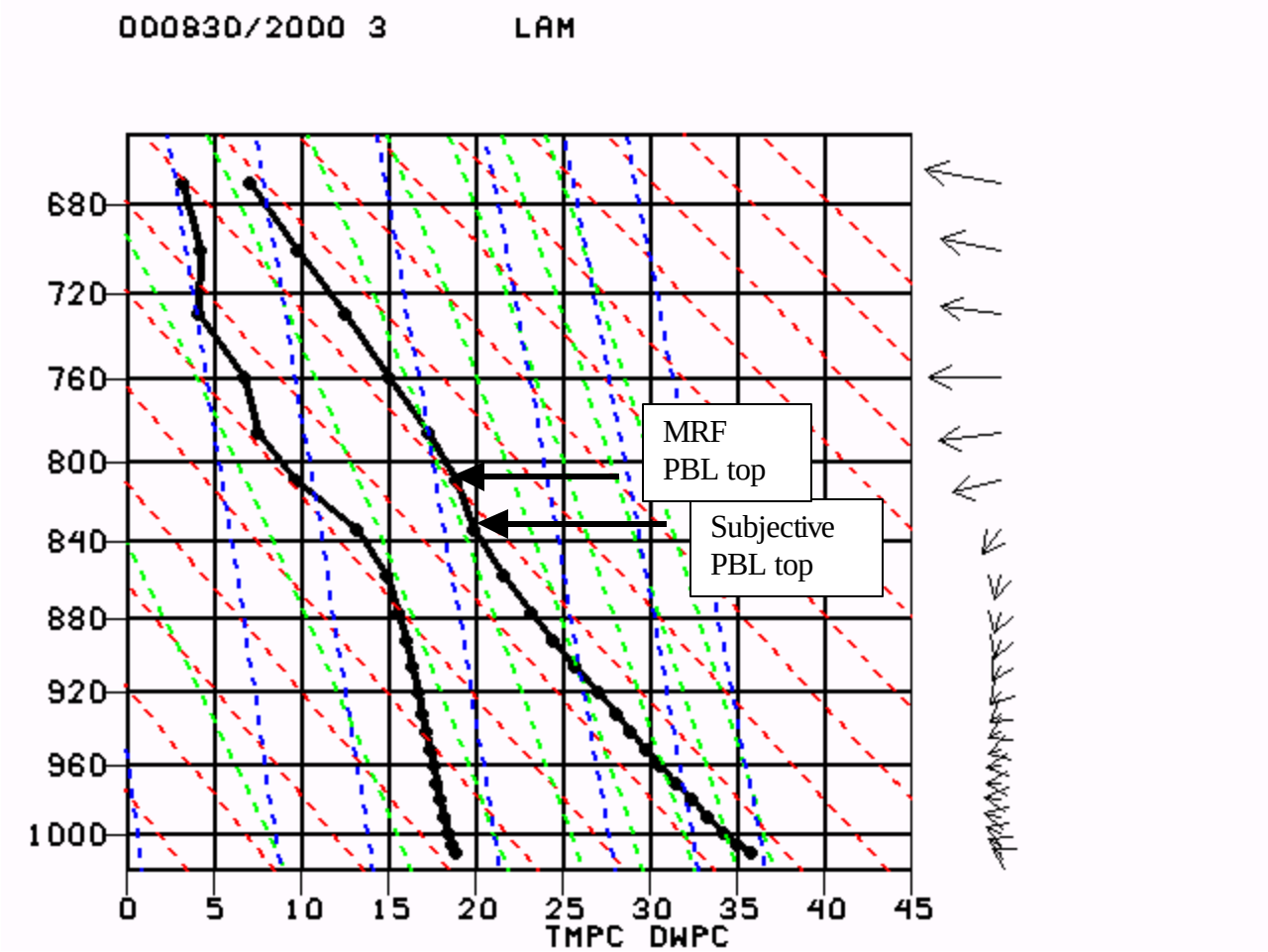

Fig. 2b: Model sounding, dec6grid4 model run, for 2000 UTC Aug. 30, 2000, at Houston Southeast/Lamarque.

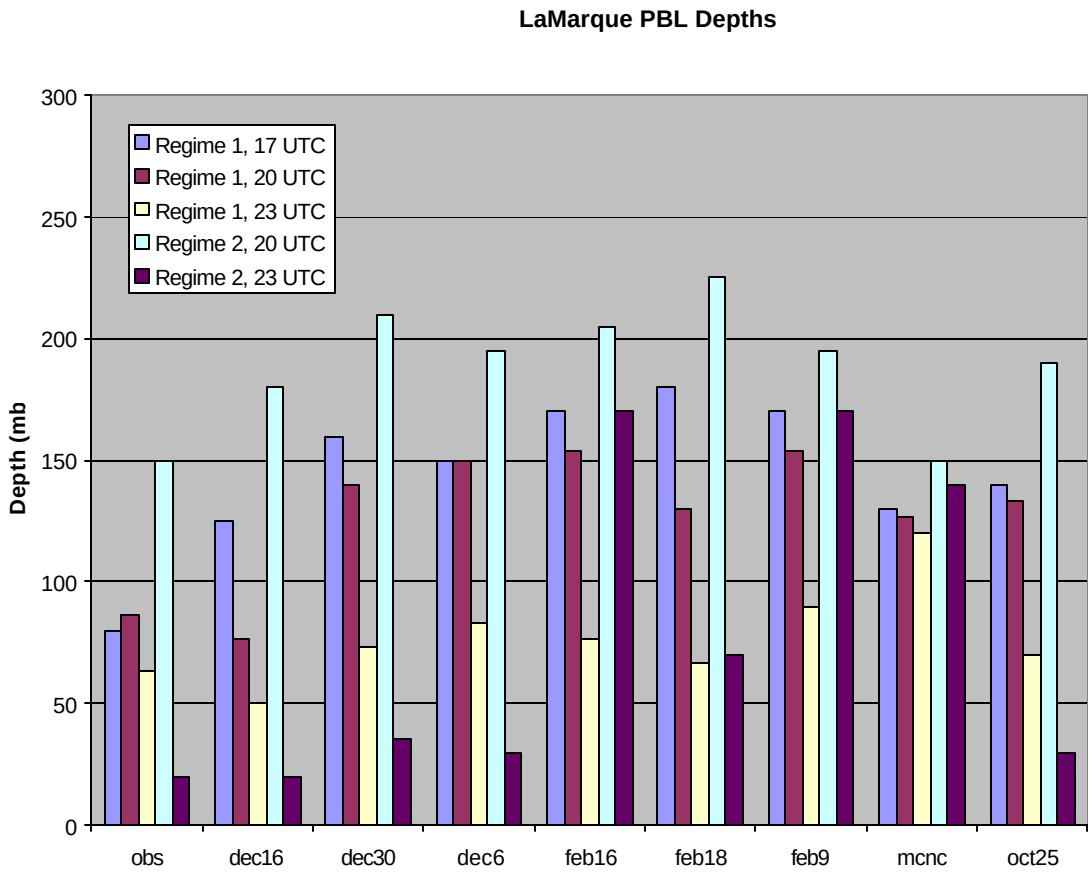

Figure 3: Daytime PBL depths, Houston Southeast/Lamarque site. First set is from Airsonde observations; other sets are from model runs.

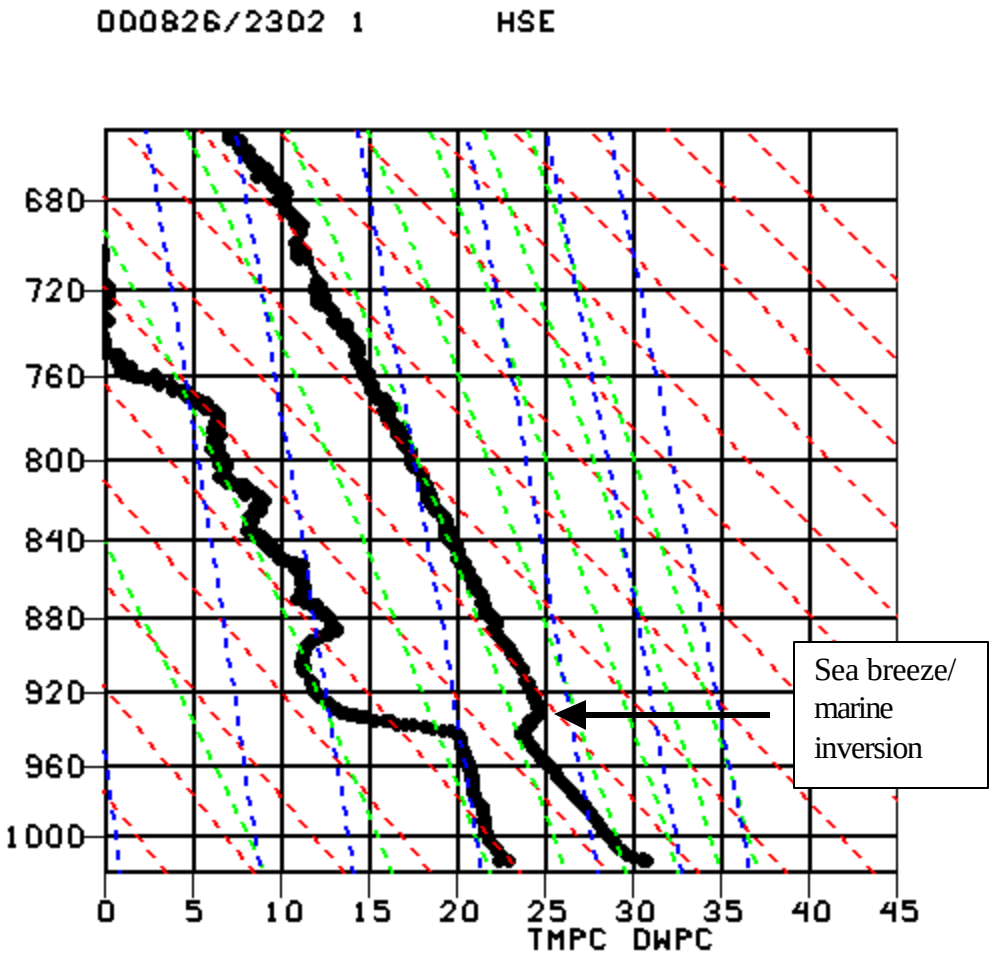

Figure 4a: Observed sounding, 2302 UTC Aug. 26, 2000, Houston Southeast/Lamarque Airsonde site.

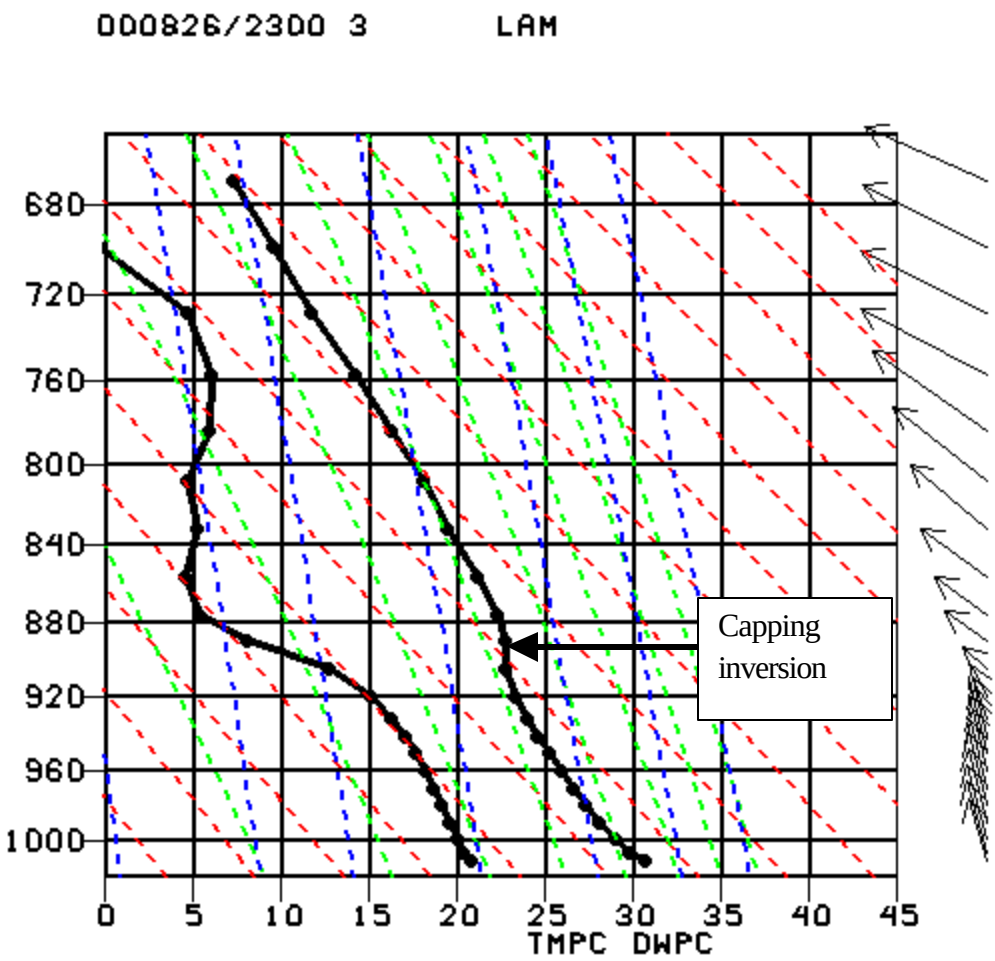

Figure 4b: Model sounding from dec6grid4 model run, Houston Southeast/Lamarque, 2300 UTC Aug. 26 2000.

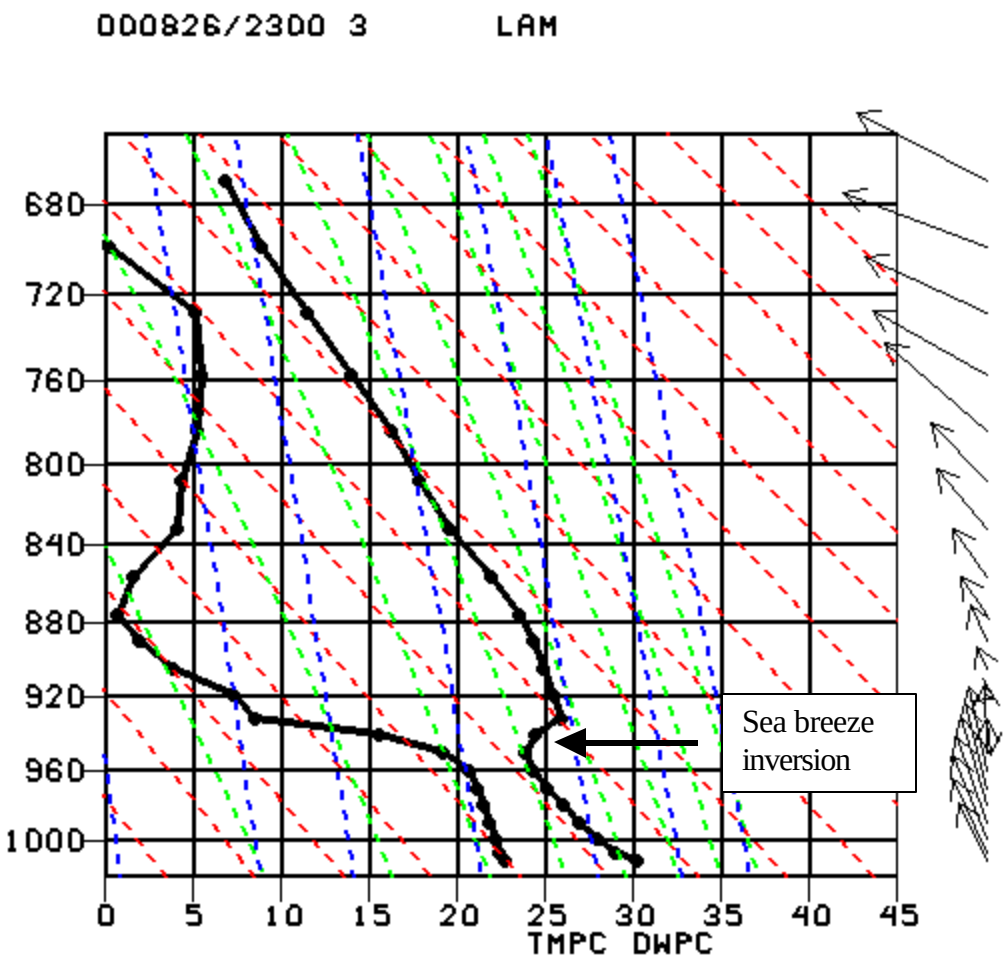

Figure 4c: Model sounding from dec16grid4 model run, Houston Southeast/Lamarque, 2300 UTC Aug. 26 2000.

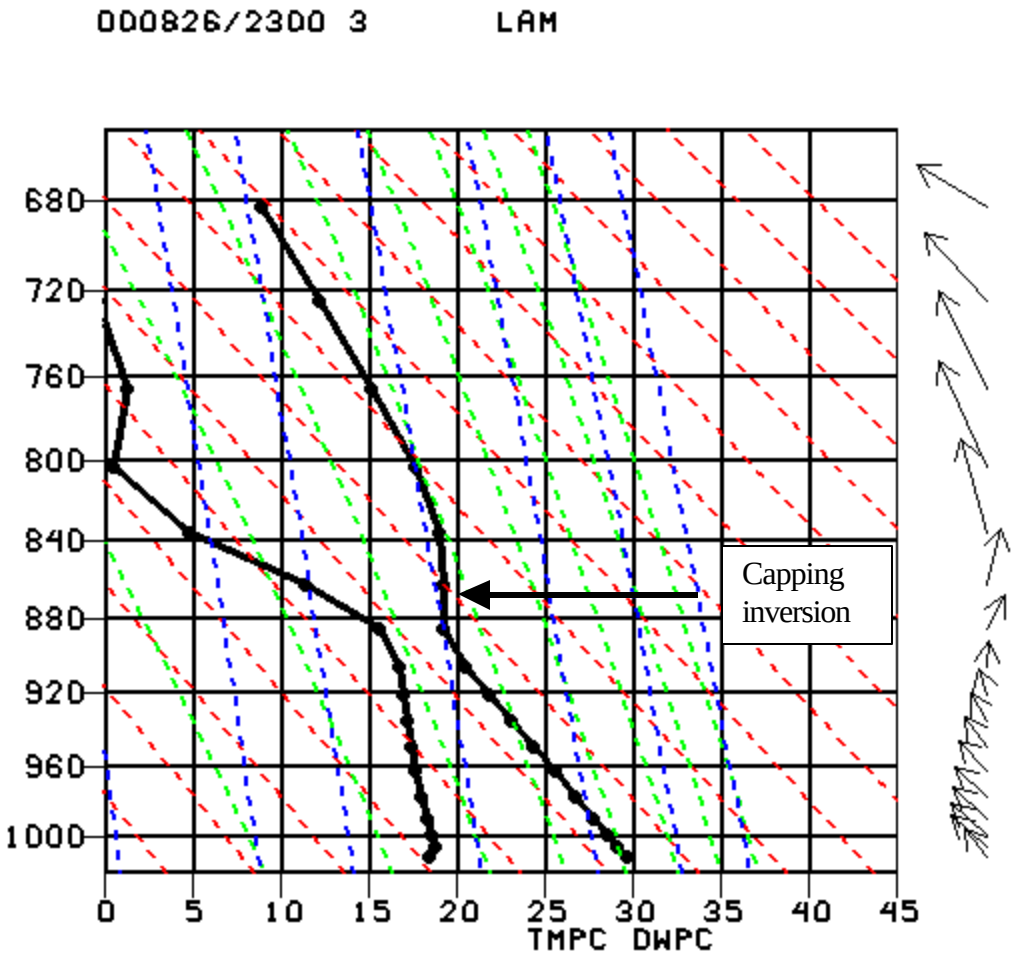

Figure 4d: Model sounding from MCNC model run, Houston Southeast/Lamarque, 2300 UTC Aug. 26 2000.

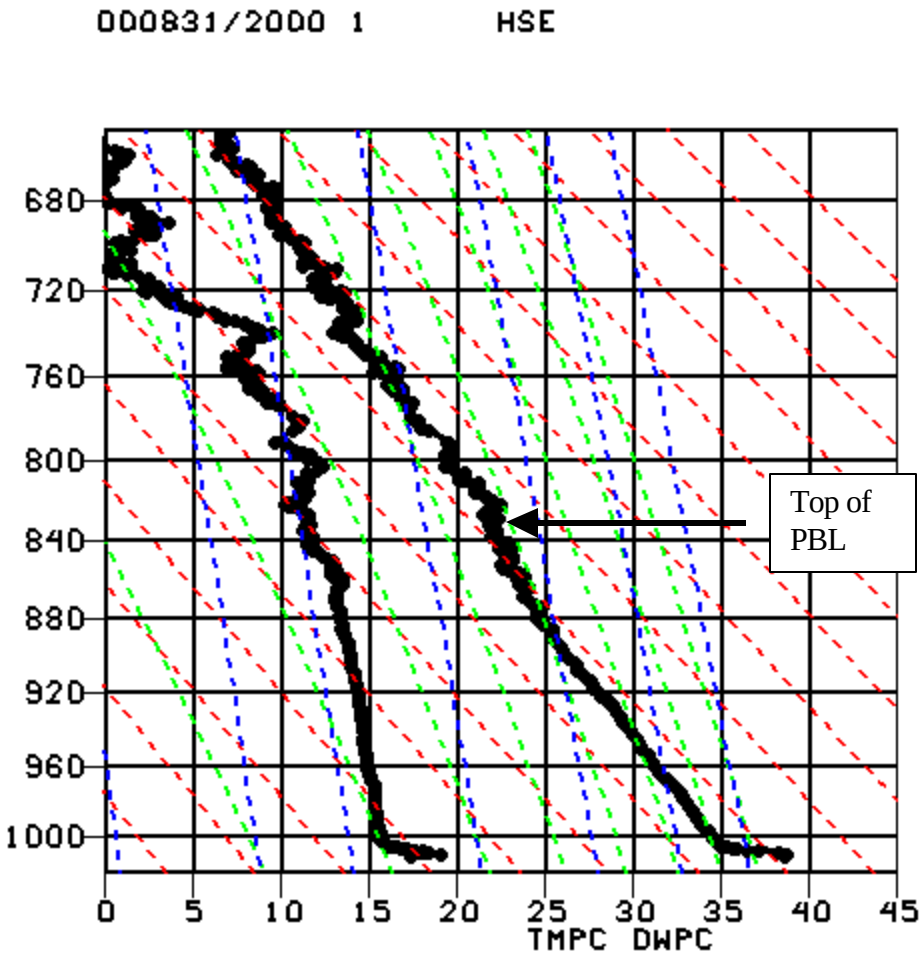

Figure 5a: Observed sounding, 2000 UTC Aug. 31, 2000, Houston Southeast/Lamarque Airsonde site.

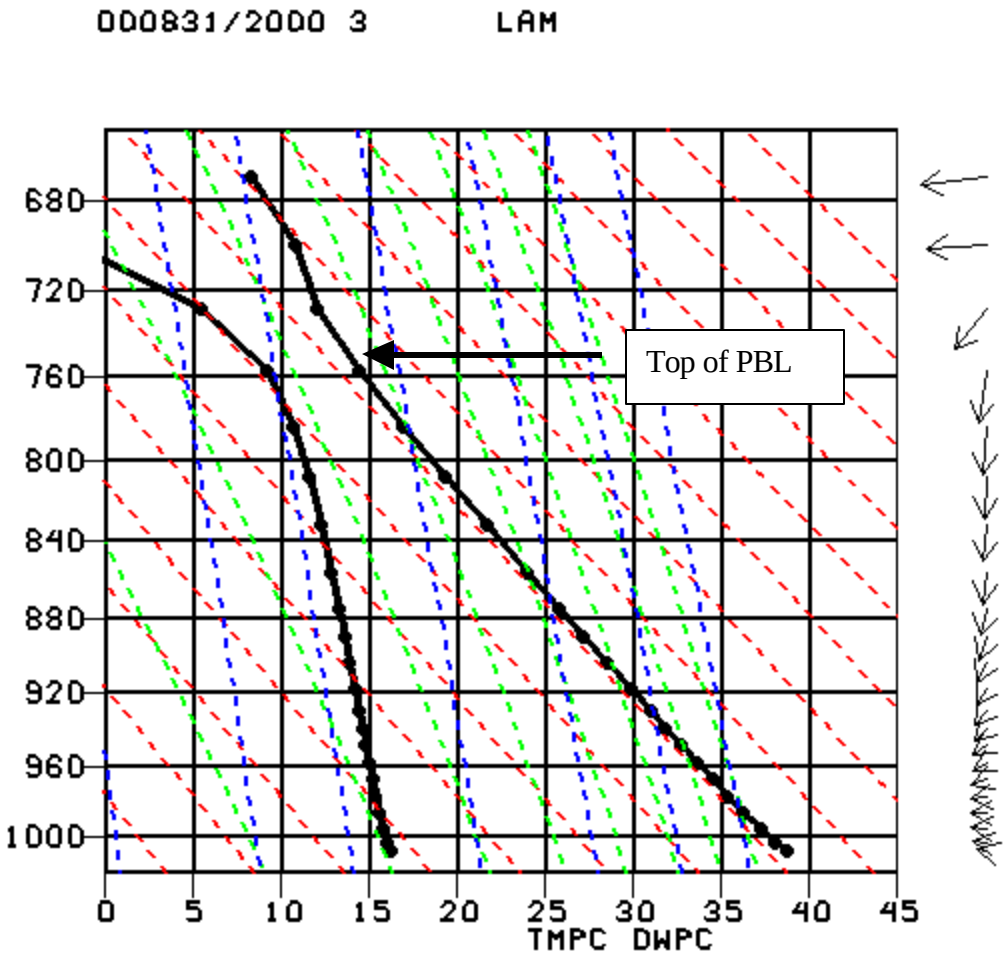

Figure 5b: Model sounding from dec30grid4 model run, Houston Southeast/Lamarque, 2000 UTC Aug. 31 2000.

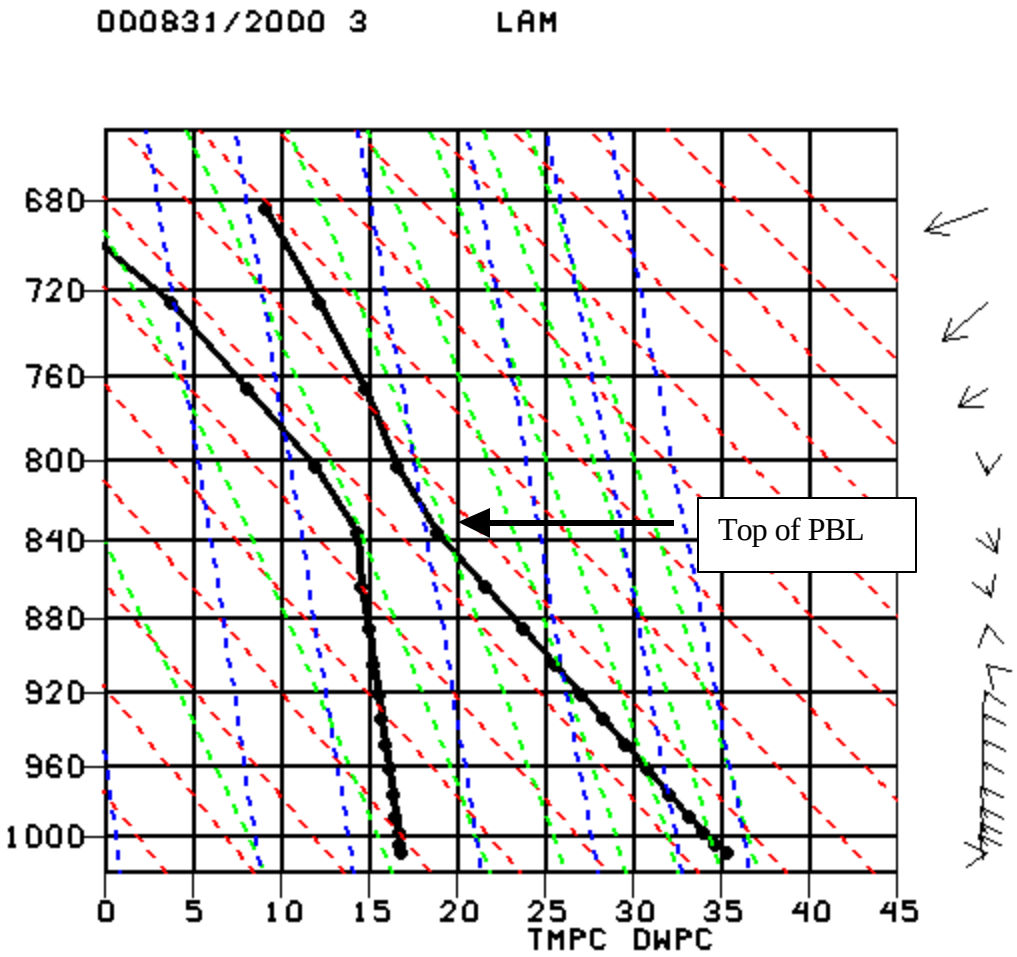

Figure 5c: Model sounding from MCNC model run, Houston Southeast/Lamarque, 2000 UTC Aug. 31 2000.

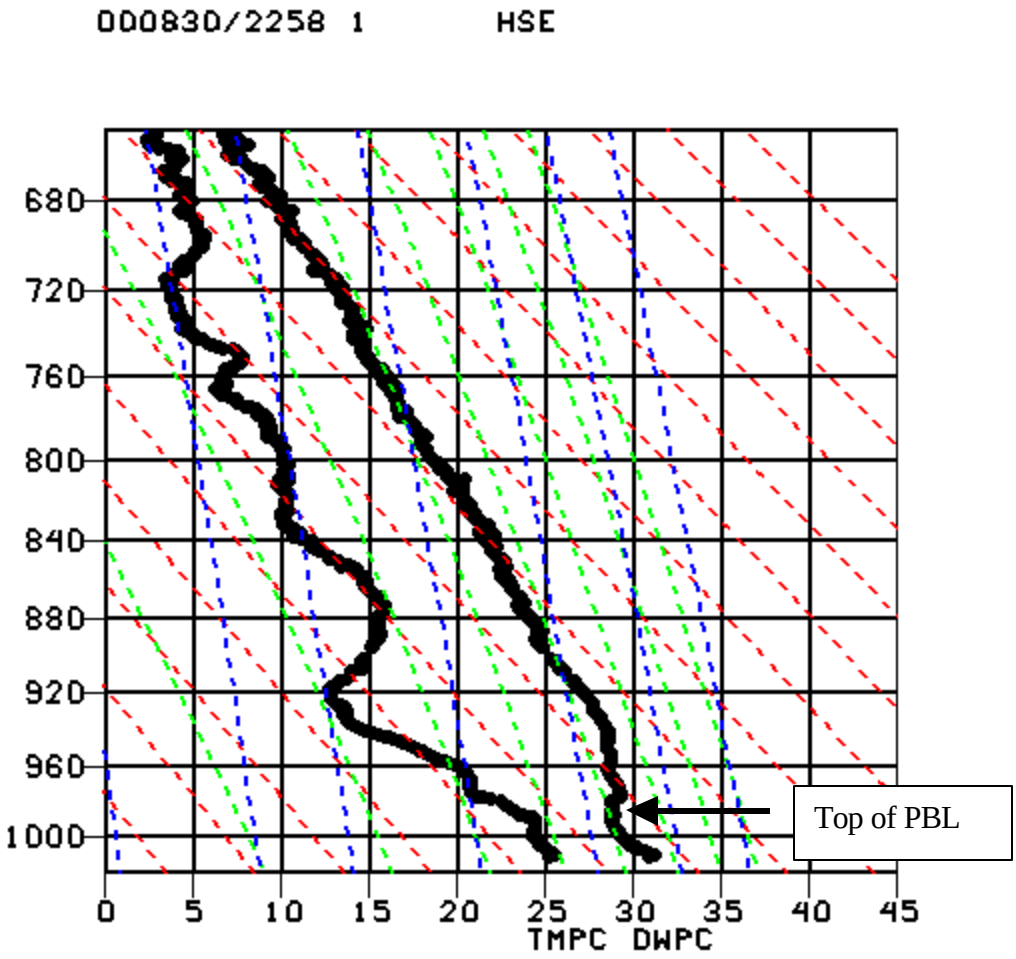

Figure 6a: Observed sounding, 2258 UTC Aug. 30, 2000, Houston Southeast/Lamarque Airsonde site.

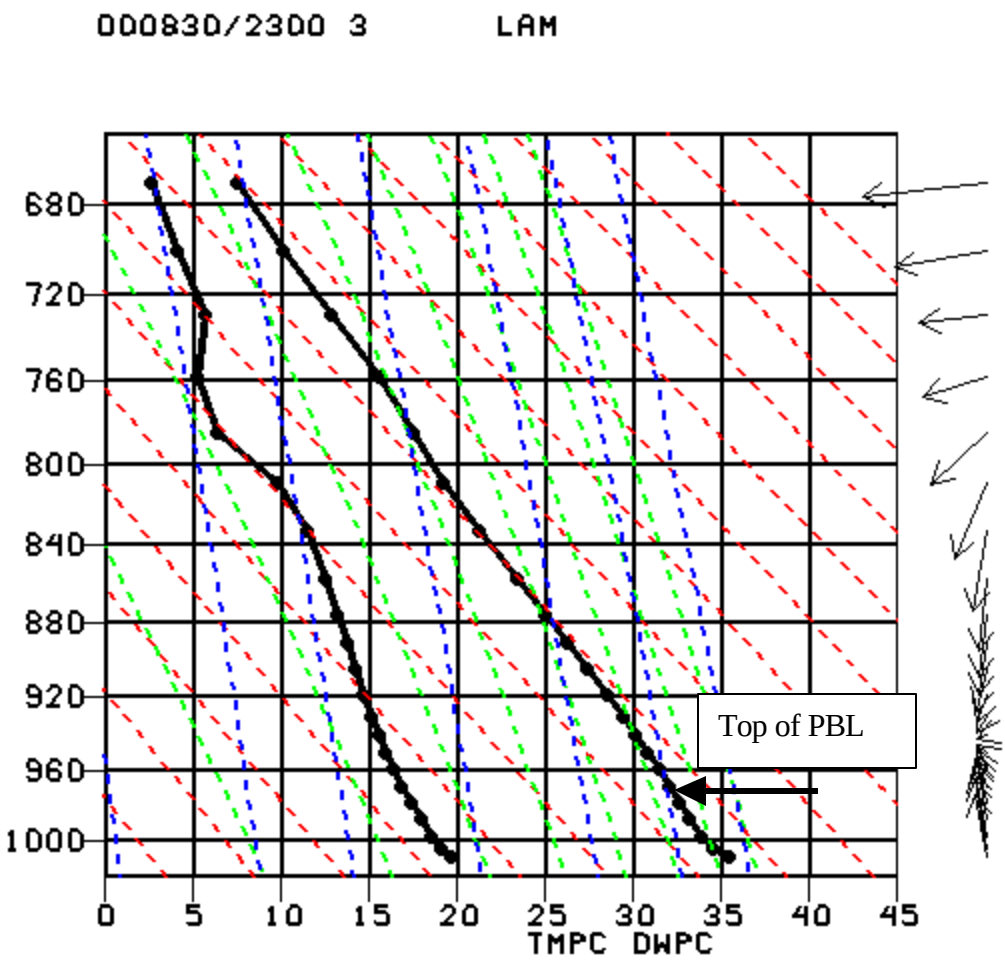

Figure 6b: Model sounding from dec30grid4 model run, Houston Southeast/Lamarque, 2300 UTC Aug. 30 2000.

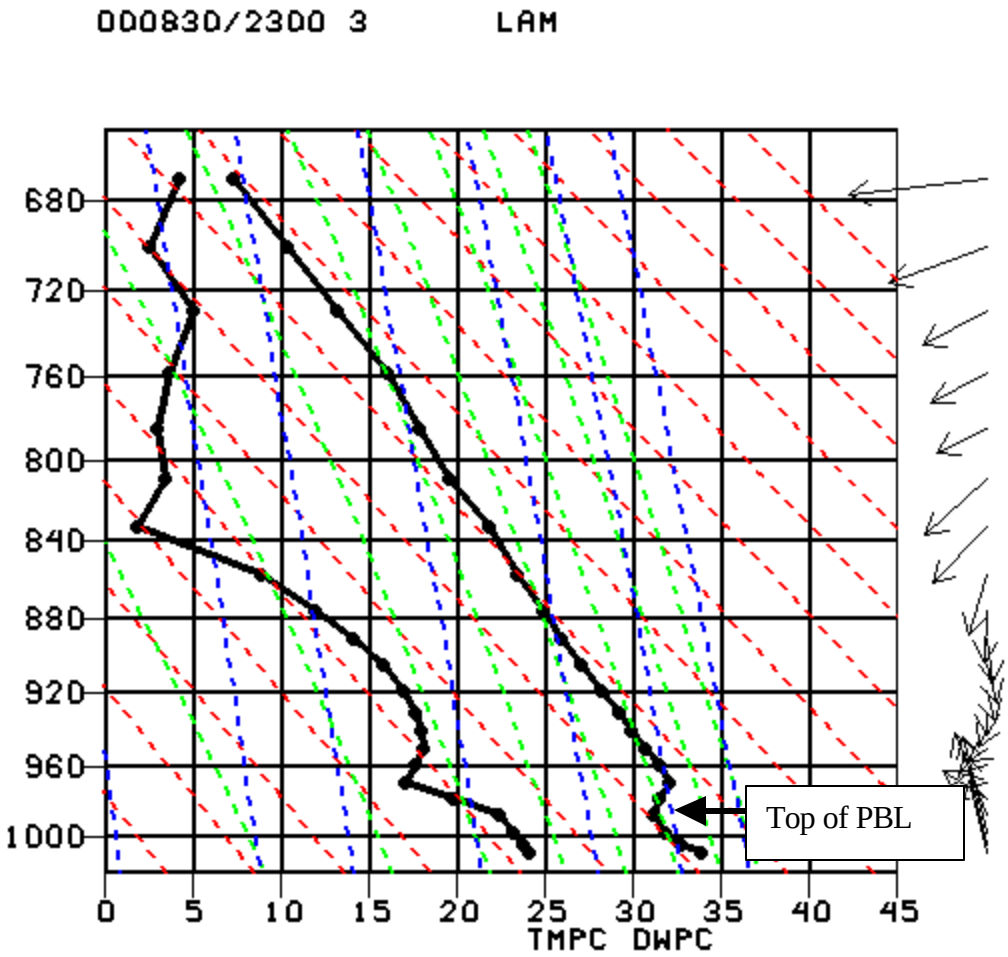

Figure 6c: Model sounding from dec16grid4 model run, Houston Southeast/Lamarque, 2300 UTC Aug. 30 2000.

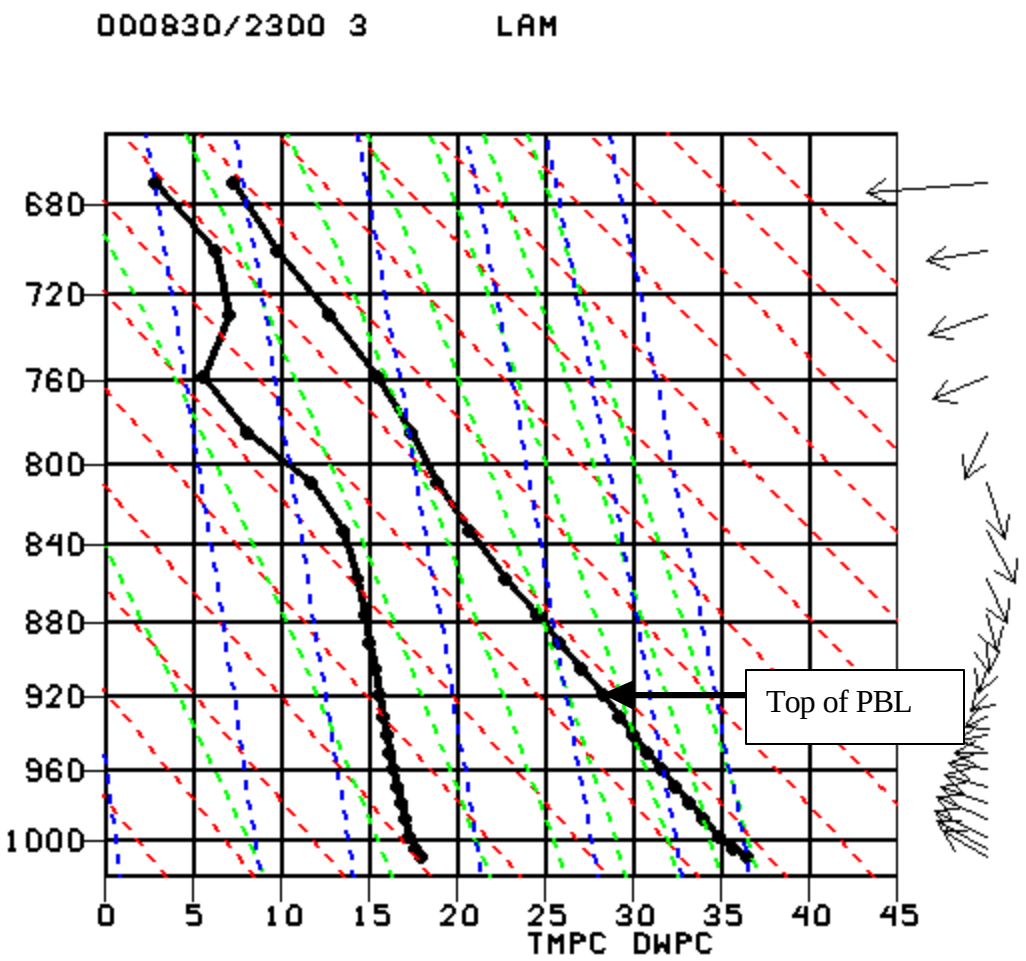

Figure 6d: Model sounding from feb9grid4 model run, Houston Southeast/Lamarque, 2300 UTC Aug. 30 2000.

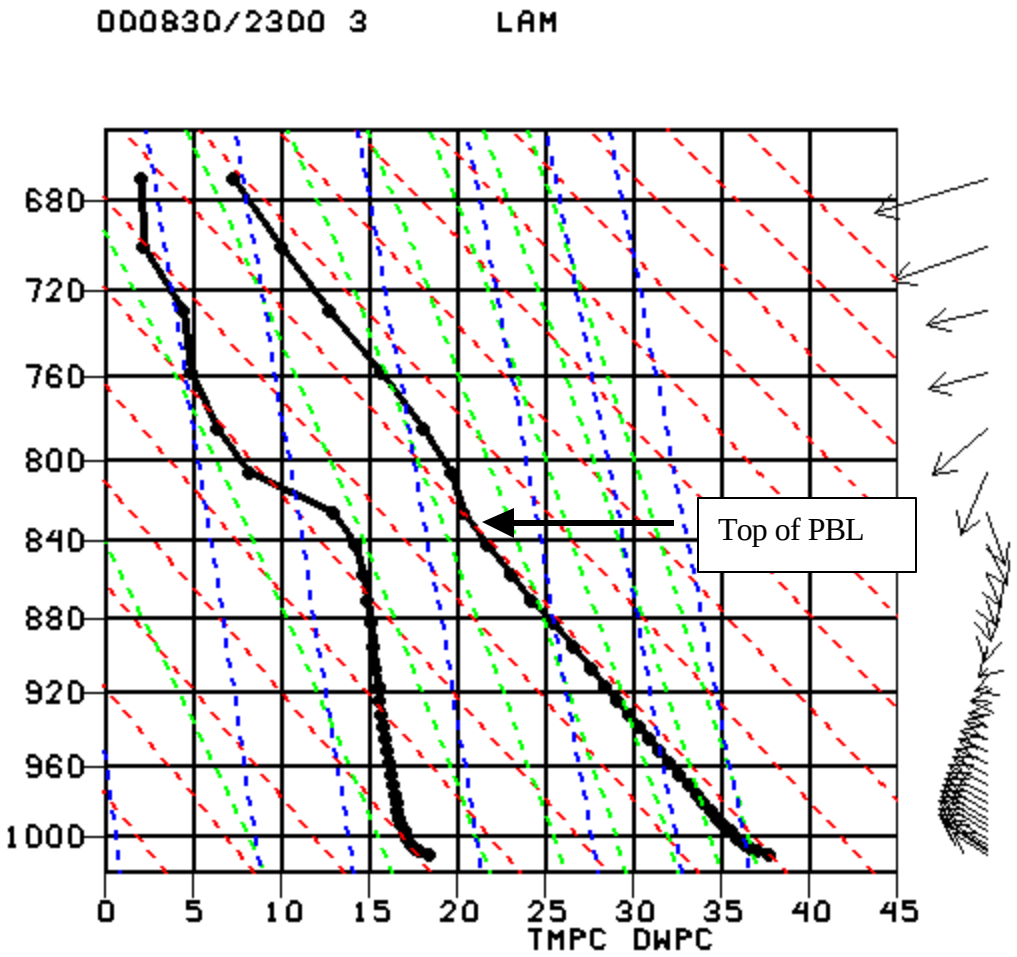

Figure 6e: Model sounding from feb16grid4 model run, Houston Southeast/Lamarque, 2300 UTC Aug. 30 2000.

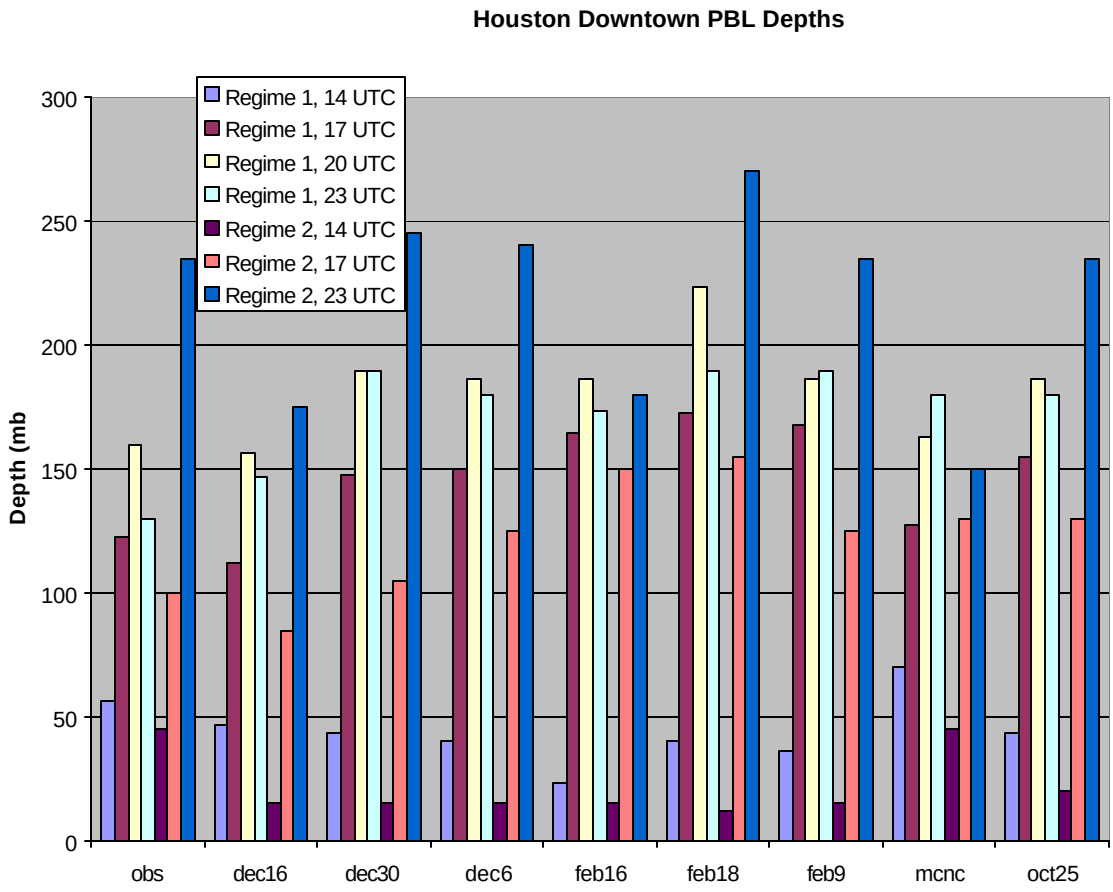

Figure 7: Daytime PBL depths, Houston Downtown site. First set is from Airsonde observations; other sets are from model runs.

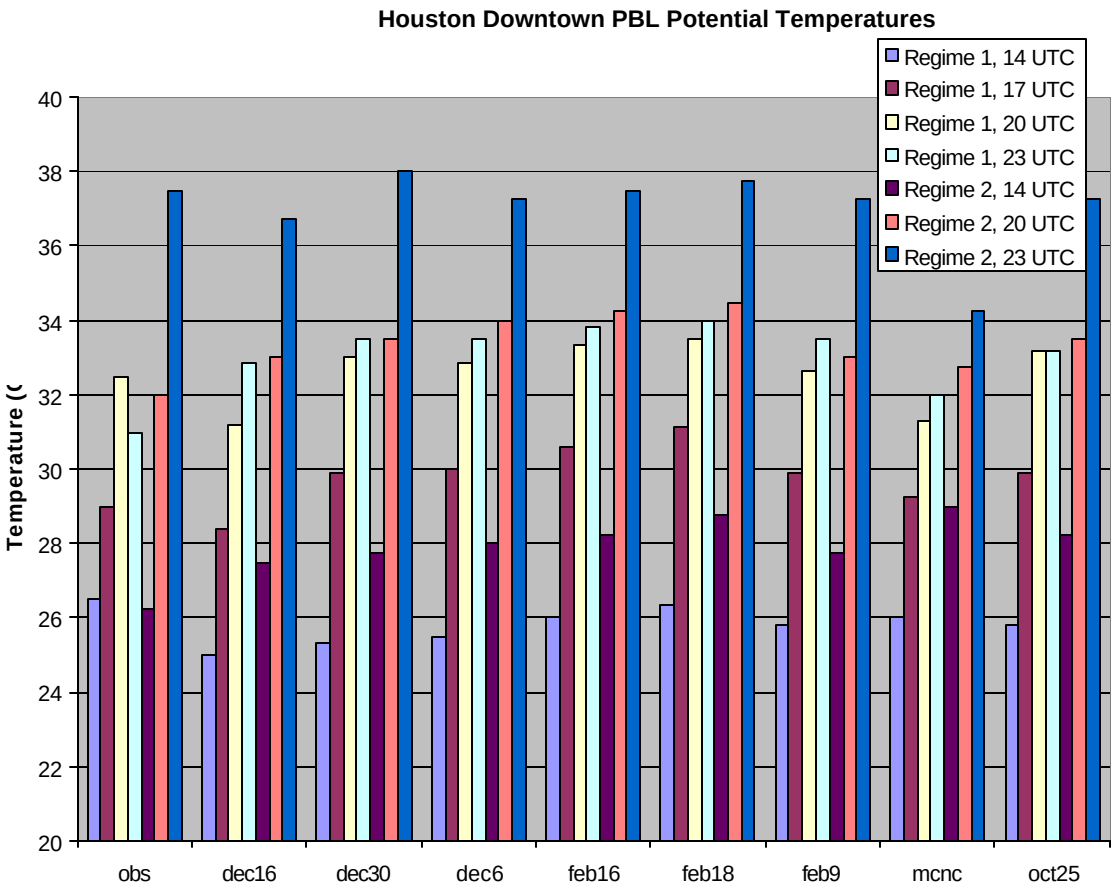

Figure 8: Mean PBL potential temperatures, Houston Downtown Airsonde site. First set is observations, remaining sets are model runs.

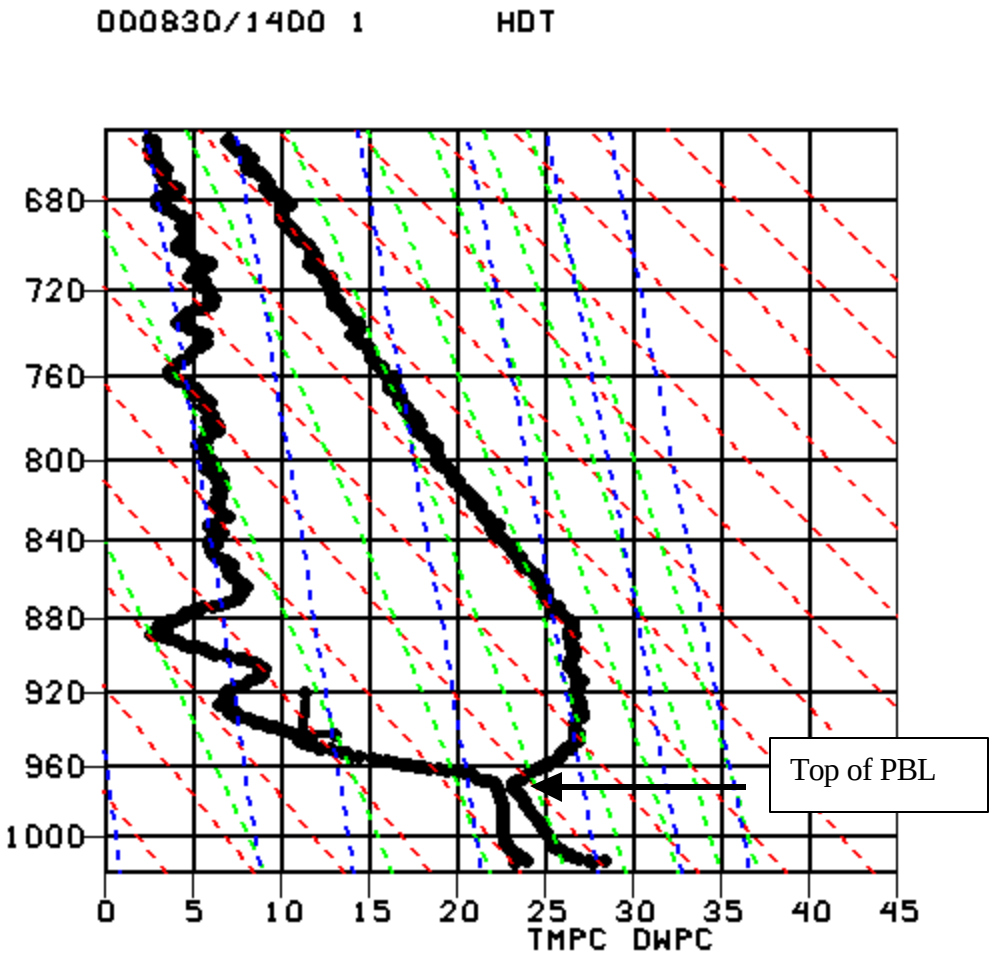

Figure 9a: Observed sounding, 1400 UTC Aug. 30, 2000, Houston Downtown Airsonde site.

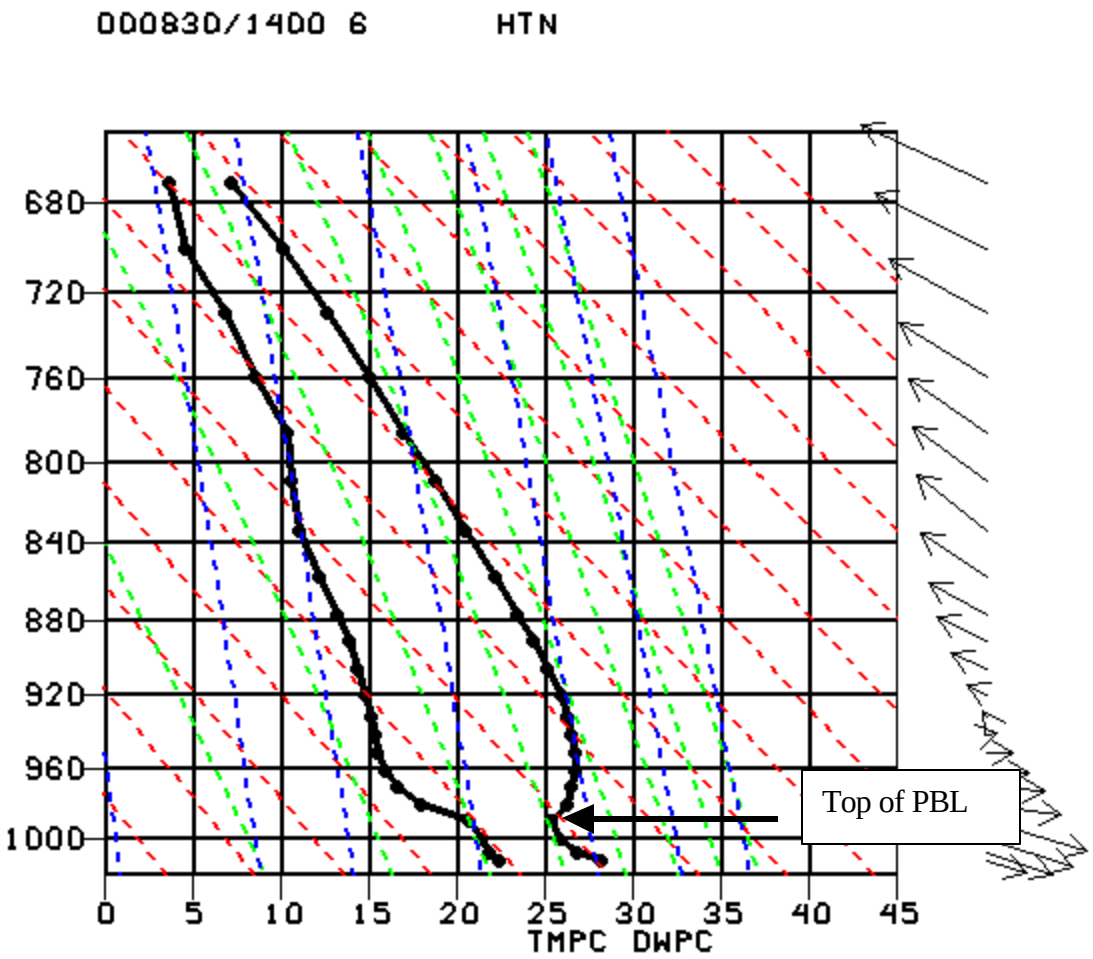

Figure 9b: Model sounding from dec30grid4 model run, Houston Downtown, 1400 UTC Aug. 30 2000.

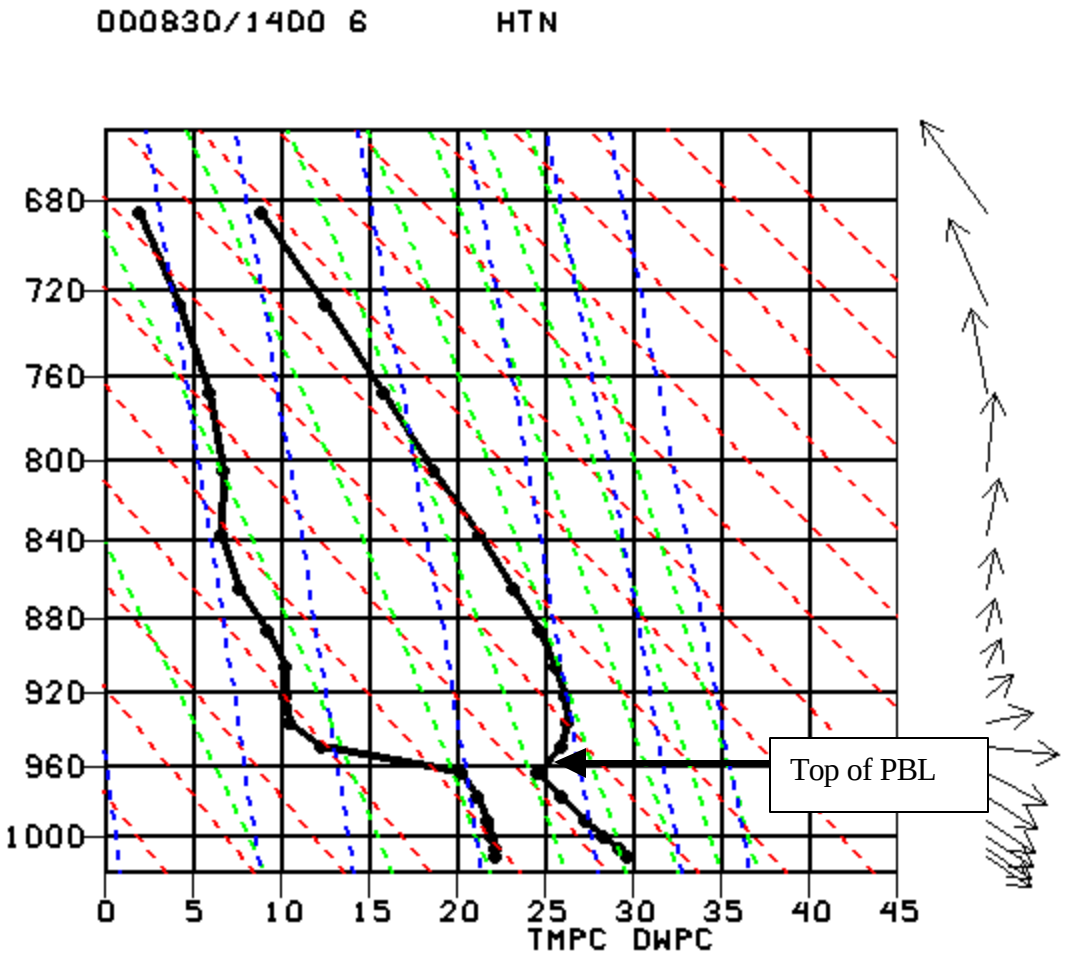

Figure 9c: Model sounding from MCNC model run, Houston Downtown, 1400 UTC Aug. 30 2000.

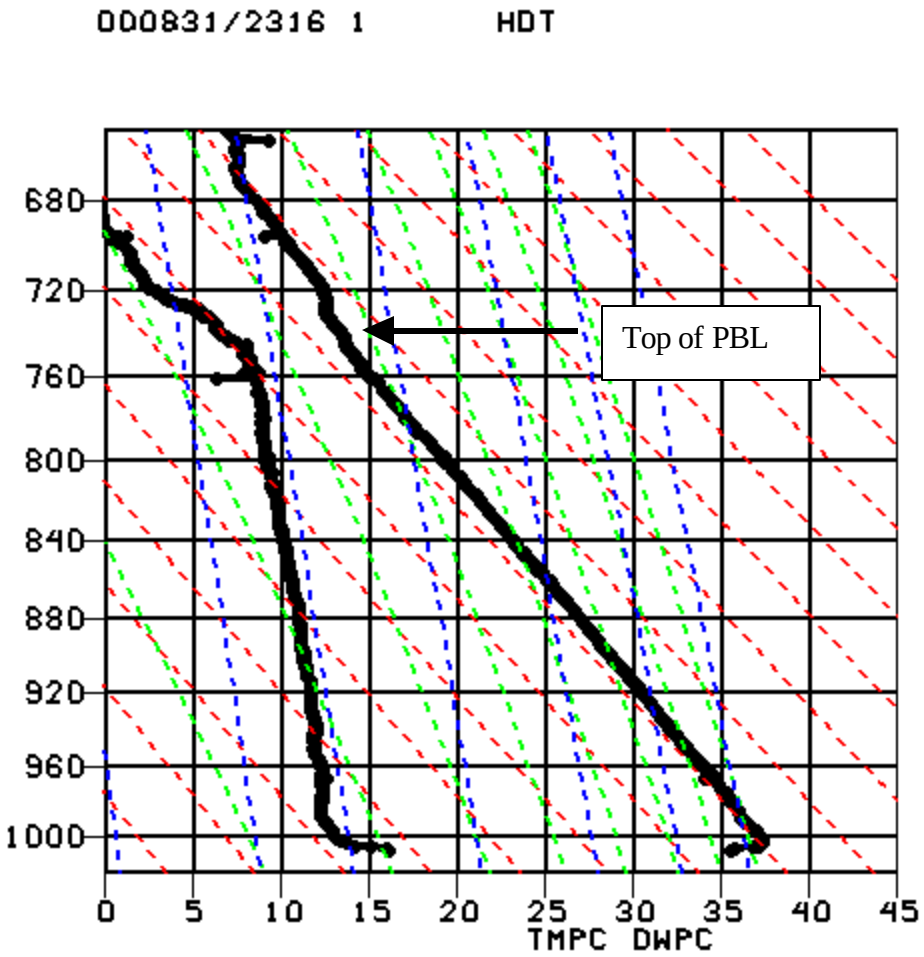

Figure 10a: Observed sounding, 2316 UTC Aug. 31, 2000, Houston Downtown Airsonde site.

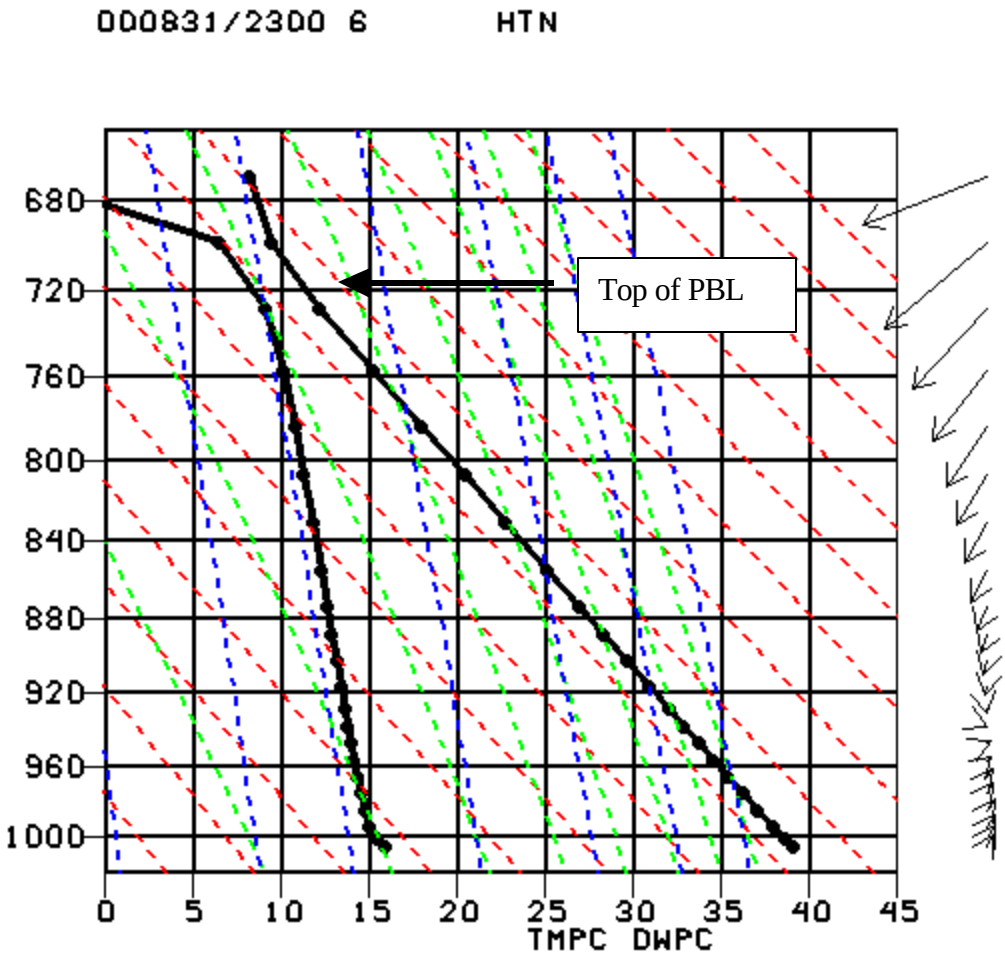

Figure 10b: Model sounding from dec30grid4 model run, Houston Downtown, 2300 UTC Aug. 31 2000.

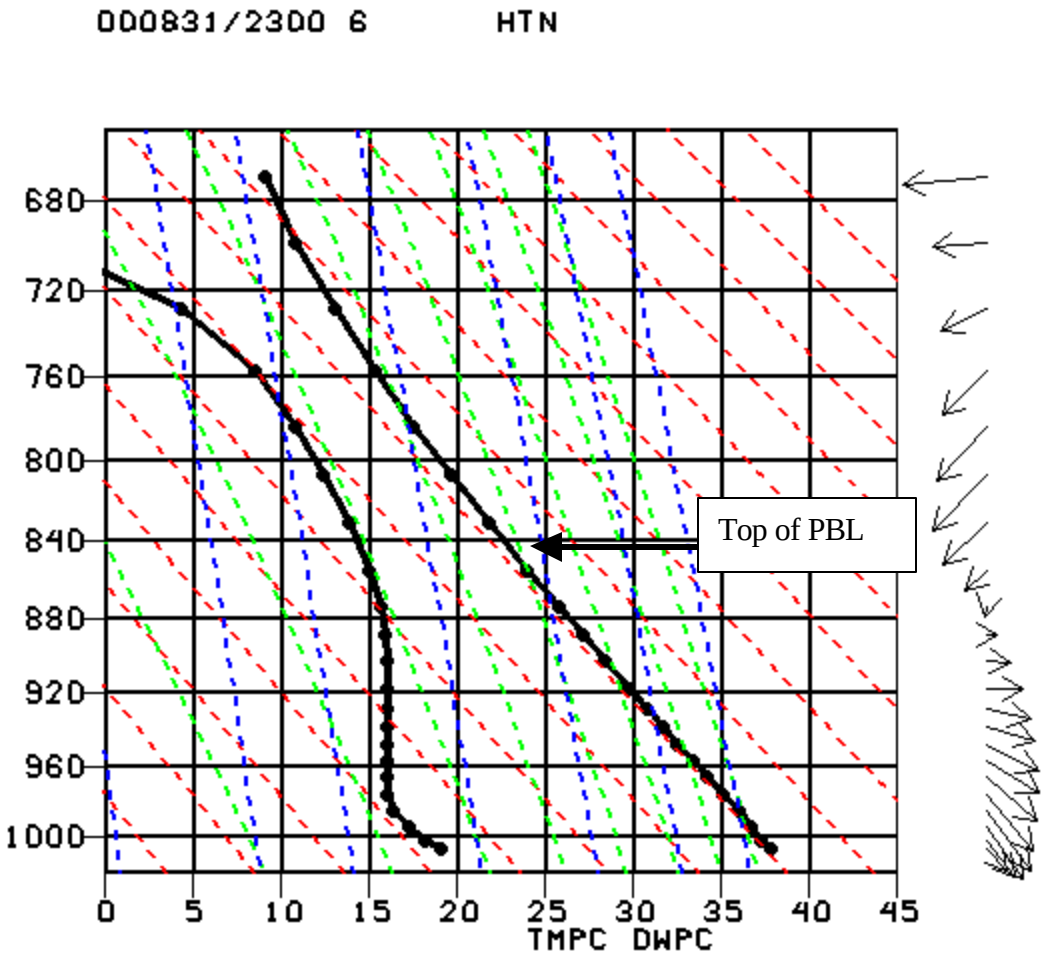

Figure 10c: Model sounding from dec16grid4 model run, Houston Downtown, 2300 UTC Aug. 31 2000.

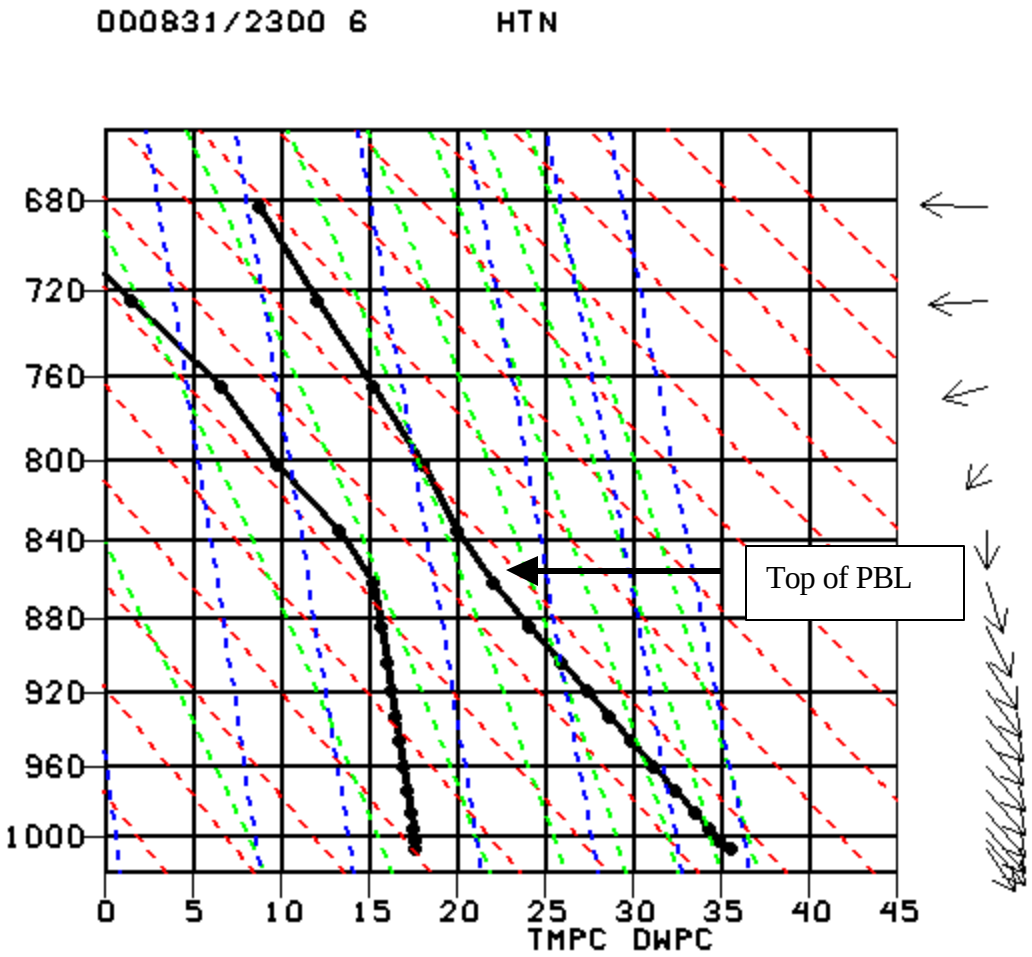

Figure 10d: Model sounding from MCNC model run, Houston Downtown, 2300 UTC Aug. 31 2000.

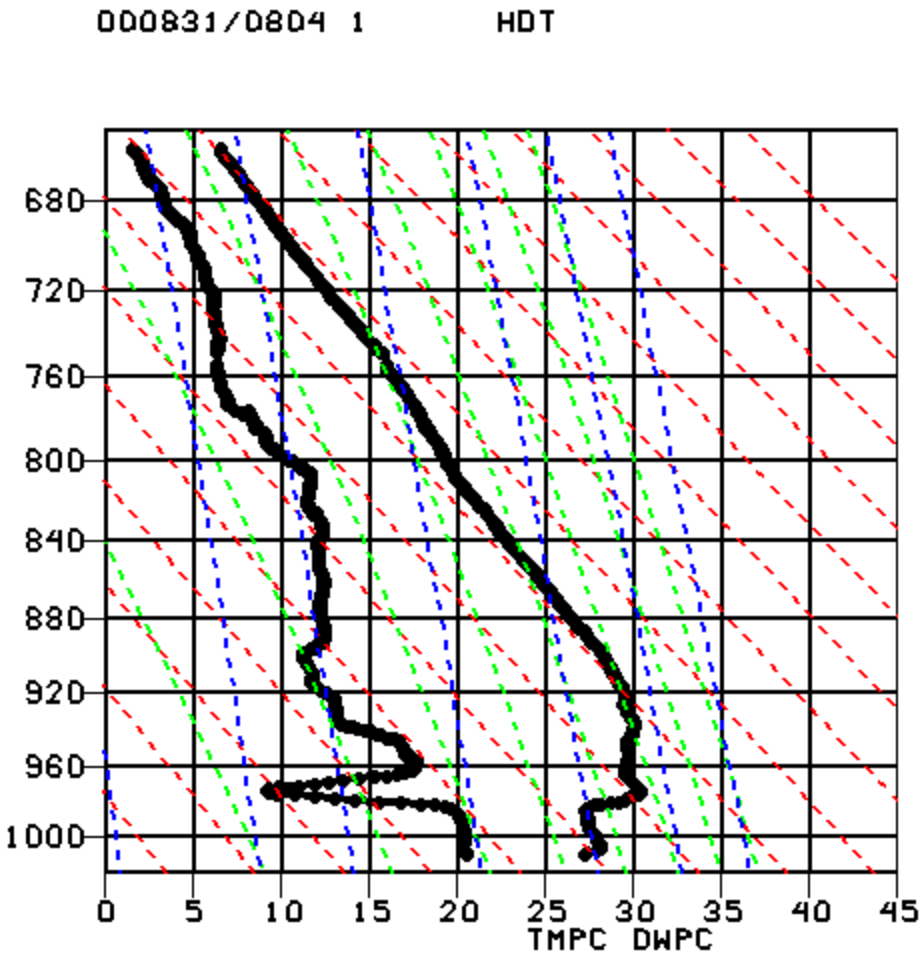

Figure 11a: Observed sounding, 0804 UTC Aug. 31, 2000, Houston Downtown Airsonde site.

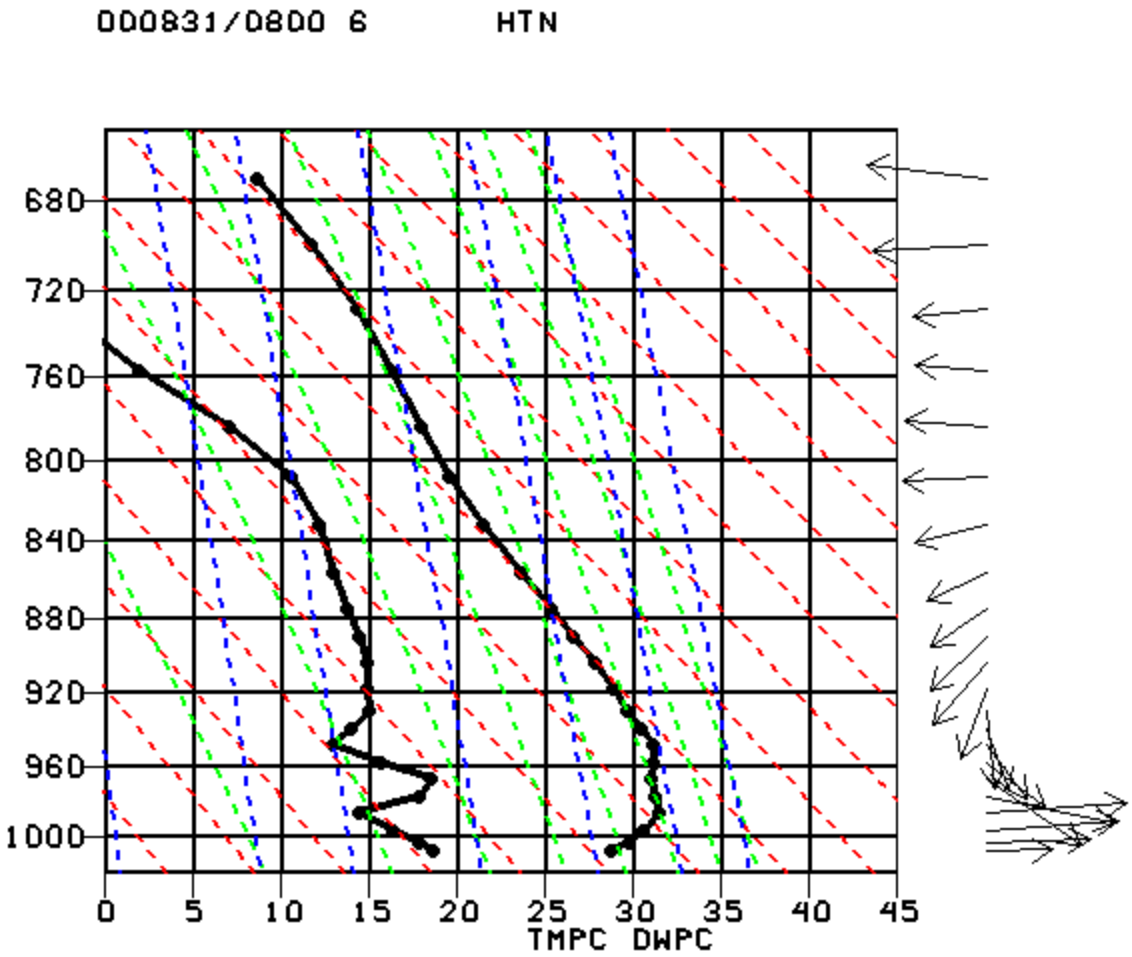

Figure 11b: Model sounding from dec16grid4 model run, Houston Downtown, 0800 UTC Aug. 31 2000.

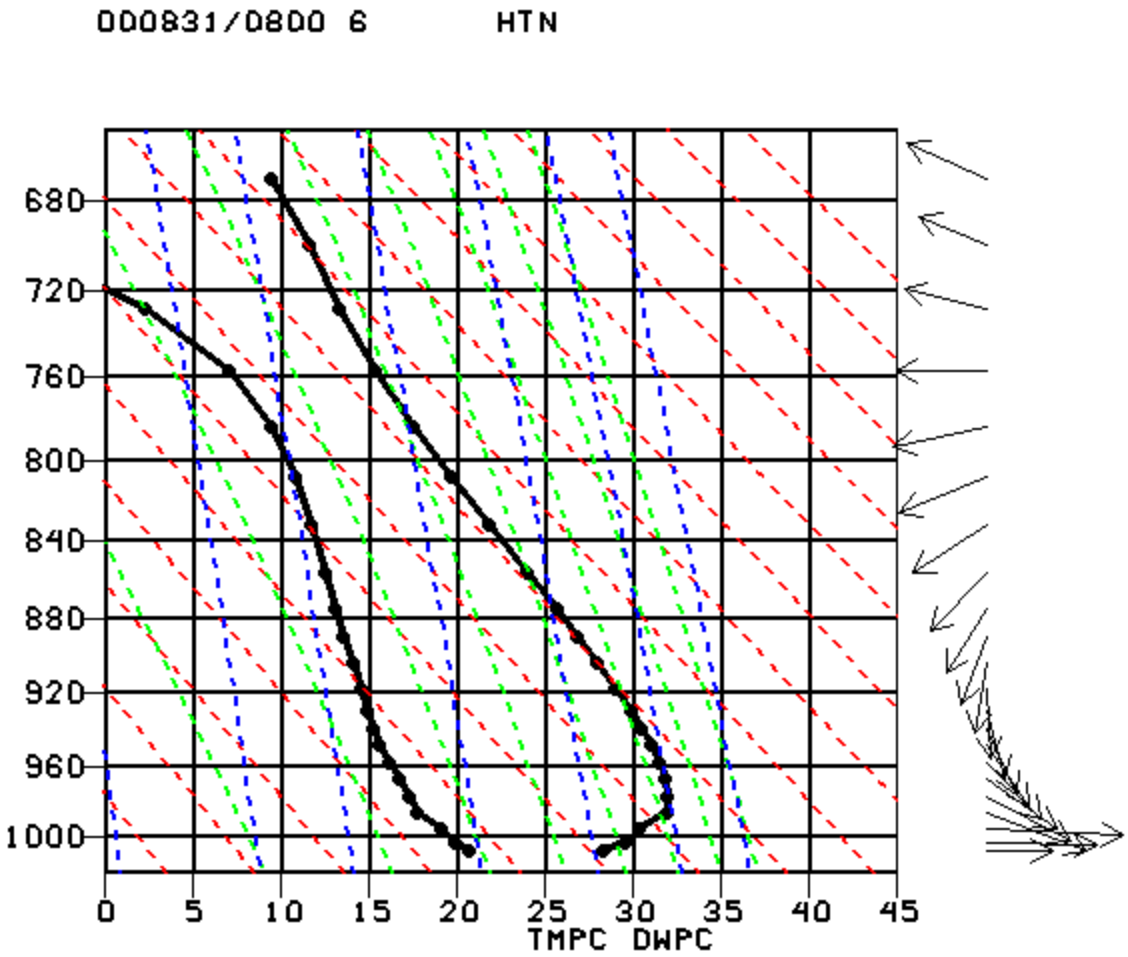

Figure 11c: Model sounding from dec30grid4 model run, Houston Downtown, 0800 UTC Aug. 31 2000.

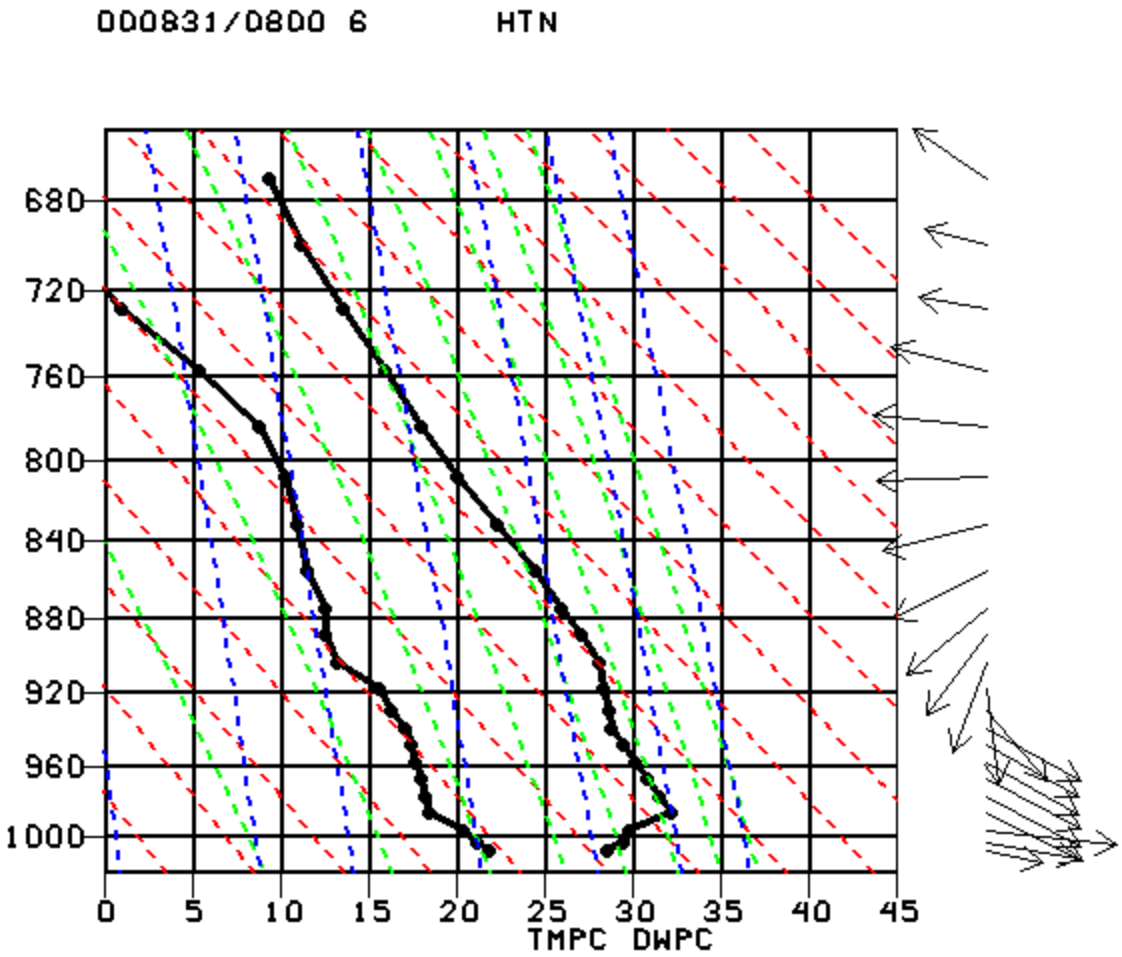

Figure 11d: Model sounding from feb9grid4 model run, Houston Downtown, 0800 UTC Aug. 31 2000.

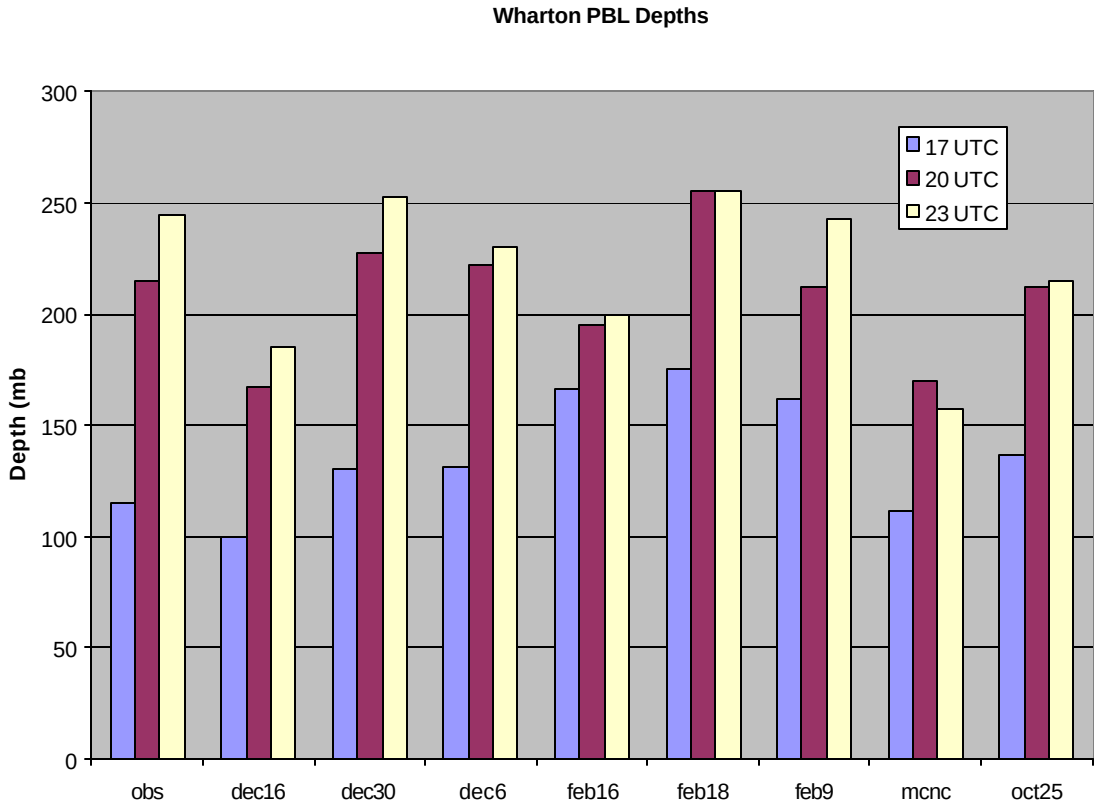

Figure 12: Daytime PBL depths, Wharton Power Plant site. First set is from GPS rawinsonde observations; other sets are from model runs.

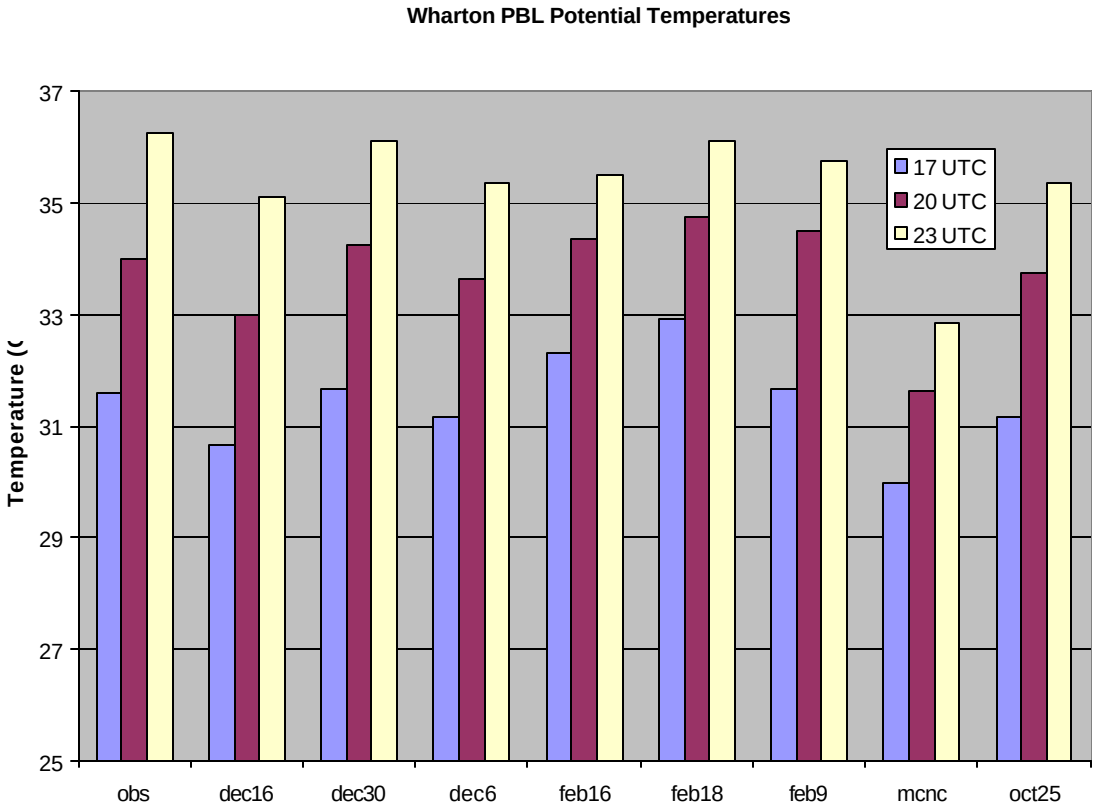

Figure 13: Mean PBL potential temperatures, Wharton Power Plant GPS rawinsonde site. First set is observations, remaining sets are model runs.

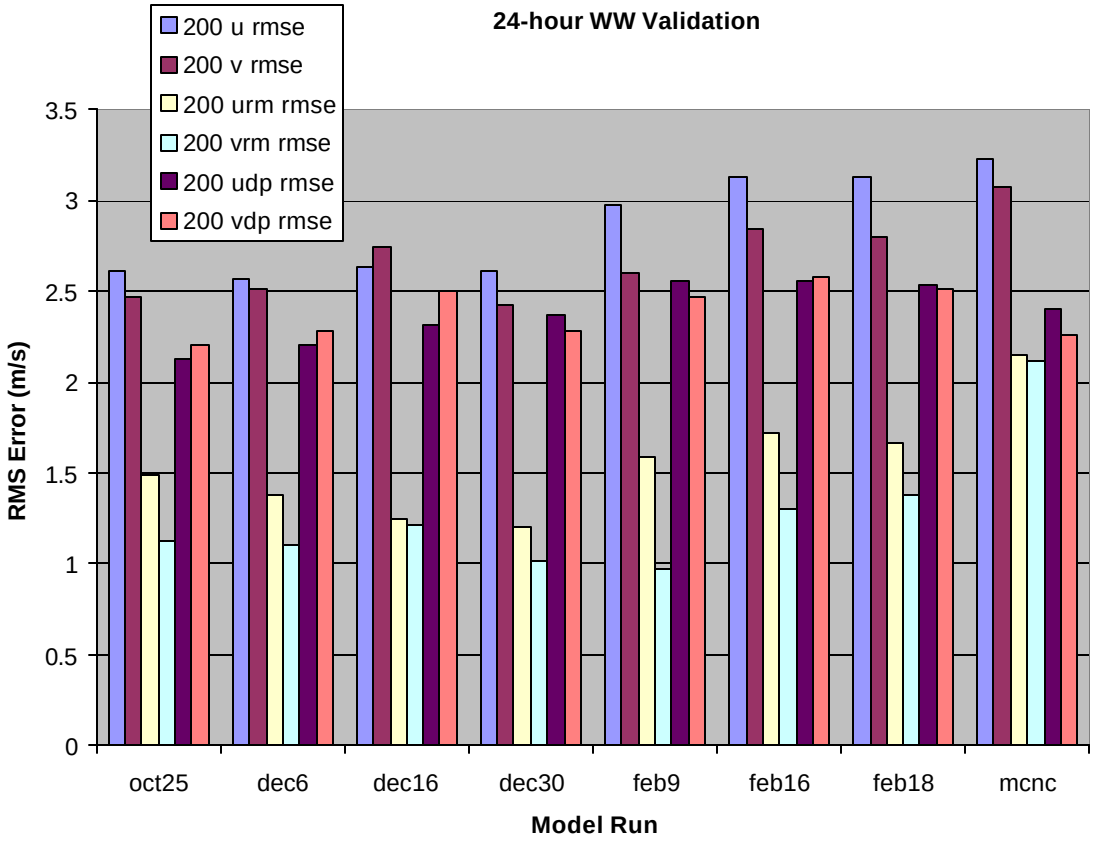

Figure 14a: RMS Errors between model runs and profiler data, vertical level nearest to 200 m. (u,v): total wind components. (urm,vrm) 24-hour running mean wind components. (udp,vdp) departures from 24-hour running mean. Profiler data set has been passed through ETL quality control.

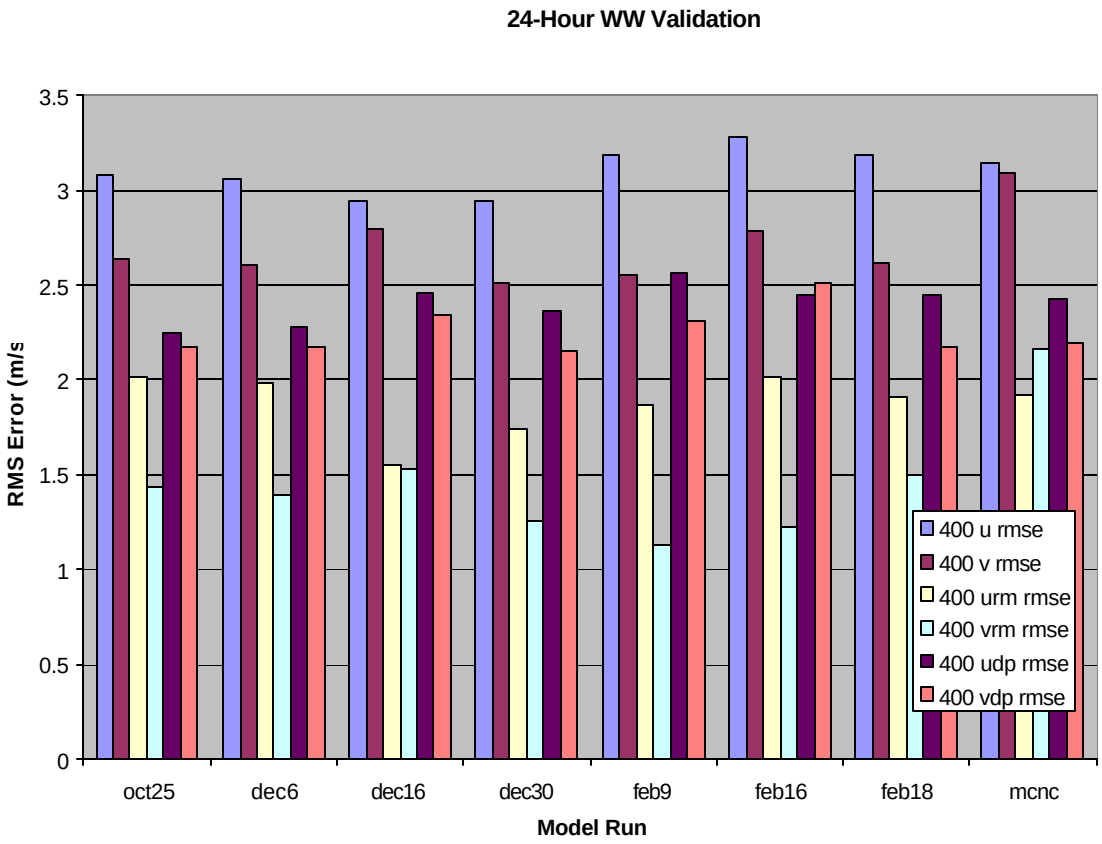

Figure 14b: RMS Errors between model runs and profiler data, vertical level nearest to 400 m.

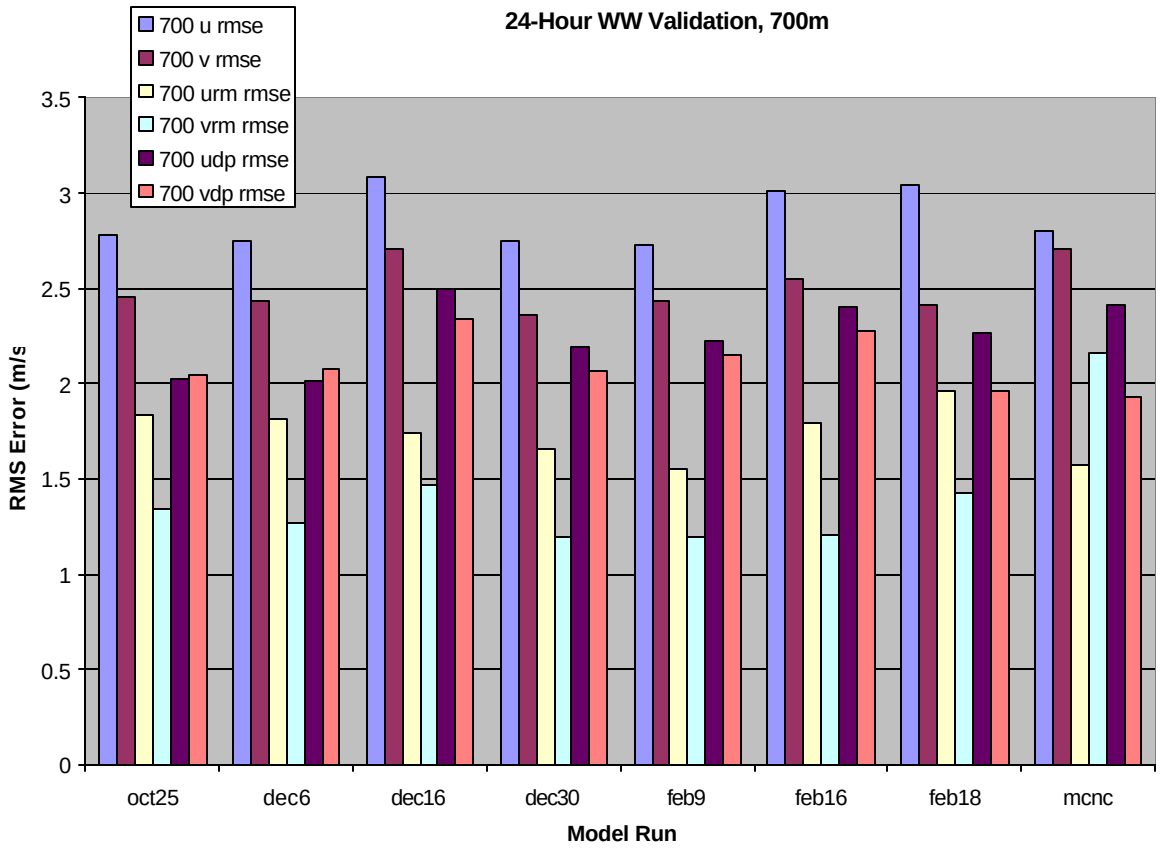

Figure 14c: RMS Errors between model runs and profiler data, vertical level nearest to 700 m.

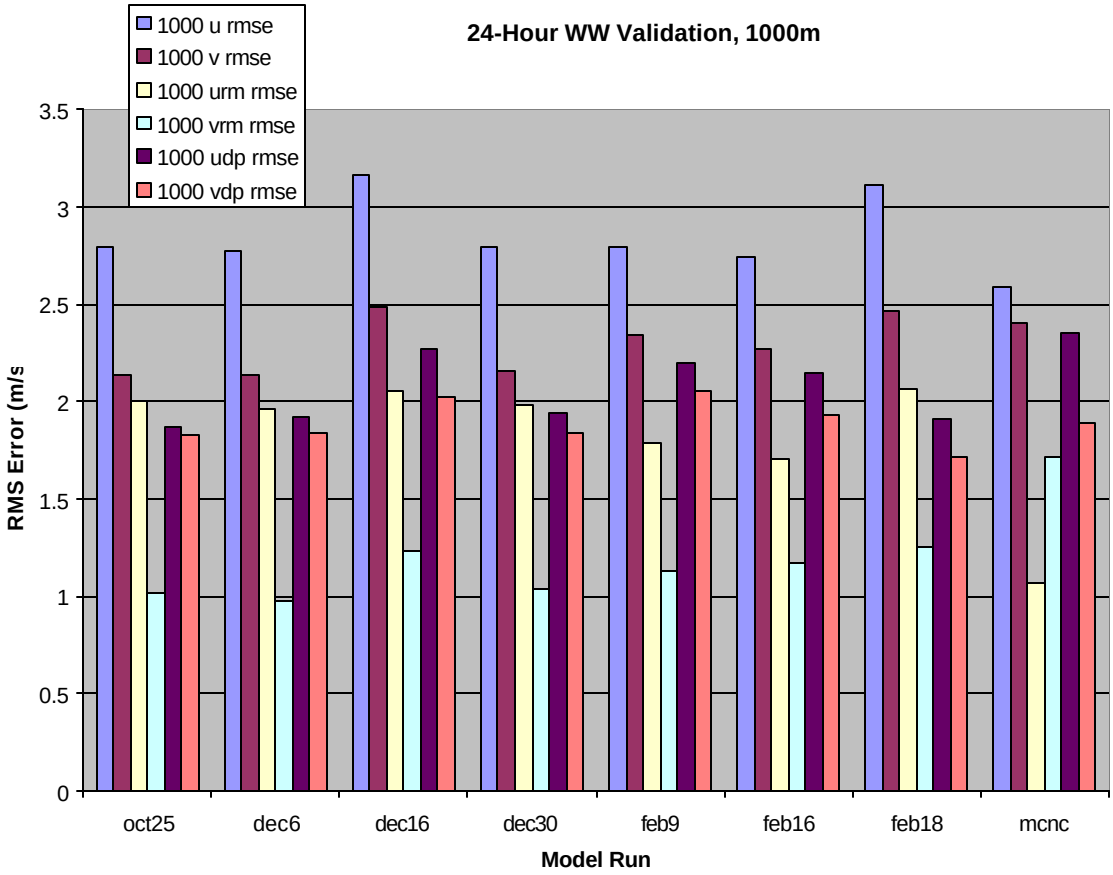

Figure 14d: RMS Errors between model runs and profiler data, vertical level nearest to 1000 m.

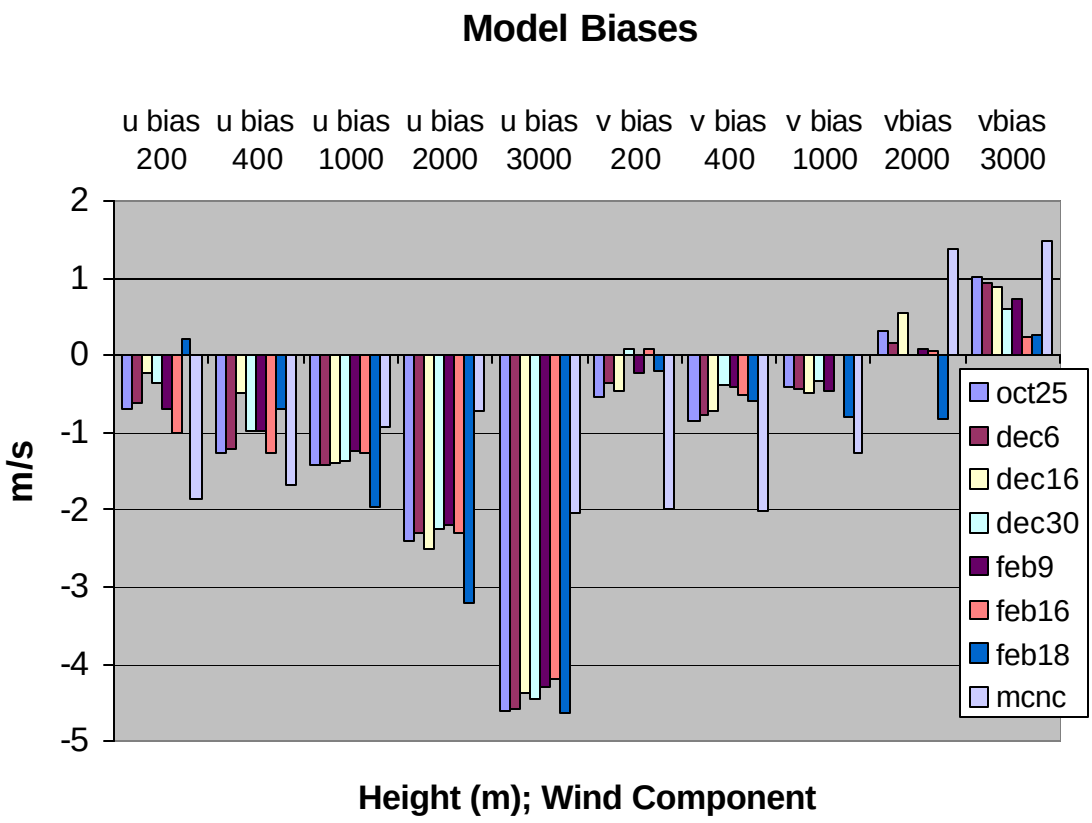

Figure 15: Biases of modeled wind components at indicated levels (m), measured against ETL quality-controlled profiler data.

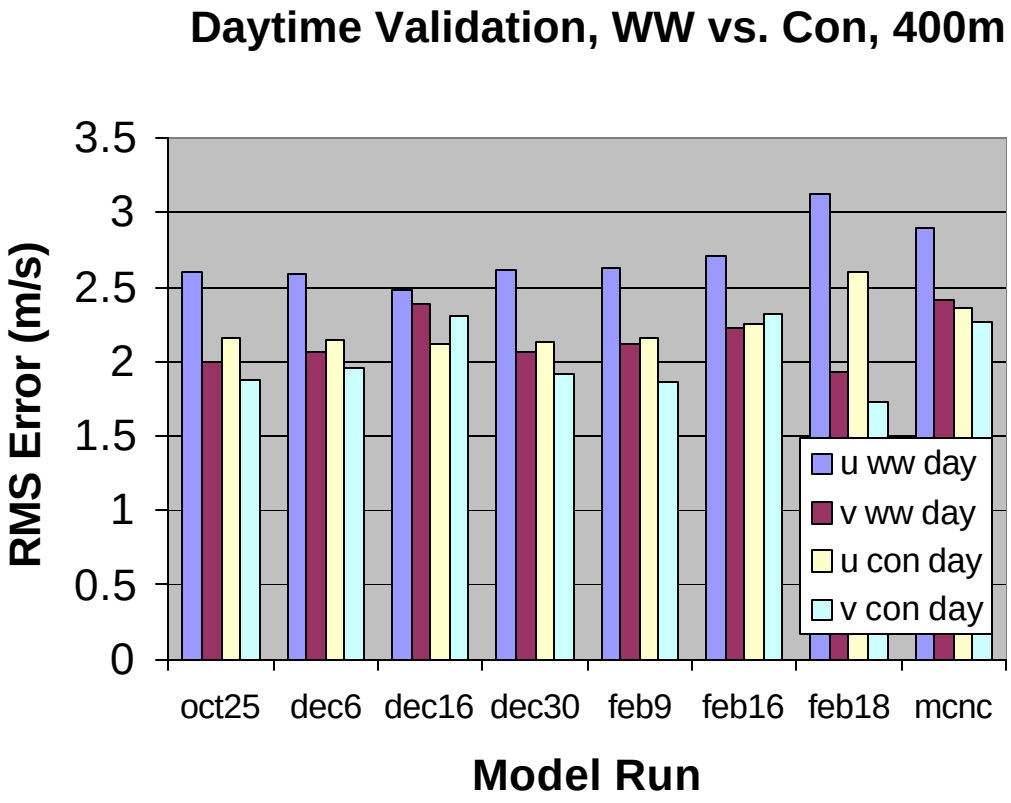

Figure 16: Comparison of model RMS error using ETL quality-controlled profiler data (ww) and AL quality-controlled profiler data (con).

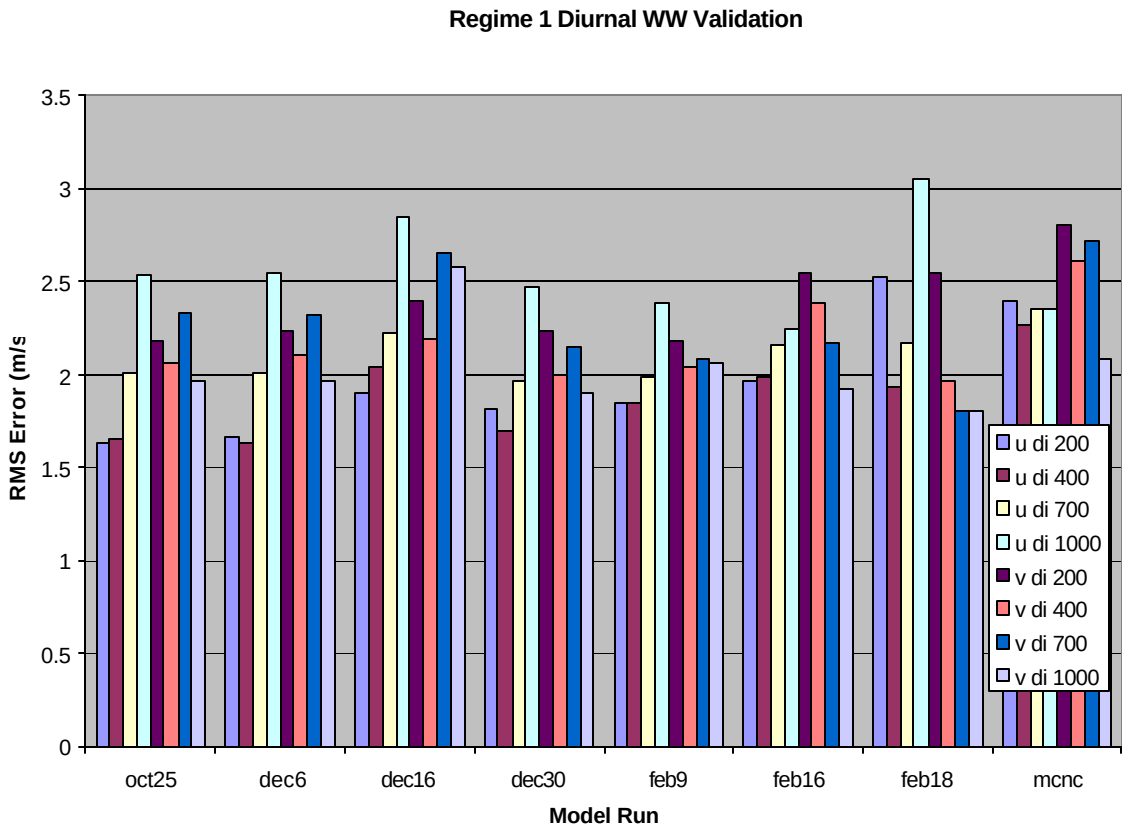

Figure 17a: RMS error of the departures from the 24-hour running mean of each wind component during Regime 1, measured against ETL quality-controlled profiler data.

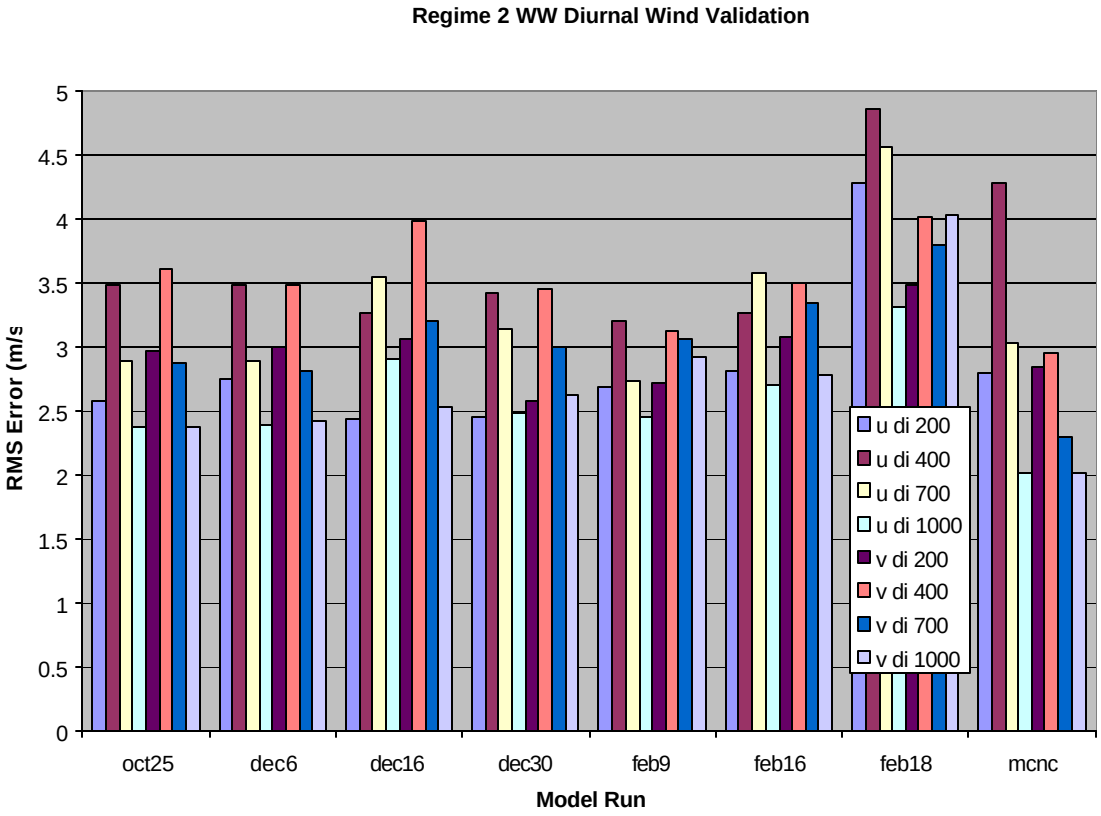

Figure 17b: RMS error of the departures from the 24-hour running mean of each wind component during Regime 2, measured against ETL quality-controlled profiler data.

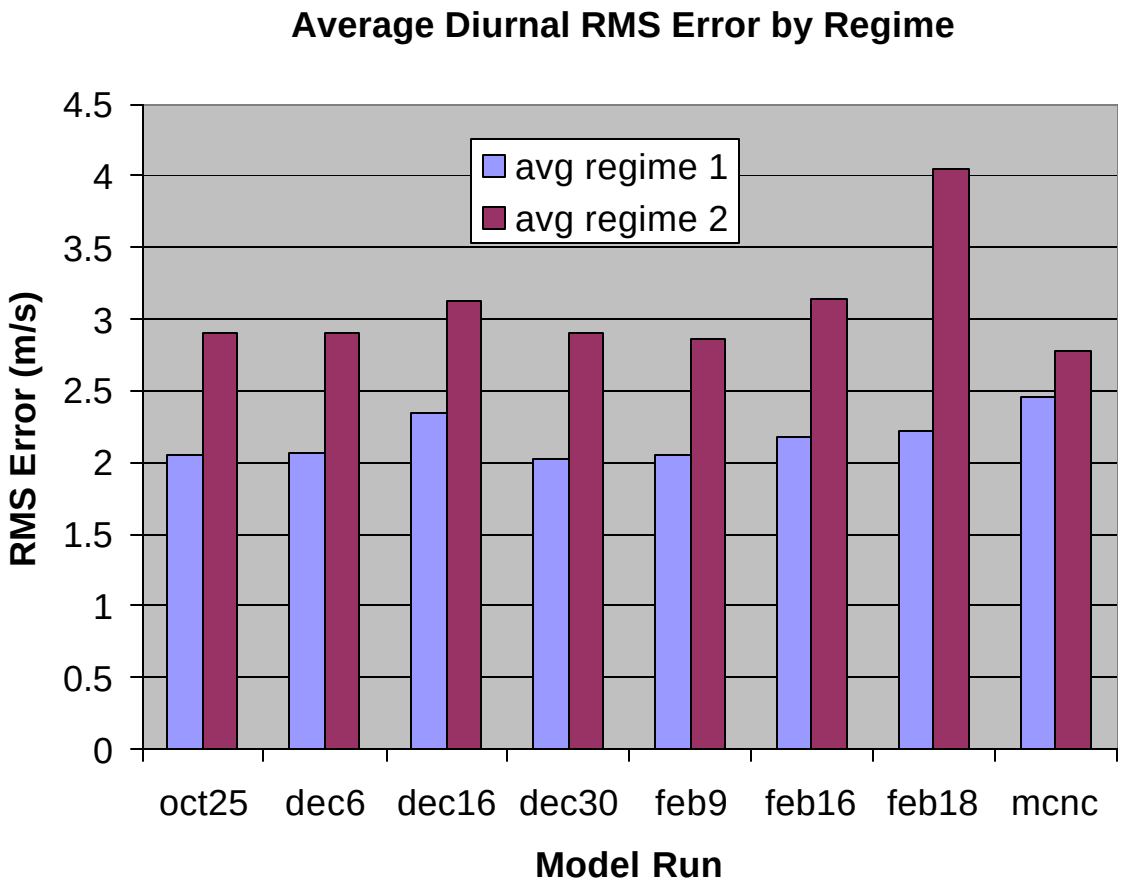

Figure 18: RMS error of the departure from 24-hour running means for Regime 1 and Regime 2, measured against ETL quality-controlled profiler data. RMS errors are computed at the 200m, 400m, 700m, and 1000m levels and averaged.

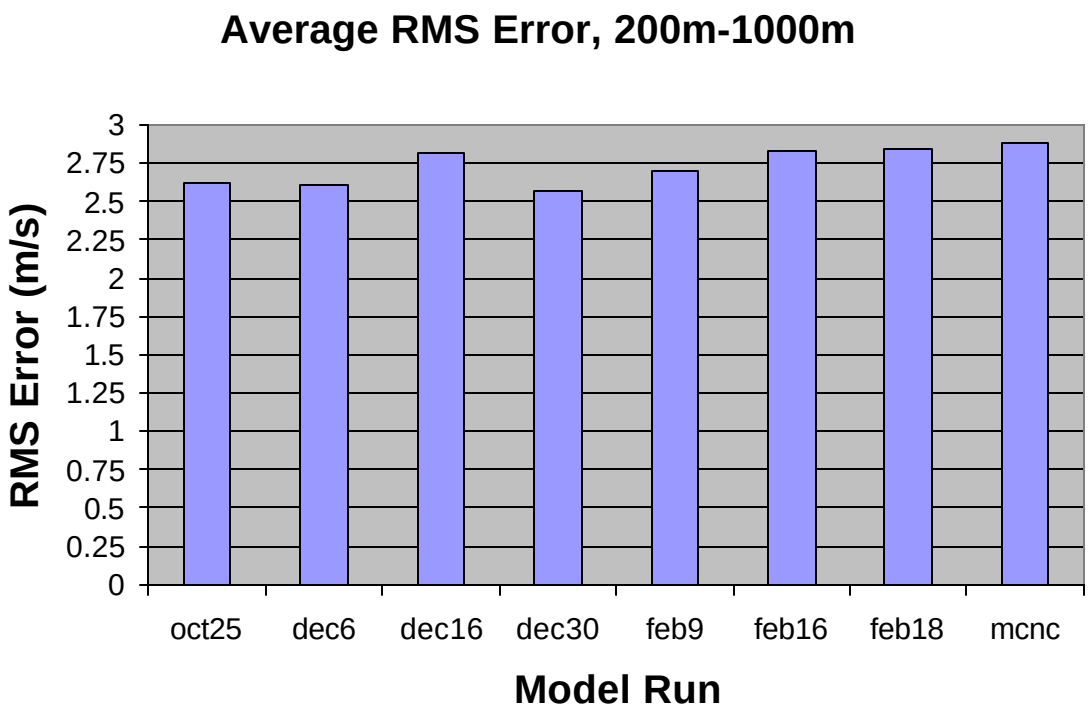

Figure 19: RMS error of the departure from 24-hour running means for entire ozone episode, measured against ETL quality-controlled profiler data. RMS errors are computed at the 200m, 400m, 700m, and 1000m levels and averaged.

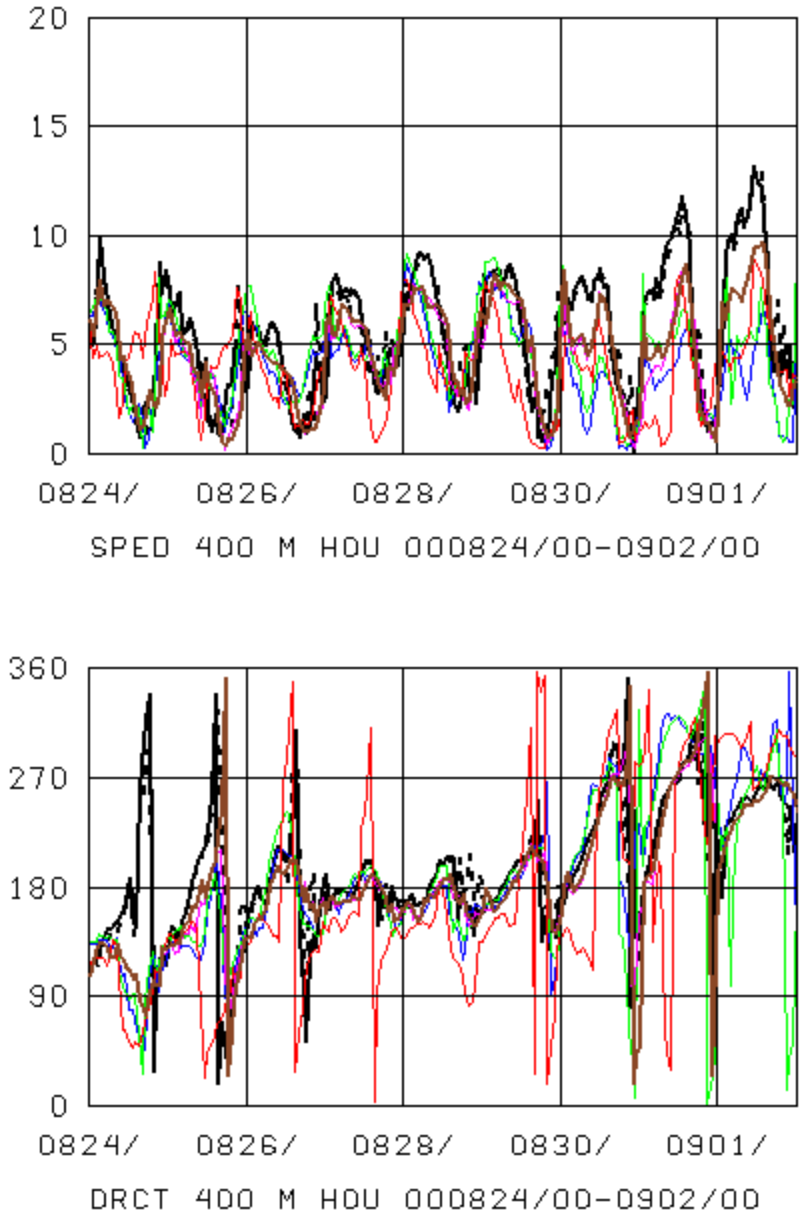

Figure 20: Time series of wind speed (top, m/s) and direction (bottom, degrees) at the 400 m level at the Houston Southwest profiler site. Solid black: AL profiler data; Dashed black: ETL profiler data; Blue: dec6grid4; Green: dec30grid4; Red: MCNC; Purple: Obs nudging with default soil moisture; Brown: Driver run (with obs nudging)

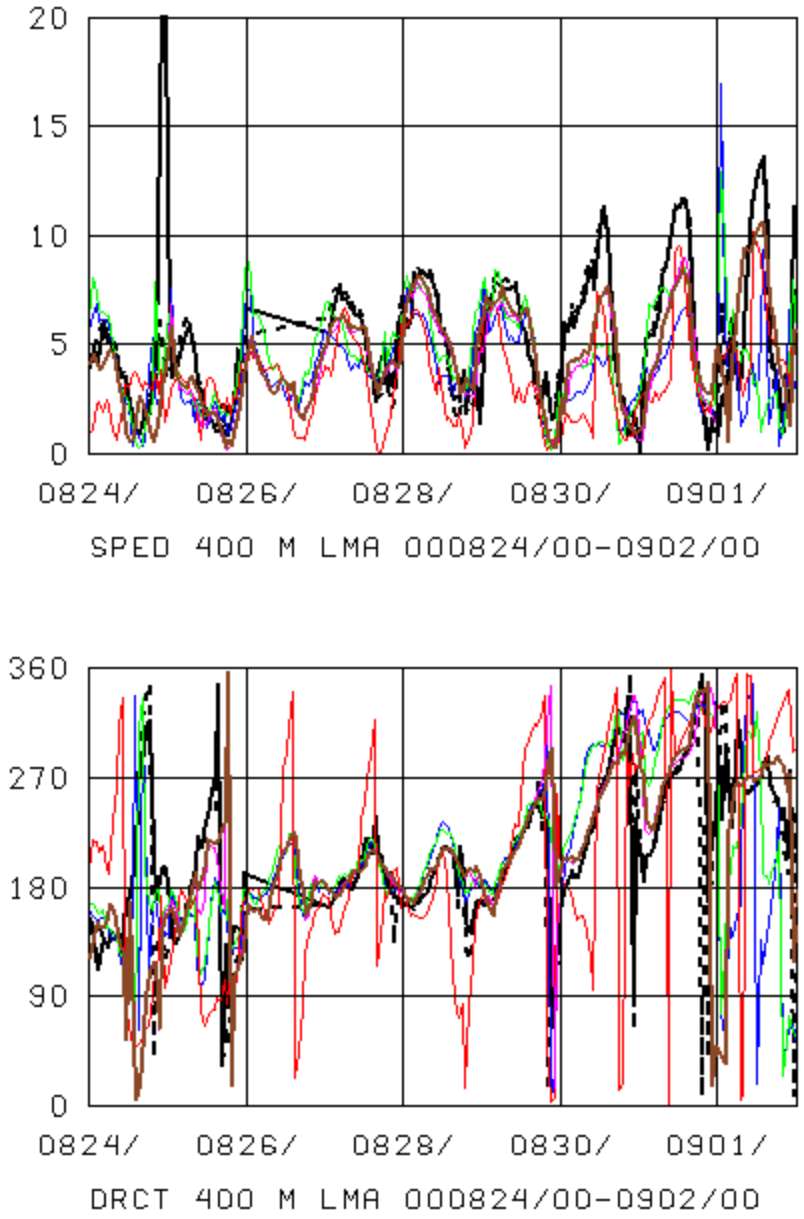

Figure 21: Time series of wind speed (top, m/s) and direction (bottom, degrees) at the 400 m level at the Liberty profiler site. Colors as in Fig. 20.

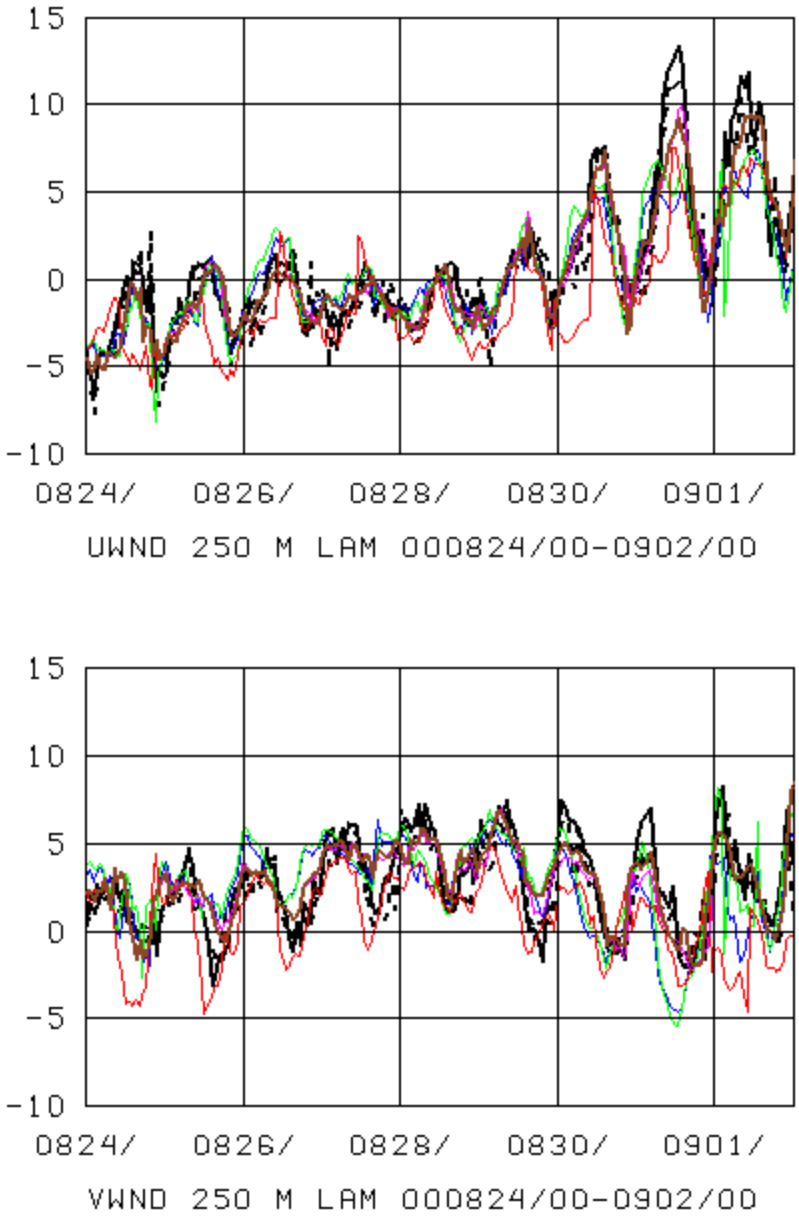

Figure 22: Time series of u (east-west) component of wind (top, m/s) and v (north-south component of wind (bottom, m/s) at the 250 m level at the Lamarque profiler site. Colors as in Fig. 20.

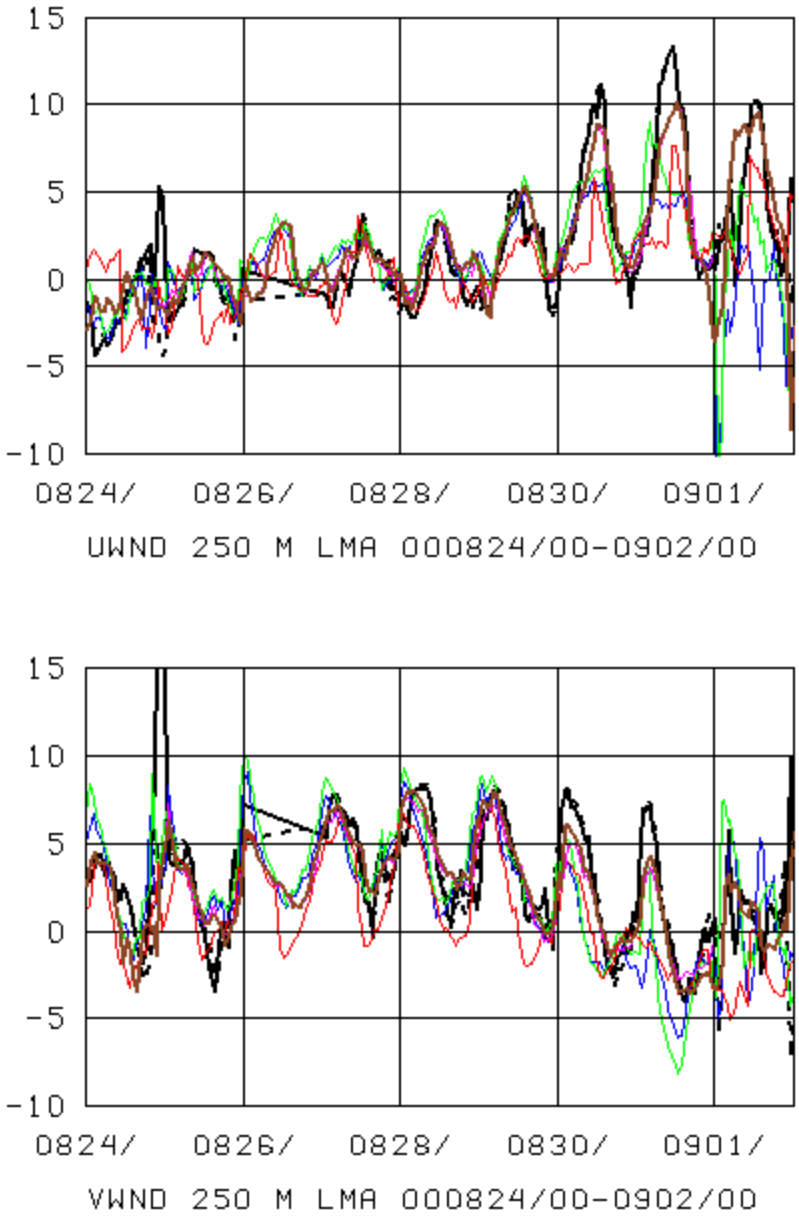

Figure 23: Time series of u (east-west) component of wind (top, m/s) and v (north-south component of wind (bottom, m/s) at the 250 m level at the Liberty profiler site. Colors as in Fig. 20.

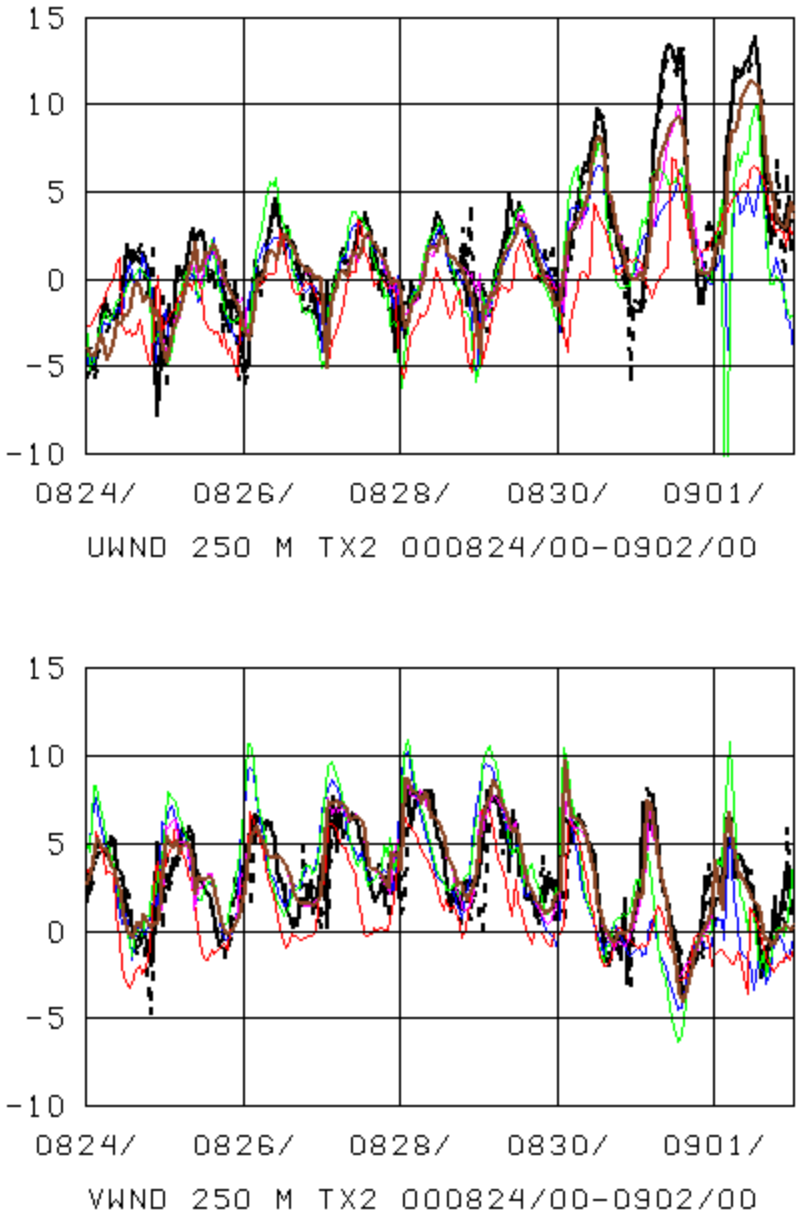

Figure 24: Time series of u (east-west) component of wind (top, m/s) and v (north-south component of wind (bottom, m/s) at the 250 m level at the Wharton Power Plant profiler site. Colors as in Fig. 20.

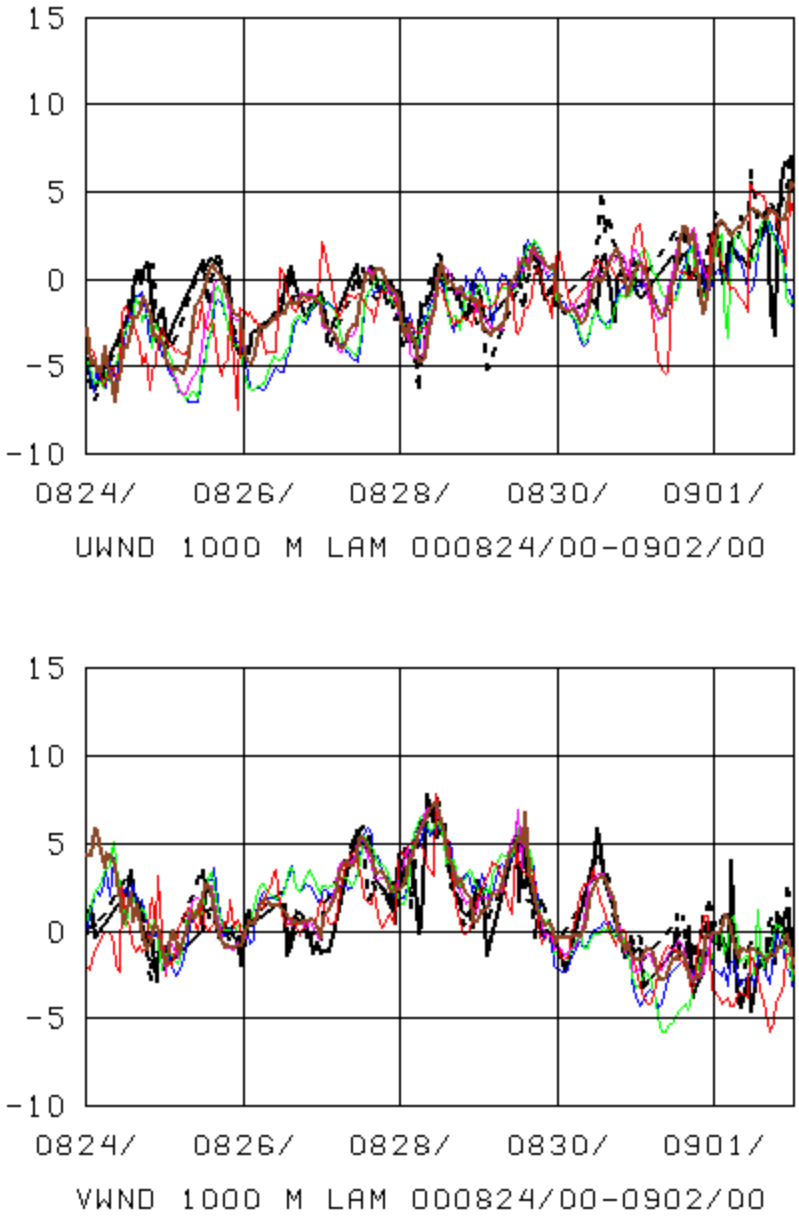

Figure 25: Time series of u (east-west) component of wind (top, m/s) and v (north-south component of wind (bottom, m/s) at the 1000 m level at the Lamarque profiler site. Colors as in Fig. 20.

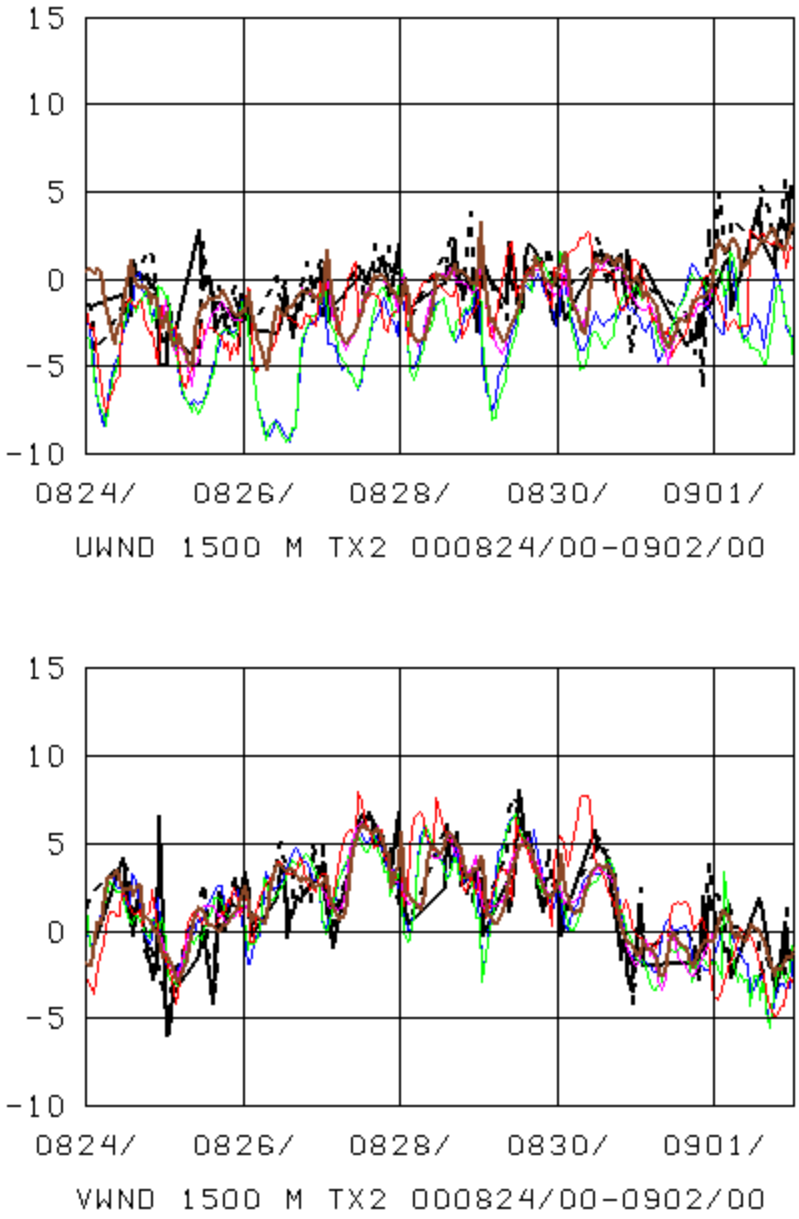

Figure 26: Time series of u (east-west) component of wind (top, m/s) and v (north-south component of wind (bottom, m/s) at the 1500 m level at the Wharton Power Plant profiler site. Colors as in Fig. 20.

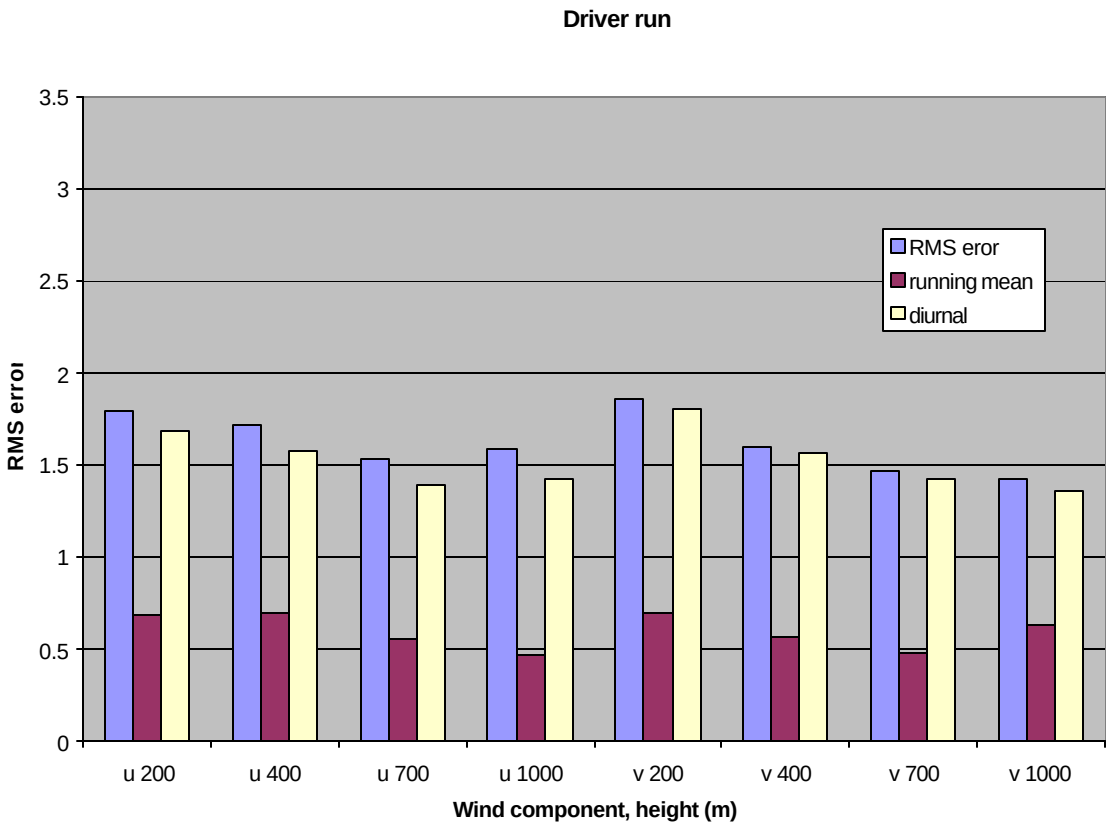

Figure 27: Total RMS error, RMS error of the 24-hour running mean, and RMS error of the departure from the 24-hour running mean, by wind component and height above ground, driver model run. Compare with Fig. 14.

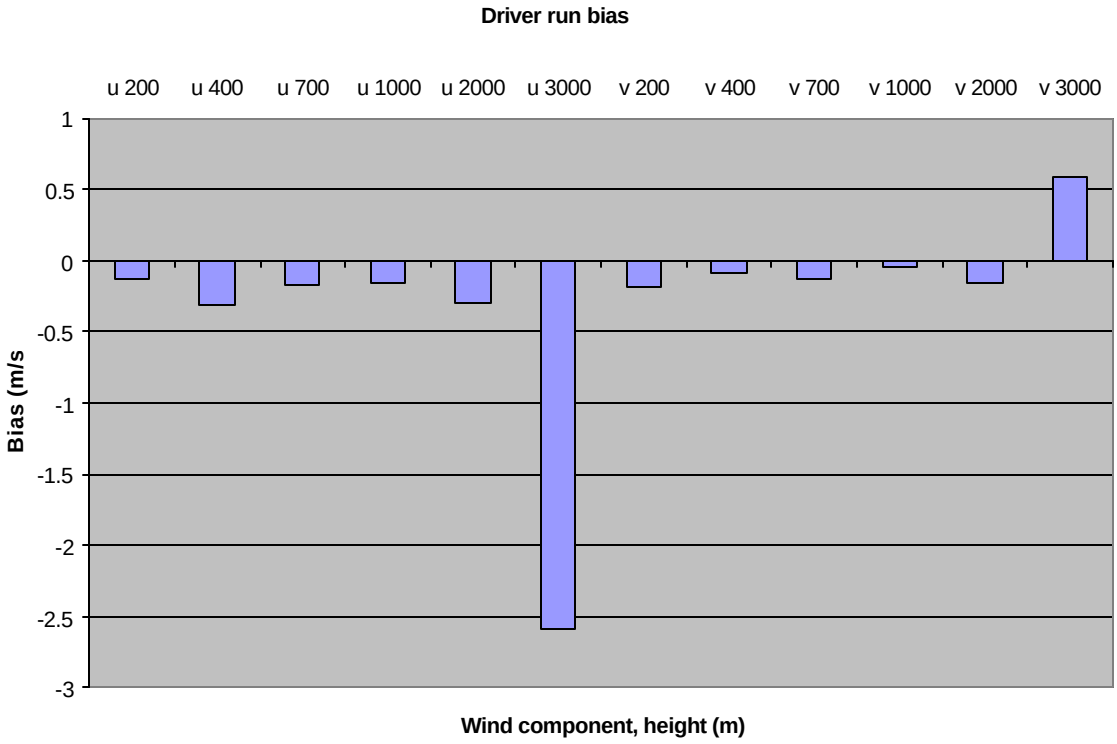

Figure 28: Bias as a function of wind component and height, driver model run. Compare with Fig. 15.

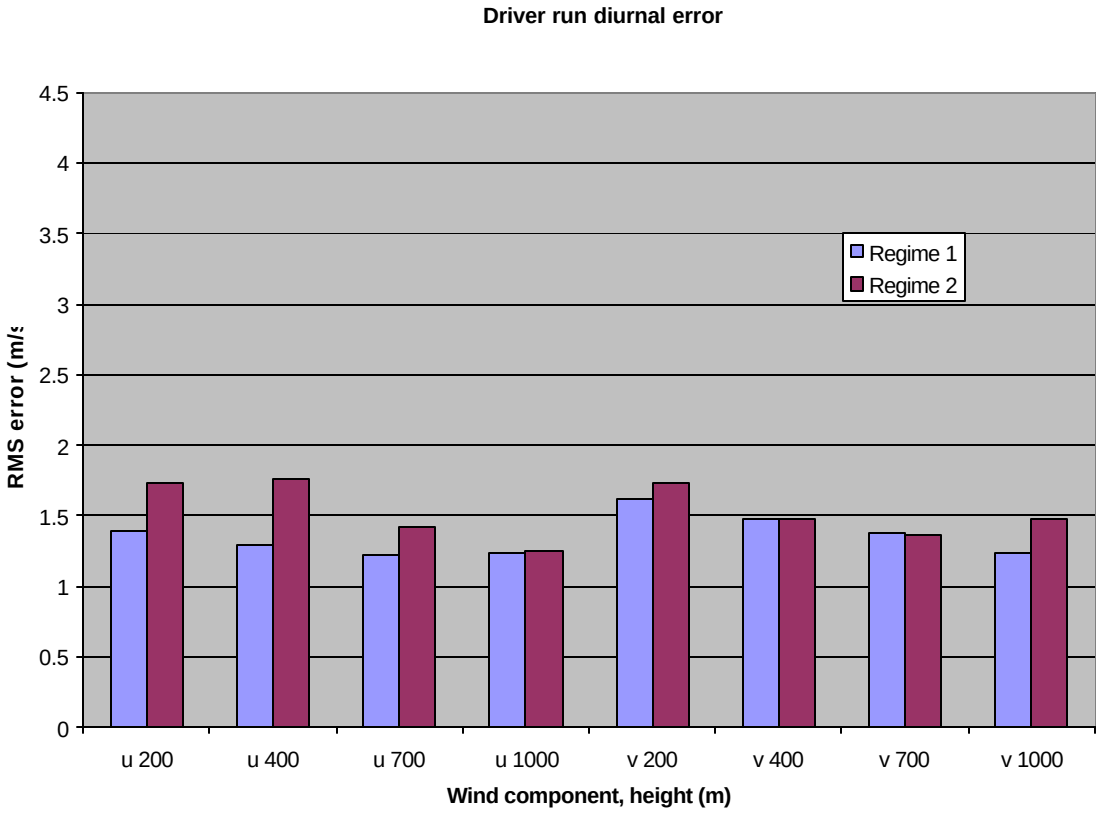

Figure 29: Driver model run RMS error of the departure from 24-hour running mean by regime, as a function of wind component and height. Compare with Fig. 18.

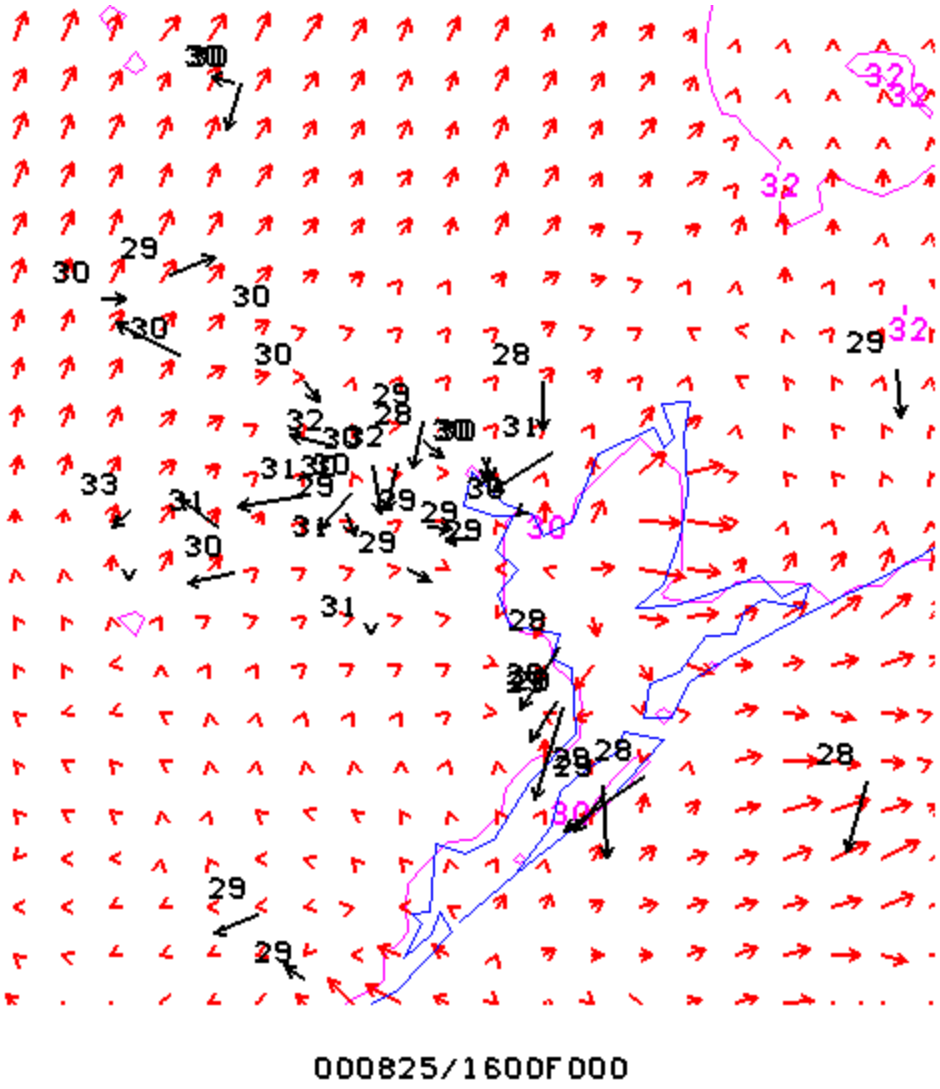

Figure 30a: Surface observations (black) and driver model run simulated winds (red) and temperatures (purple, C), 16 UTC August 25 2000.The observed wind speed in the lower right corner is 3.2 m/s; this scale is retained in the figures that follow. The model data is 2 m temperature and 10 m wind, output from the MRF PBL scheme.

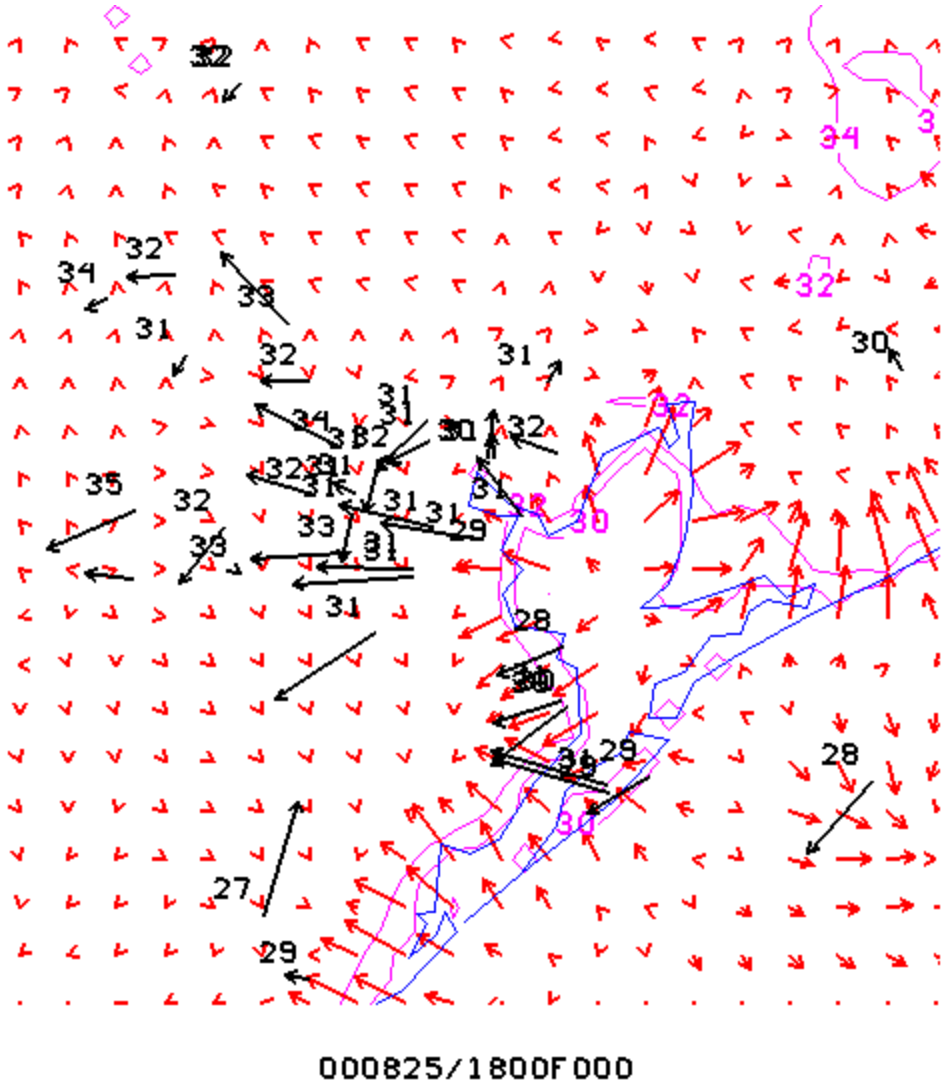

Figure 30b: Observations and driver model simulation, 18 UTC August 25.

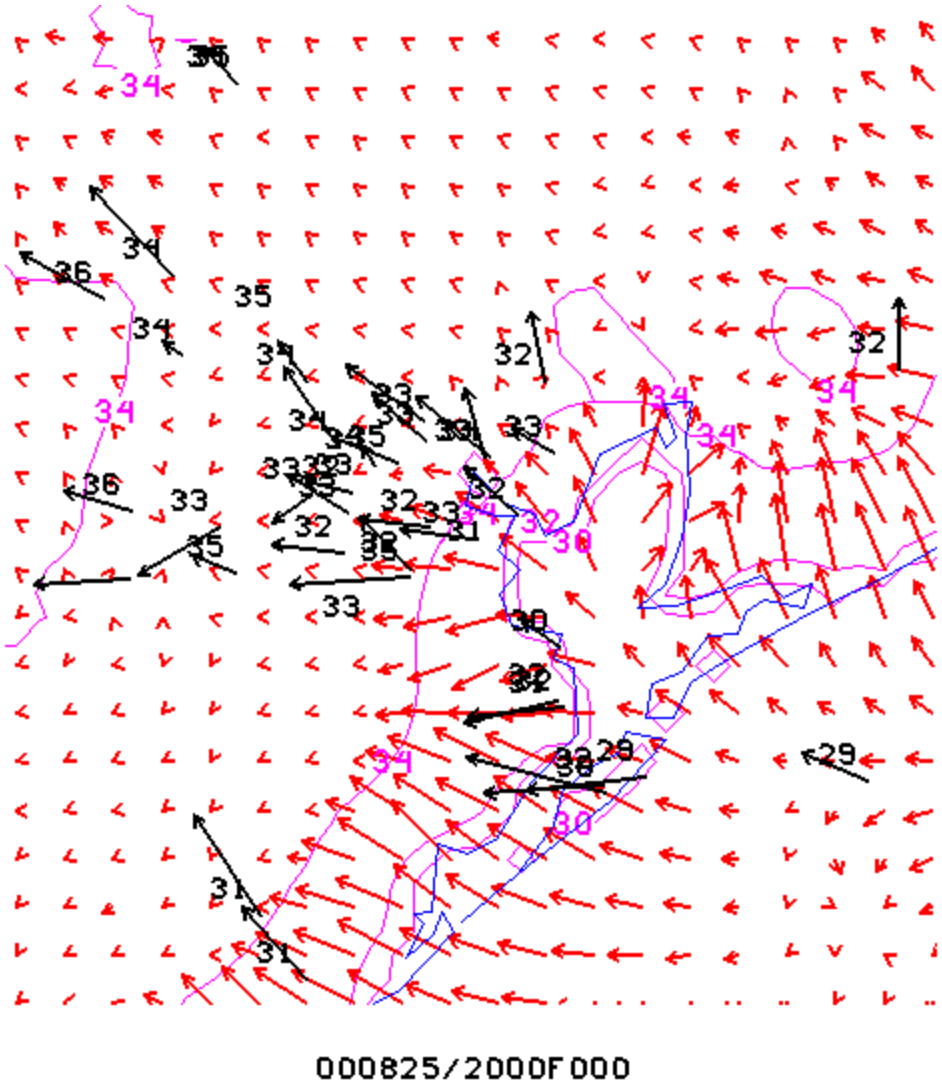

Figure 30c: Observations and driver model simulation, 20 UTC August 25.

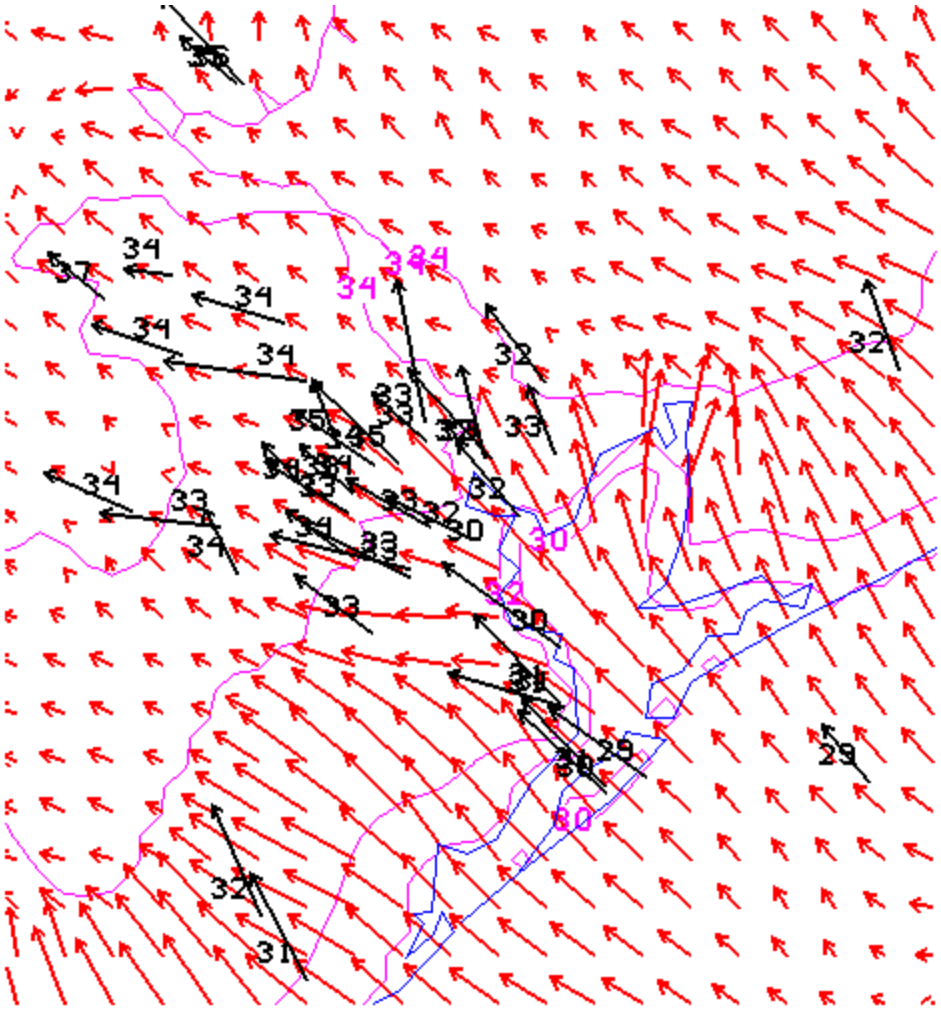

Figure 30d: Observations and driver model simulation, 22 UTC August 25.

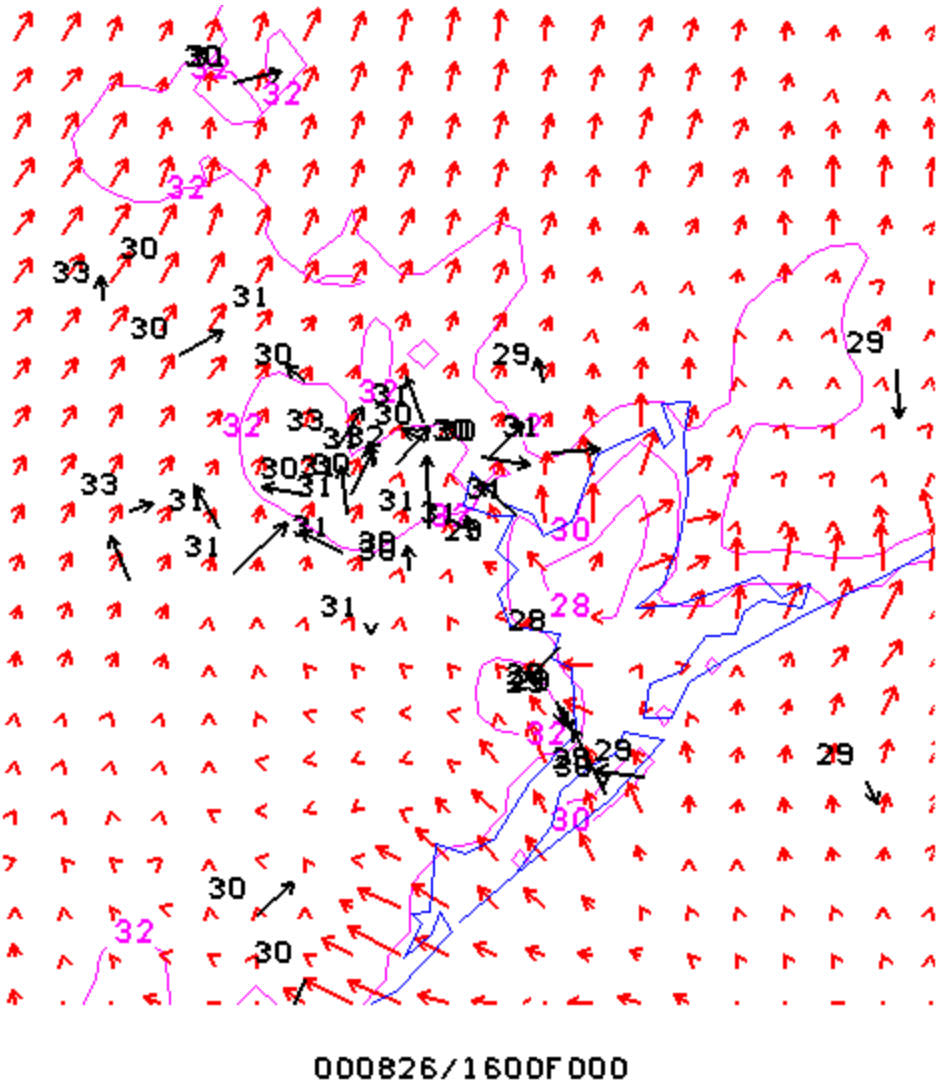

Figure 31a: Observations and driver model simulation, 16 UTC August 26.

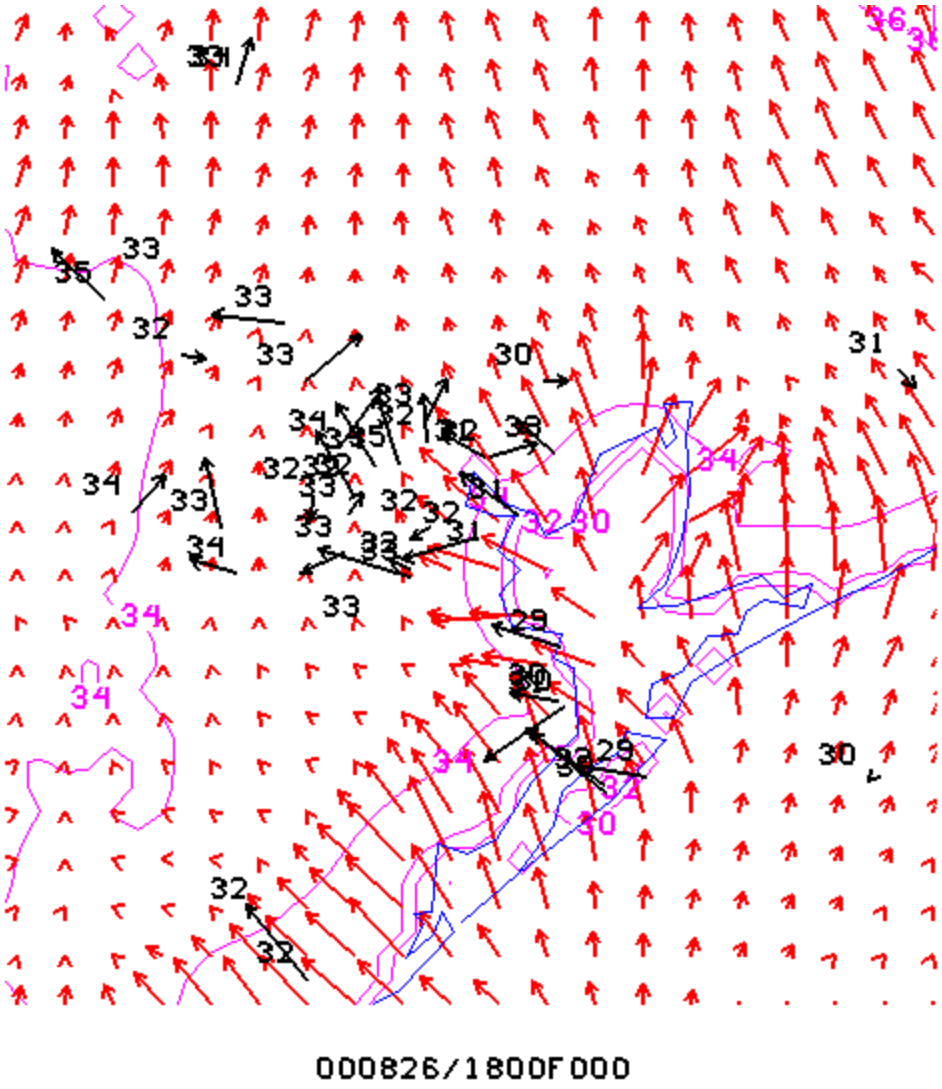

Figure 31b: Observations and driver model simulation, 18 UTC August 26.

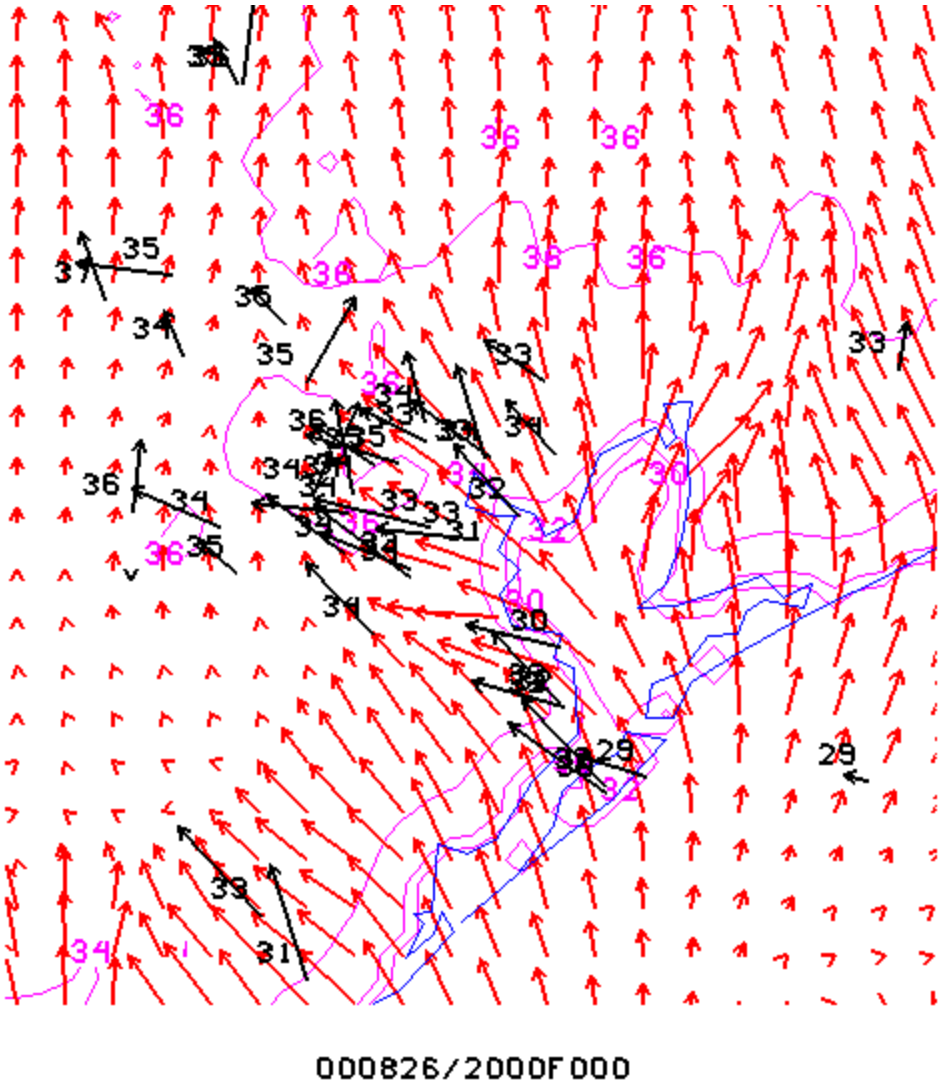

Figure 31c: Observations and driver model simulation, 20 UTC August 26.

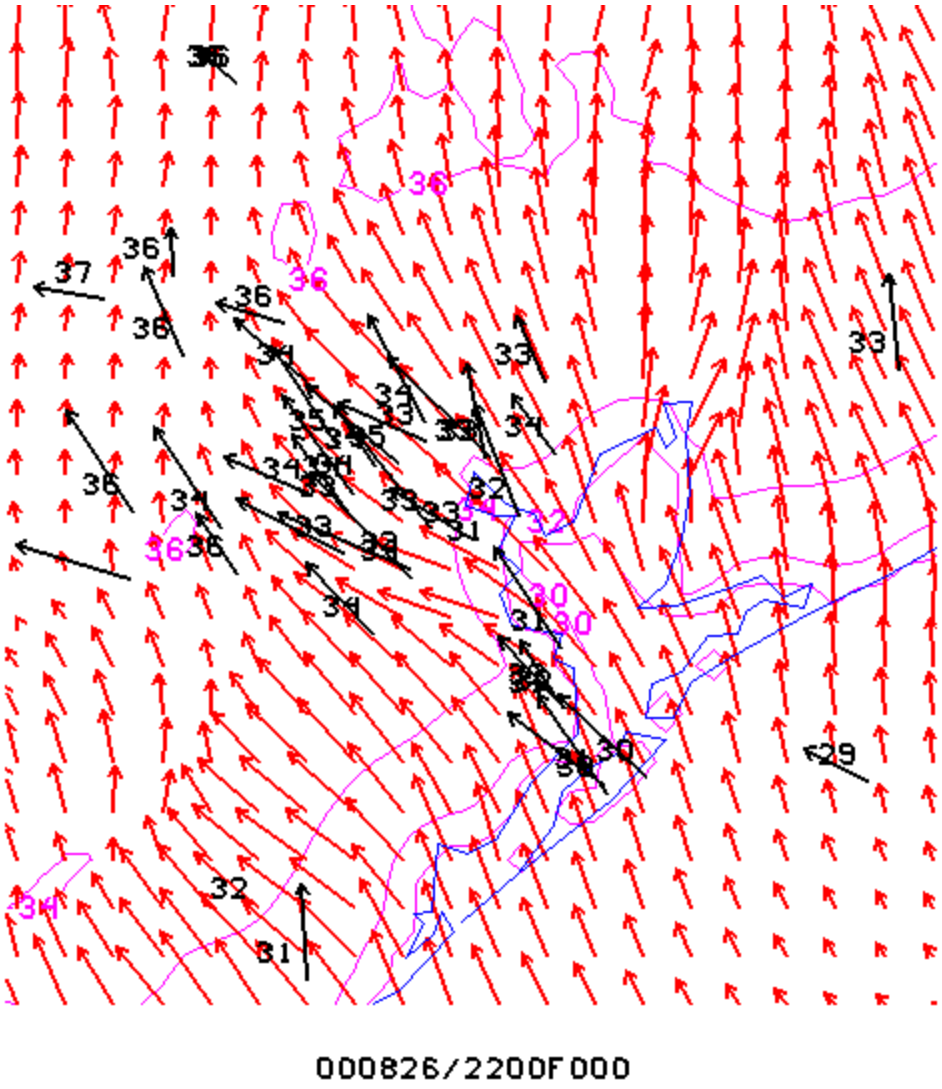

Figure 31d: Observations and driver model simulation, 22 UTC August 26.

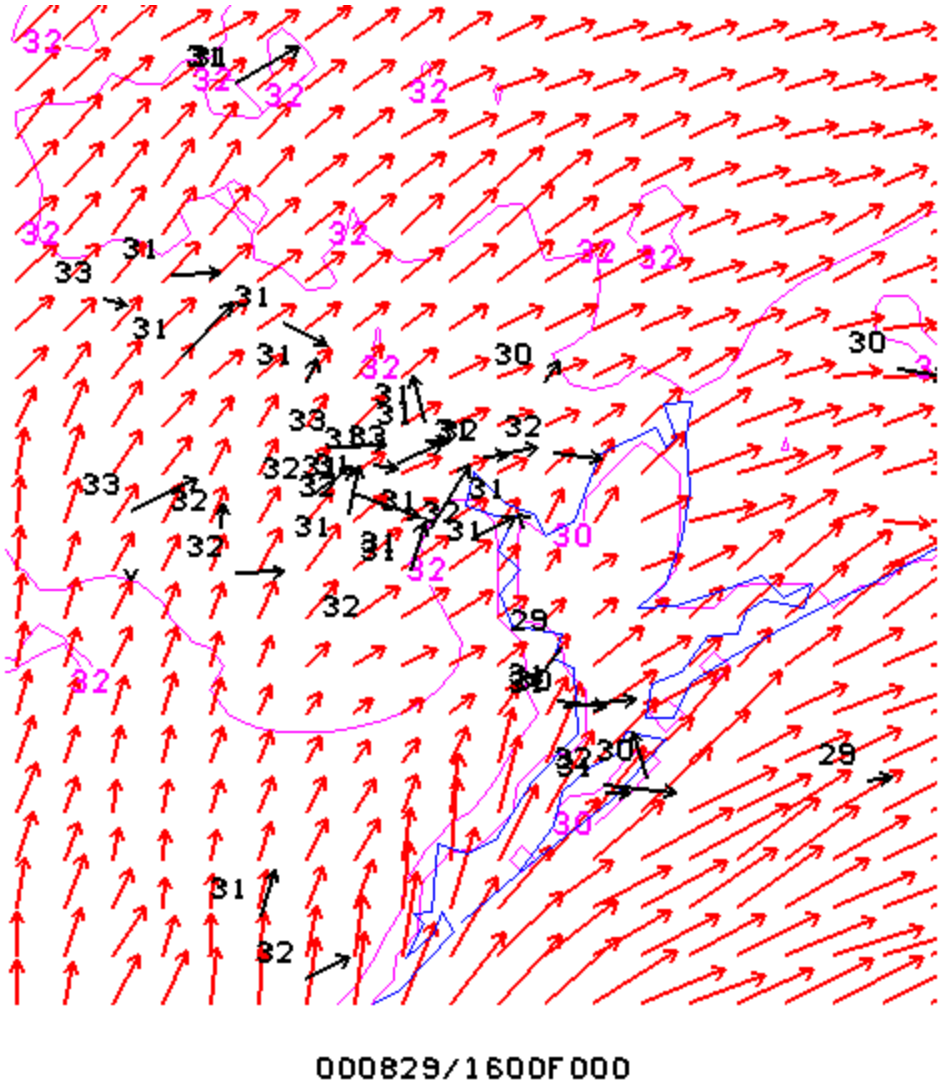

Figure 32a: Observations and driver model simulation, 16 UTC August 29.

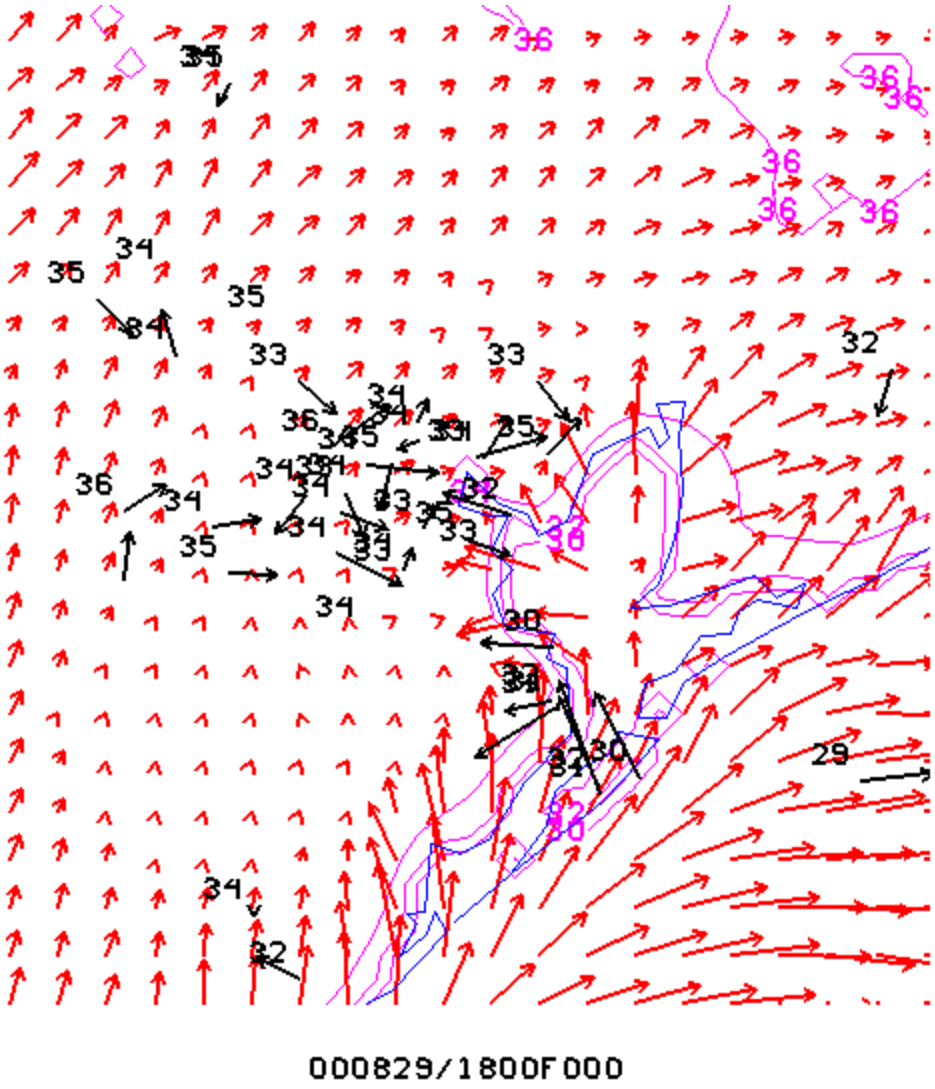

Figure 32b: Observations and driver model simulation, 18 UTC August 29.

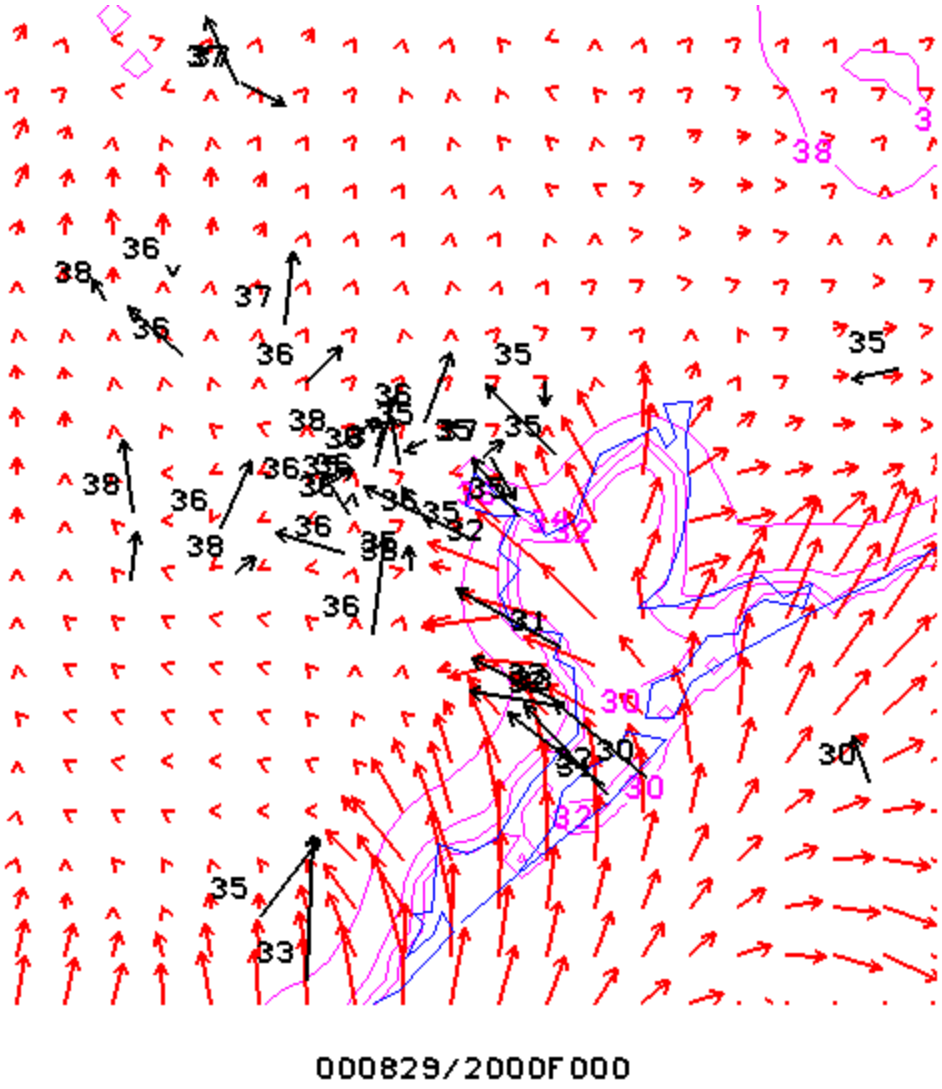

Figure 32c: Observations and driver model simulation, 2000 UTC August 29.

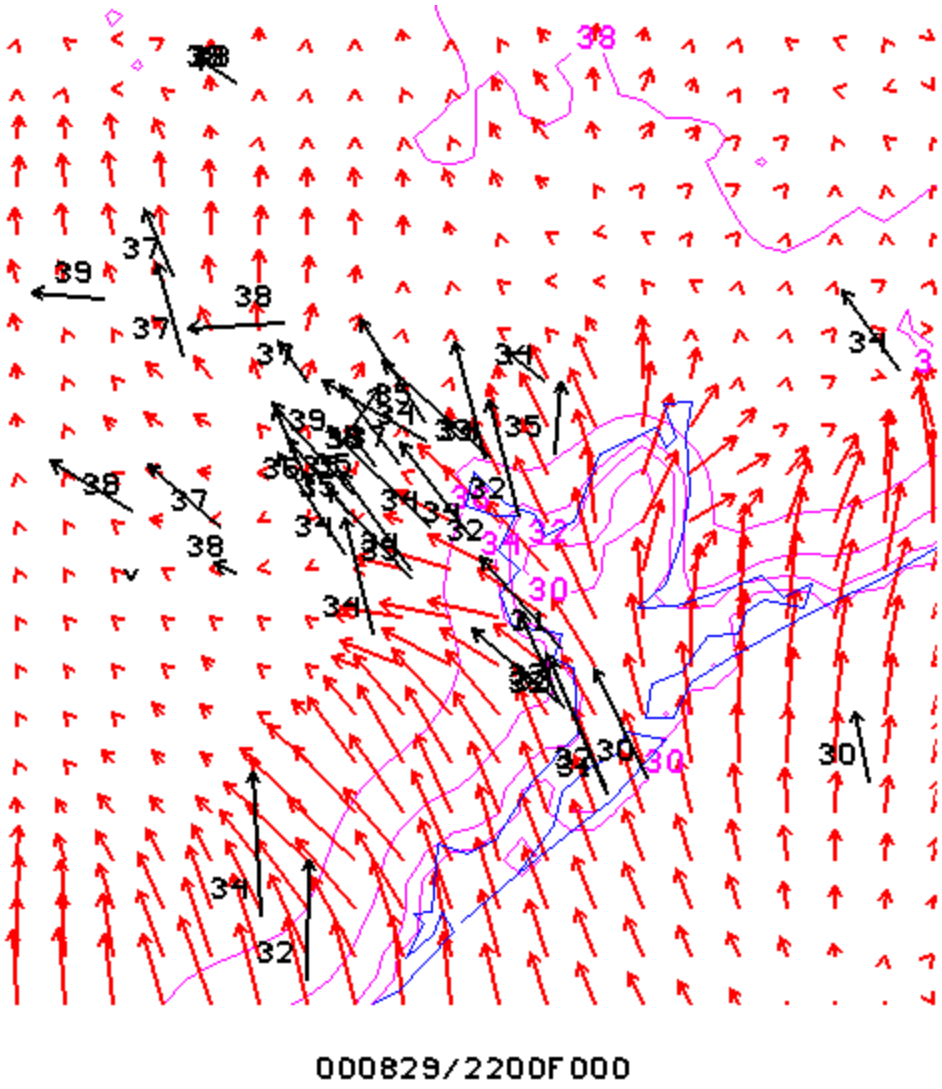

Figure 32d: Observations and driver model simulation, 22 UTC August 29.

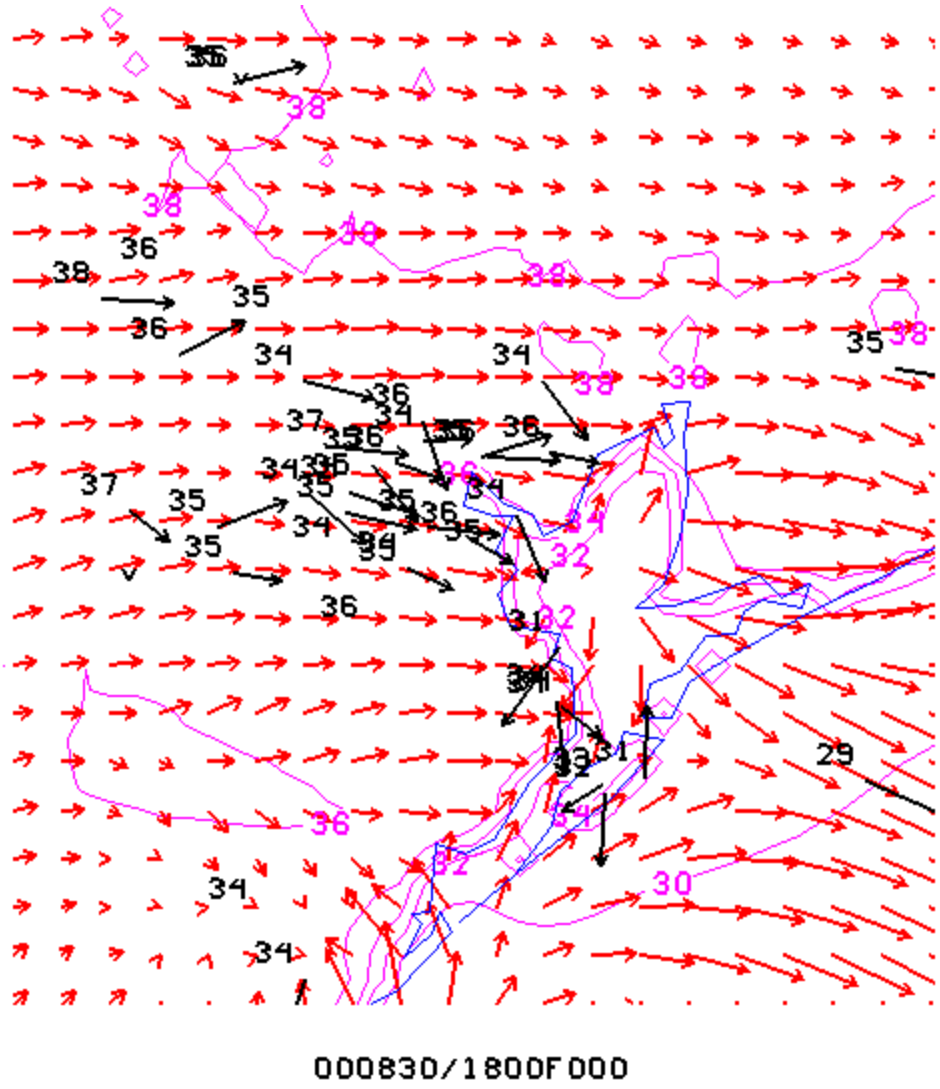

Figure 33a: Observations and driver model simulation, 18 UTC August 30.

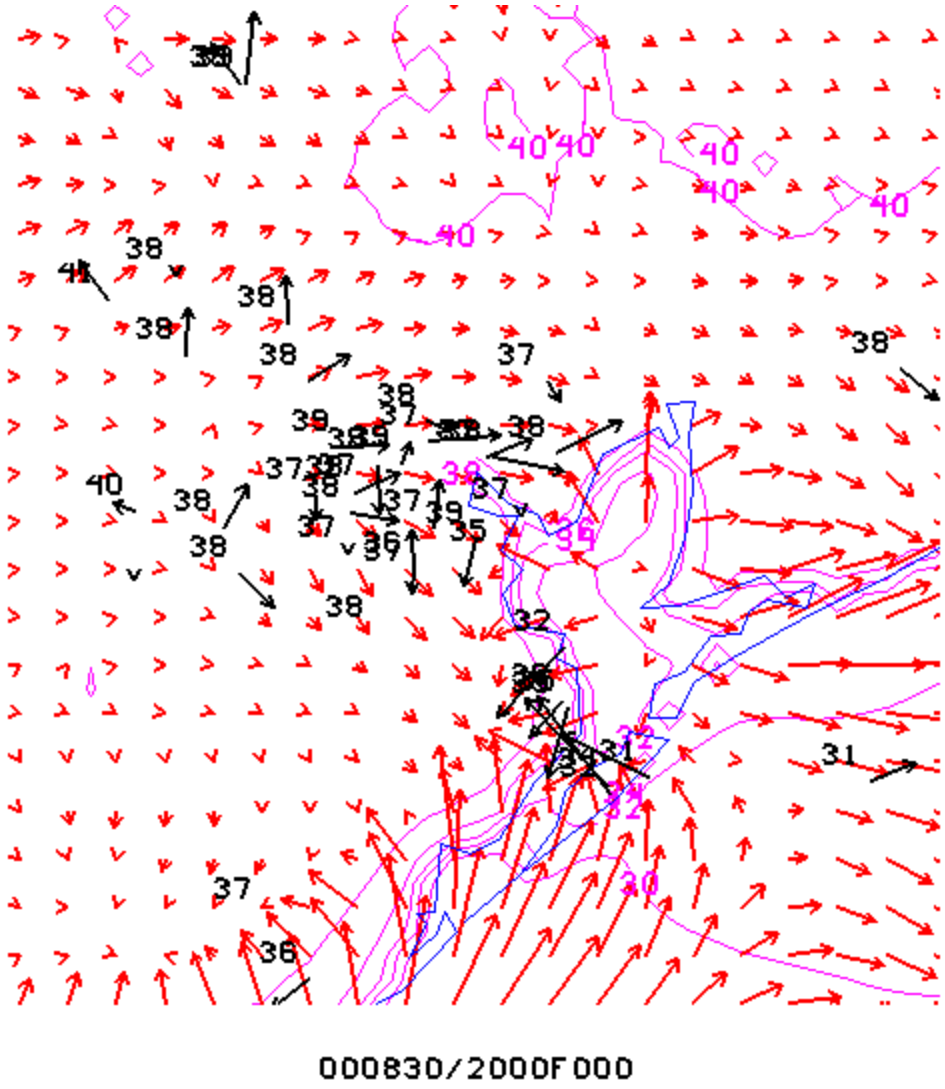

Figure 33b: Observations and driver model simulation, 20 UTC August 30.

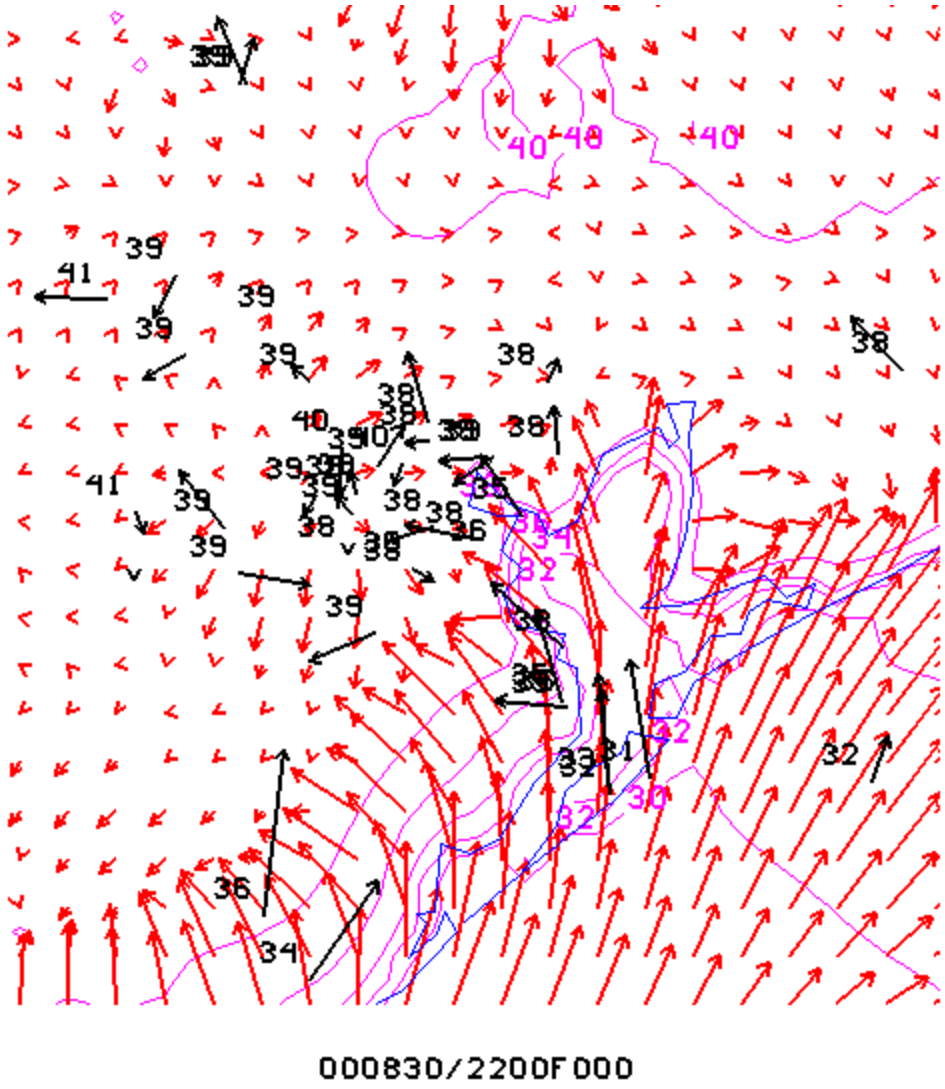

Figure 33c: Observations and driver model simulation, 22 UTC August 30.

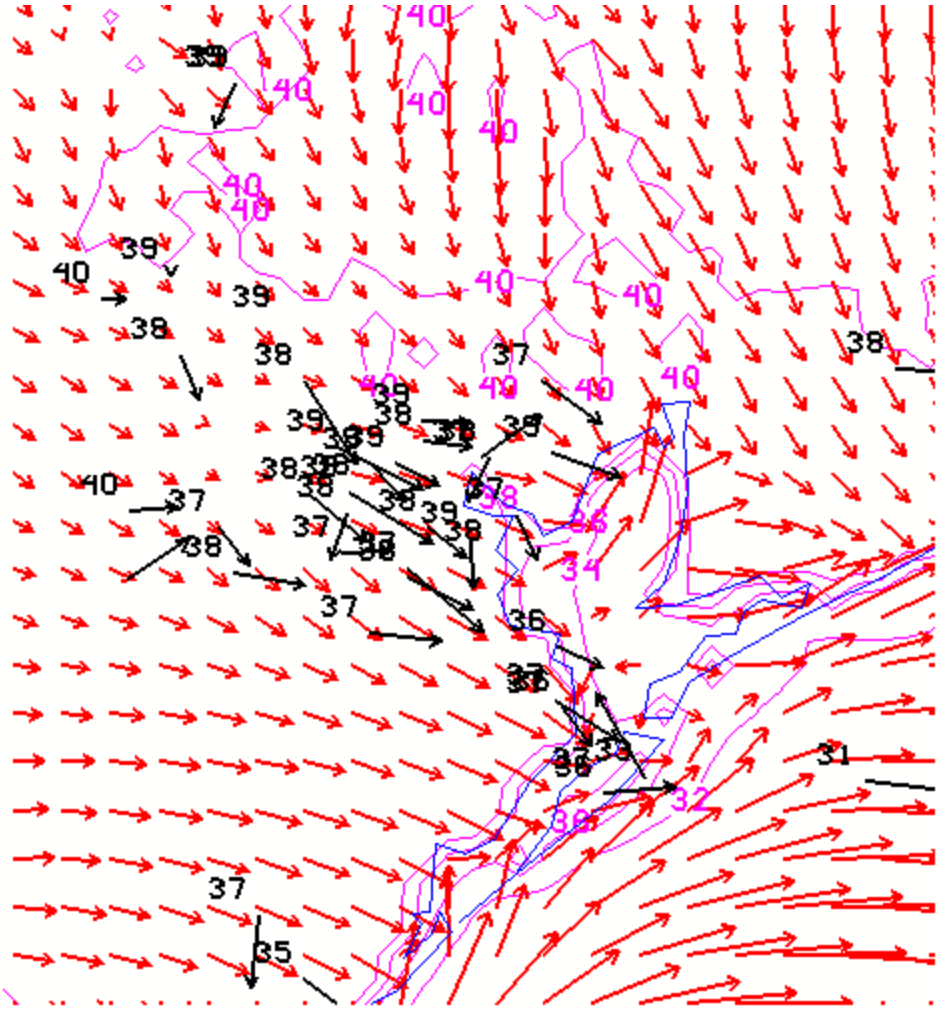

Figure 34a: Observations and driver model simulation, 18 UTC August 31.

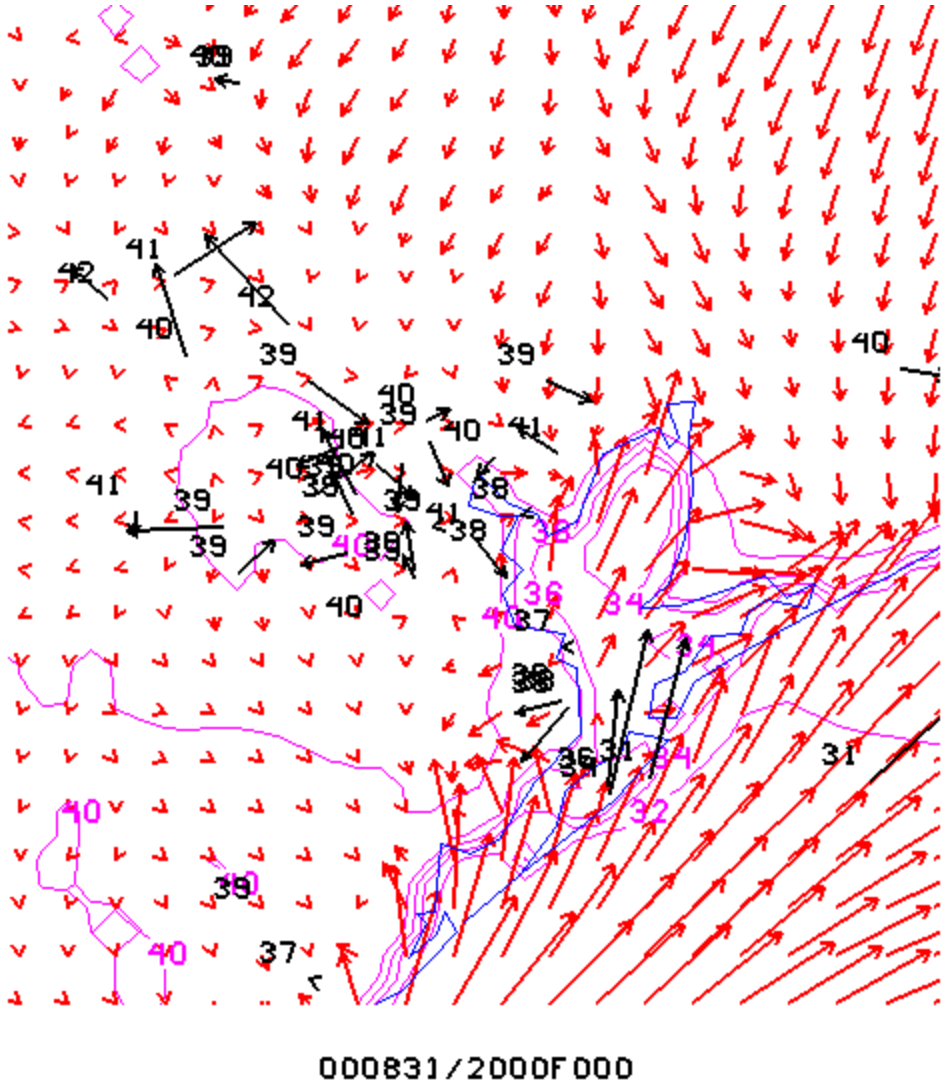

Figure 34b: Observations and driver model simulation, 20 UTC August 31.

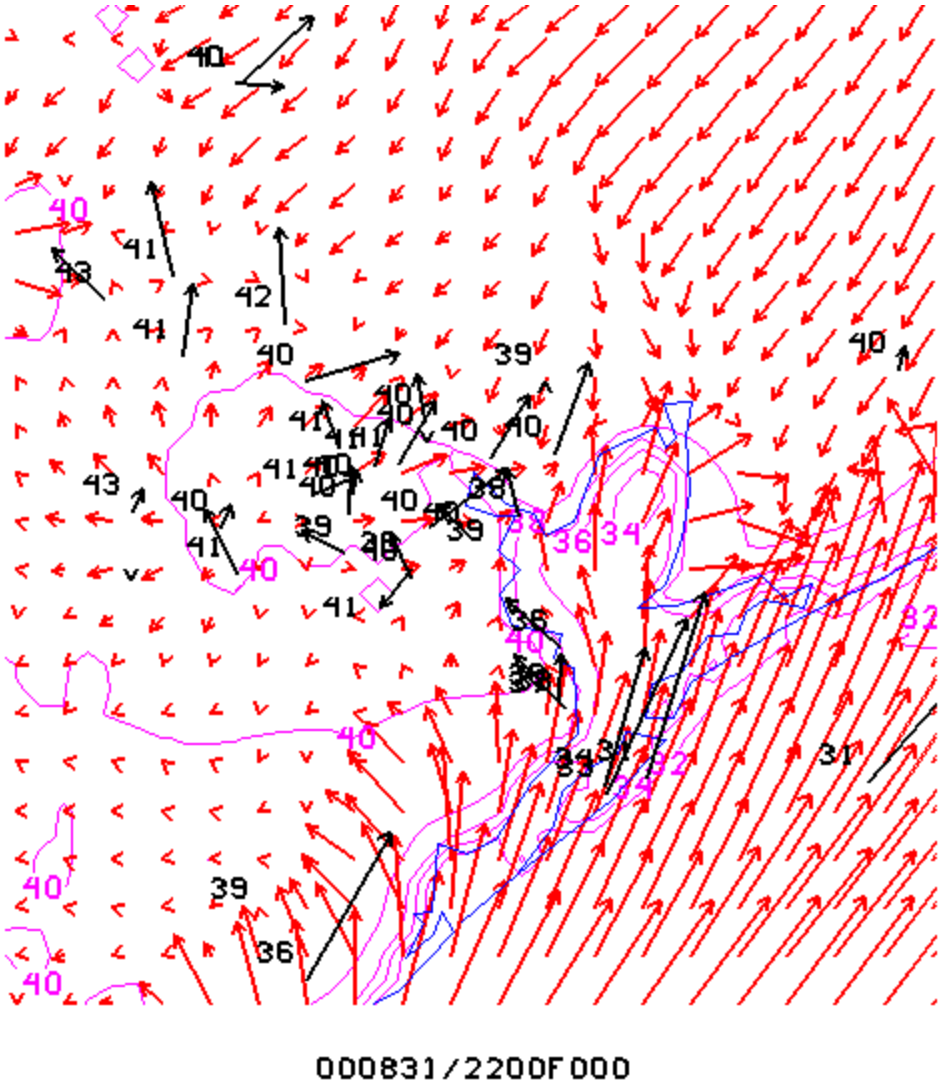

Figure 34c: Observations and driver model simulation, 22 UTC August 31.

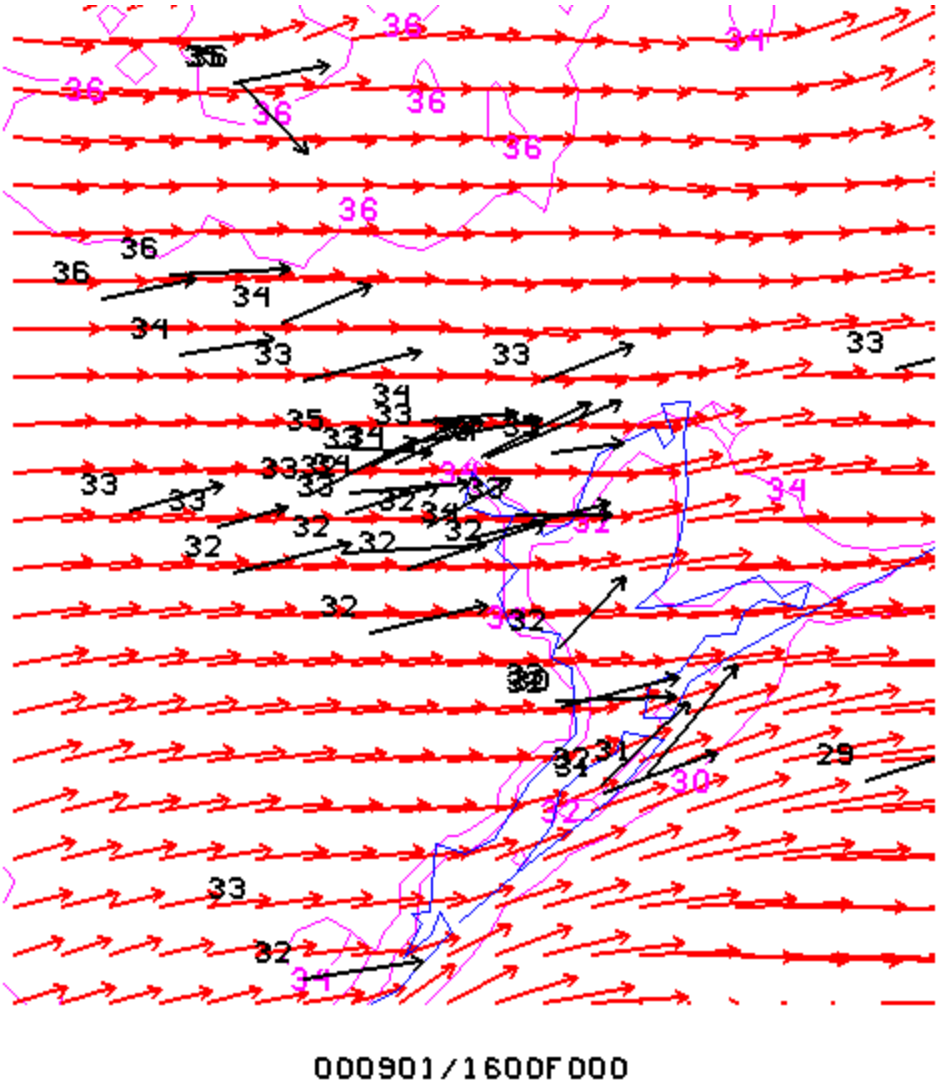

Figure 35a: Observations and driver model simulation , 16 UTC September 1.

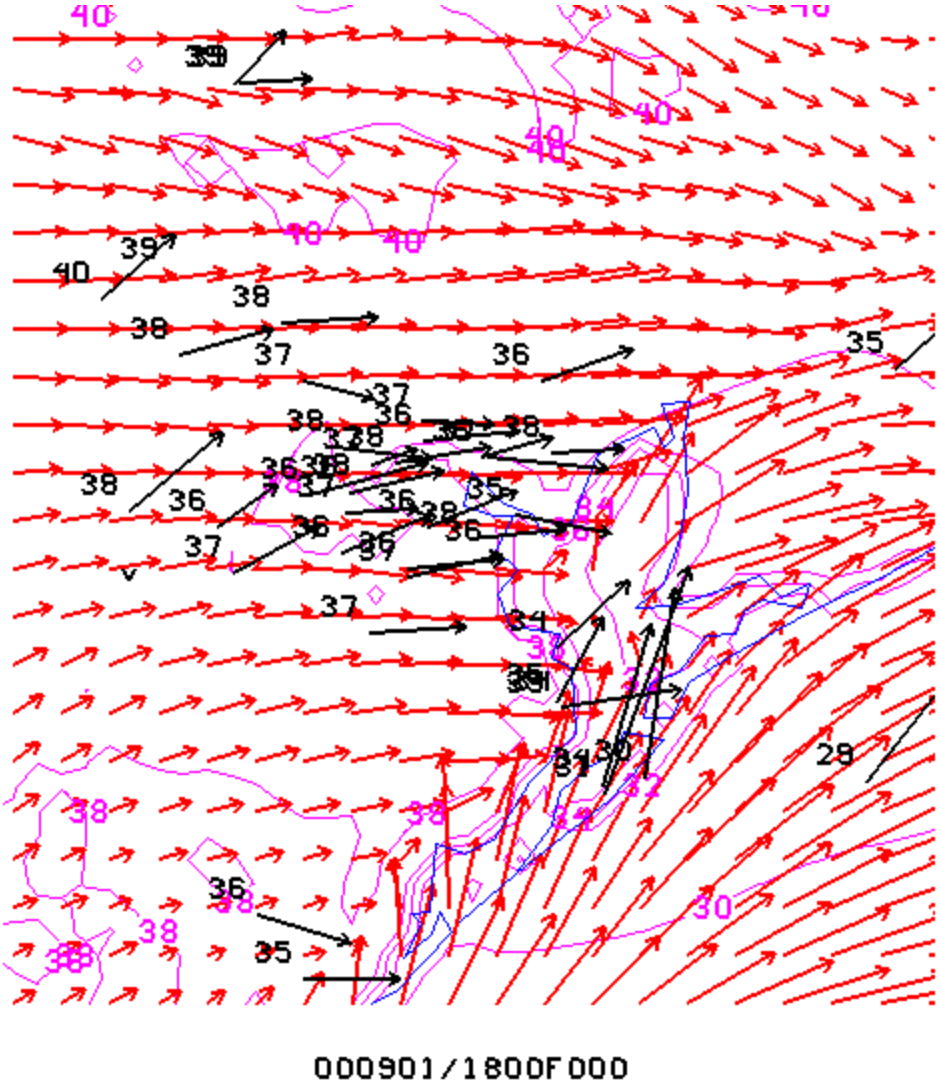

Figure 35b: Observations and driver model simulation, 18 UTC September 1.

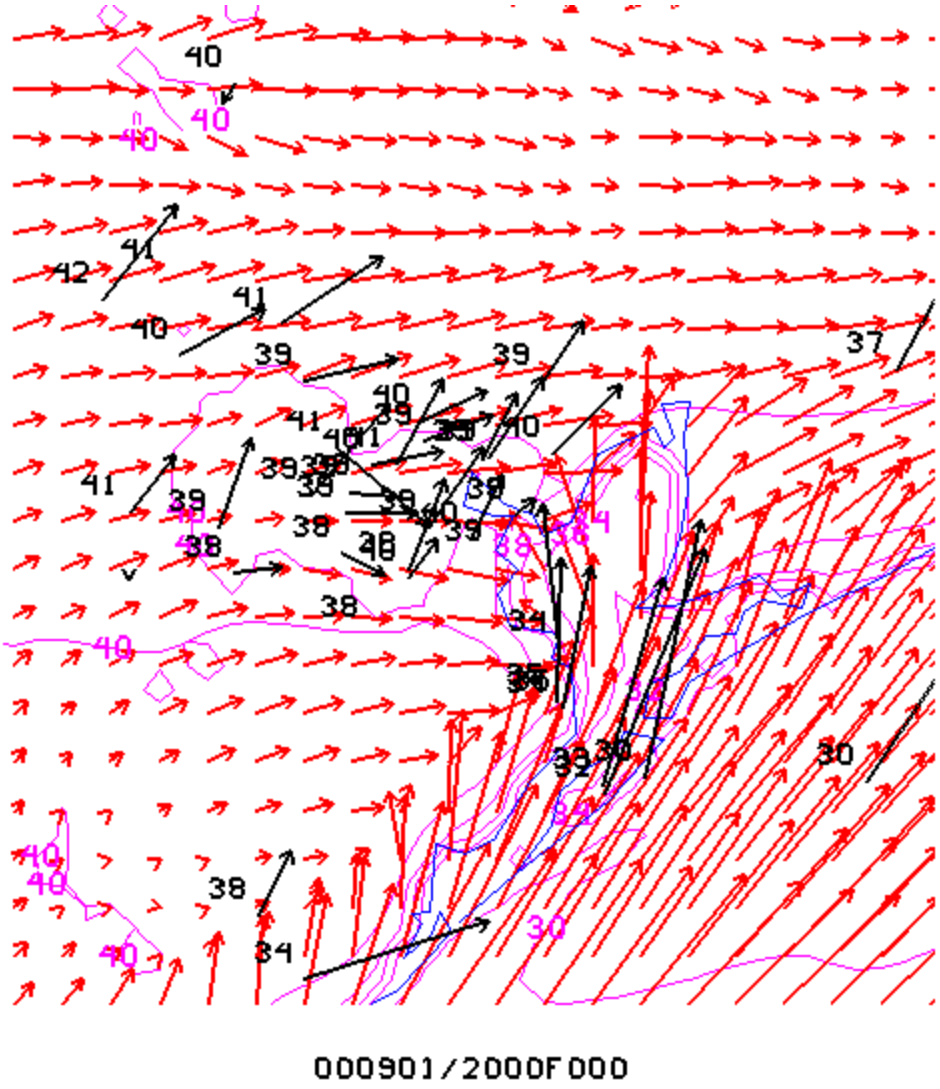

Figure 35c: Observations and driver model simulation, 20 UTC September 1.

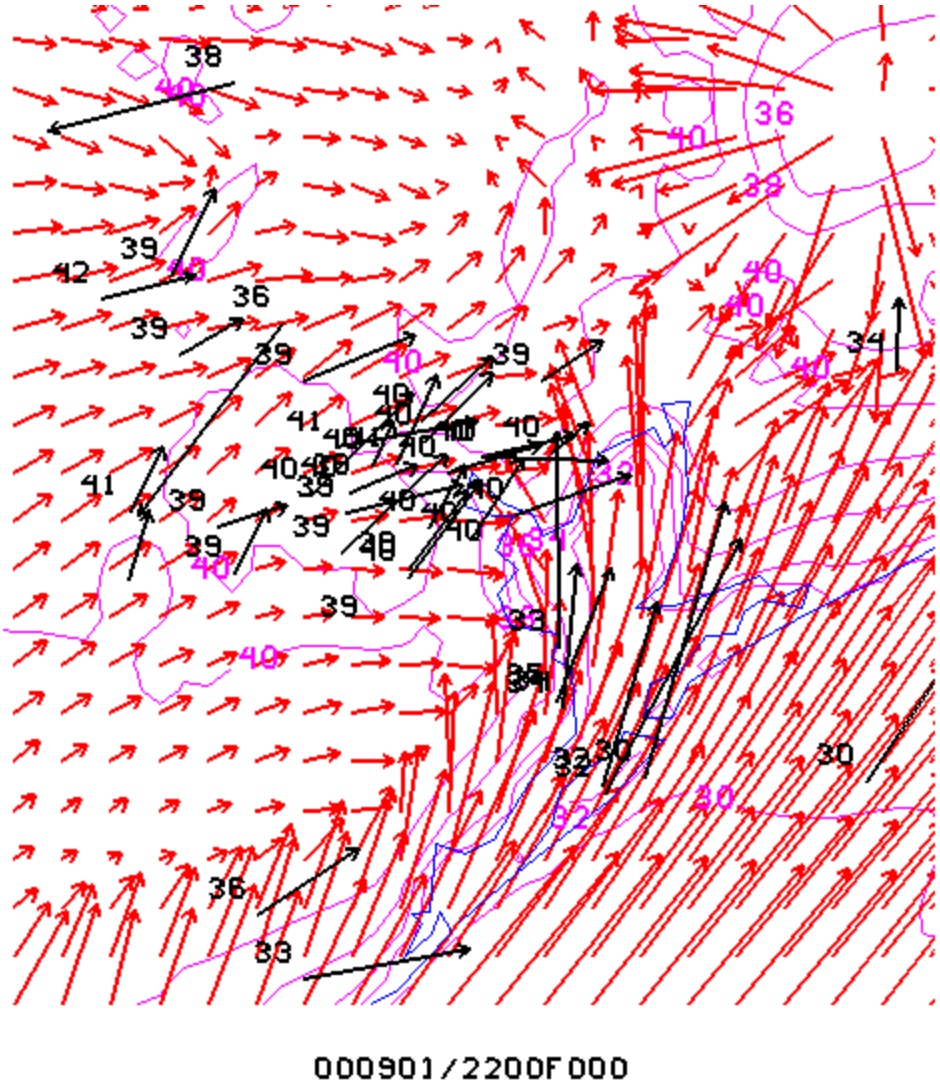

Figure 35d: Observations and driver model simulations, 22 UTC September 1.